DESIGN AND ANALYSIS OF MICROCRYSTALLINE PHOTONIC STRUCTURES FOR MICRO SENSORS

Thesis submitted in partial fulfillment of the requirements for the award of degree of

Master of Technology

in

VLSI Design & CAD

Submitted By:

Anshul Tuteja

Roll No. 600961005

Under the Guidance of

Dr. Sanjay Sharma

Associate Professor

Department of Electronics & Communication Engineering

Thapar University, Patiala

June 2011

CERTIFICATE

I hereby declare that the work which is being presented in the thesis entitled, **"Design and Analysis of Microcrystalline Photonic Structures for Micro Sensors"** in partial fulfillment of the requirement for the award of degree of M.Tech. (VLSI Design & CAD) at Electronics and Communication Engineering Department of Thapar University, Patiala, is an authentic record of my own work carried out under the supervision of Dr. Sanjay Sharma, Associate Professor, ECED.

The matter presented in this thesis has not been submitted in any other University/Institute for the award of my degree.

Date: 30/06/11

Anshul Tuteja
Roll. No. 600961005

It is certified that the above statement made by the student is correct to the best of my knowledge and belief.

30/6/2011

Dr. Sanjay Sharma
Associate Professor
ECED, Thapar University

Counter signed by:

Dr. A. K. Chatterjee
Professor & Head
ECED, Thapar University
Patiala-147004

Dr. S. K. Mohapatra
Dean of Academic Affairs
Thapar University
Patiala-147004

ACKNOWLEDGEMENTS

I take this opportunity to express my profound sense of gratitude and respect to all those who helped me through the duration of this thesis. I would have never succeeded in completing my task without the cooperation, encouragement and help provided to me by various people. Words are often too less to reveals one's deep regards. I acknowledge with gratitude and humility my indebtedness to **Dr. Sanjay Sharma, Associate Professor,** Electronics and Communication Engineering Department, Thapar University, Patiala, under whose guidance I had the privilege to complete this thesis. I wish to express my deep gratitude towards him for providing individual guidance and support throughout the thesis work.

I convey my sincere thanks to **Head of the Department, Dr. A. K. Chatterjee** as well as **PG Coordinator, Dr. Alpana Agrawal, Assistant Professor,** Electronics and Communication Engineering Department, entire faculty and staff of Electronics and Communication Engineering Department for their encouragement and cooperation.

My greatest thanks are to all who wished me success especially my parents. Above all I render my gratitude to the Almighty who bestowed self-confidence, ability and strength in me to complete this work for not letting me down at the time of crisis and showing me the silver lining in the dark clouds. I do not find enough words with which I can express my feelings of thanks to my dear friends for their help, inspiration and moral support which went a long way in successful competition of the present study.

Anshul Tuteja

ABSTRACT

Photonic crystals are periodic optical nanostructures that are designed to affect the motion of photons. Photonic crystal fibers (PCFs) are a class of optical fibers that uses photonic crystal cladding and were developed in early 1990s. The continuous and innovative experimental works on the photonic crystal fiber illustrates that they posses fundamentally exceptional properties and overcomes many limitations of conventional optical fiber, i.e. being endlessly single mode, high non linear coefficients, anomalous dispersion in visible region and guiding light through hollow core. Considering these unique as well as exceptional properties the thesis mainly focused on the micro sensor based properties of photonic crystal and photonic crystal fiber that include the transmittance and reflectance features and also the band gap analysis to define the range of frequencies in the band gap that would be strongly reflected from periodic arrangement of the designed photonic structure.

The thesis starts with a short review of conventional fibers as well as the some essential basics of photonic crystal structures and then proceeds to a discussion on the guiding mechanism including modified total internal reflection and photonic band gap guidance are reviewed. The main properties of solid core PCFs that includes dispersion tailoring, ultra high nonlinearities, birefringent features are being studied. A short review of the loss mechanisms is also presented. The numerical modeling techniques for modeling as well as simulation of photonic crystal designs are introduced. The modeling techniques include finite difference time domain (FDTD) method and Plane Wave Expansion (PWE) method. The FDTD method has been represented in context to modal and polarization properties of the photonic design and PWE method has been represented in context to band gap analysis of the designed photonic structure.

The FDTD modeling of photonic crystal in one dimensional and two dimensional forms is done by taking the rectangular lattice waveguide structure and dielectric material of user defined refractive index. The default material is taken to be air with unit refractive index. The FDTD simulation and analyses of modeled crystal is done that presents the reflectance and transmittance properties of the photonic crystal-the electric and magnetic field component for

transverse electric polarization and the poynting vector also. The band gap analysis for the modeled photonic crystal is done by PWE method by taking a same tolerance factor for both one and two dimensional photonic crystal design and thus band gaps are located and analyzed.

After analyzing the properties of photonic crystal a hollow core photonic crystal fiber is modeled by FDTD method, having the hollow core and rectangular lattice of user defined refractive index channel. The modal distributions as well as the polarization properties are analyzed. Also the band analysis of the same is done by PWE method to locate and observe the band gap in the structure so as to determine which range of frequencies of the input wave that would be totally reflected through the designed PCF when considering it for PCF sensor design.

TABLE OF CONTENTS

LIST OF FIGURES

LIST OF TABLES

ABBREVIATIONS

ABC	Absorbing Boundary Condition
ADE	Auxiliary Differential Equation
CFL	Courant-Friedrichs-Levy
CMOS	Complementary Metal oxide Semiconductor
CW	Continuous Wave
E	Electric Field
FBG	Fiber Braggs Grating
FDTD	Finite Difference Time Domain
H	Magnetic Field
HF	Holey Fiber
LMA	Large Mode Area
MFD	Mode Field Diameter
NA	Numerical Aperture
PBC	Periodic Boundary Condition
PBG	Photonic Band Gap
PCF	Photonic Crystal Fiber
PDE	Partial Differential Equation
PEC	Perfect Electric Conductor
PMC	Perfect Magnetic Conductor
PML	Perfectly Matched Layer
PWE	Plane Wave Expansion
RC	Recursive Convolution
SMF	Single Mode Fiber
TE	Transverse Electric
TIR	Total Internal Reflection
TM	Transverse Magnetic
UPML	Un-split Perfectly Matched Layer
UV	Ultra violet

CHAPTER

1

INTRODUCTION

Optical fibers, integrated optical waveguides and a plethora of associated devices and systems are today finding wide use in areas covering telecommunications, sensor technology, medicine and spectroscopy. The operation of such devices is usually based on the well-known effect of index guiding which assures controlled transmission of light in dielectric or semiconductor materials. This effect has been exploited for many years and the technology based on it is now approaching its limits of physical performance. Only very recently research on new materials has opened up the possibilities of guiding and controlling light by an entirely new photonic bandgap (PBG) effect. This discovery has created a huge interest in photonic crystals, the novel materials utilizing the PBG effect. It has been predicted that their utilization will soon have a major impact on a wide range of photonic applications [1].

1.1 Micro Scale Photonic Sensors

In recent years, photonic design has focused on ever smaller devices expected to operate over broad wavelength ranges and that make use of highly dispersive materials. Emerging photonic technologies including plasmonics and silicon photonics exploit dispersive material characteristics and modern semiconductor manufacturing techniques to provide new functionality to the optical designer. While such technologies open the door to greater innovation, the combination of dispersive, high index contrast materials and micro scale feature sizes have in turn place extreme demands on commercially available photonic design tools [1]. The integration of microscale technologies with the photonic devices can potentially lead to robust sensing devices. Using molecular and microscale surface modification and computer simulation, the concept seeks to enhance the prospects of PCF sensors, CMOS Sensors, Sensor arrays and Sensor networks for diverse applications such as remote and dynamic environmental monitoring, manufacturing process safety, medical diagnosis, early warning of biological warfare and homeland defense.

1.1.1 PCF Based Sensors

The photonic crystal fibers (PCFs) have become the base to explore the concept involving the study and implementation of a different enabling technology for photonic sensing. These fibers including micro structured and PBG or holey optical fibers, have emerged only in the last few years as a novel and important class of optical fibers as well as sensors based on them. Several leading groups of researchers have started aggressively exploring such waveguides for telecommunications applications due to the host of highly unusual and tailorable optical properties that they may display. However the entirely new optical properties that are possible in these fibers could also have a significant impact on a wide range of sensing applications [1]. A particular advantage will be that whereas all earlier sensing technologies require additional structures written on the fibers or added to them, this new sensing concept involving PCFs will rely uniquely on bare and undoped optical fibers, and as such will be obviously far less prone to unwanted external perturbations.

Sensors based on conventional optical fibers are well established while those based on PCFs are attracting considerable attention. PCFs are fibers with unique optical properties which are conferred by a periodic microstructure present all over the fiber length. Their modal and guidance properties [2] make PCFs appealing for optical sensing. So far a number of PCF sensors have been proposed, however, those based on Bragg gratings, long-period gratings and interferometers are the most promising ones [2] for practical applications due to their robustness. Most of these sensors have centimeter lengths and exhibit remarkable performance such as high stability over time, operation in a broad wavelength range or at extreme temperatures. However, they typically operate as point or single sensor. Sometimes the multiplexing of PCF-based sensors is a necessary step to widen their capabilities so as to make the PCF sensors compete with their well-established counterparts based on standard optical fibers.

The architecture of PCFs suggests a variety of strategies for optical sensing [3]. Especially two features of the PCFs have encouraged their use within sensors. One is the possibility of obtaining long interaction lengths between light propagating in the fiber and very small volumes of gasses or liquids positioned in the air holes. The other is the freedom in the design of the optical properties of the fibers including the number of guiding cores. The most common approach involves using the evanescent field of PCF modes, confined to the high-

index material in a PCF, for the detection and analysis of gas and liquid-phase species in air holes of PCF cladding. This protocol of optical sensing can be employed for the experimental demonstration of compact, practical and efficient PCF sensors of gas-phase media and biomolecules in aqueous solution [3].

Myaing et al [4] have demonstrated another method of biosensing using PCFs. In those experiments, a double-clad PCF served to improve the efficiency of two-photon fluorescence detection of biomolecules with the fluorescence signal delivered to the detector in the backward direction through the same fiber. The possibility of extending the concept of fiber grating-based sensing to PCFs has been demonstrated by Eggleton et al [5].

Air-guided modes of hollow-core PCFs have been shown to be ideally suited for gas phase sensing using linear and nonlinear optical methods [5]. Hollow-core PCFs adapted to transmit high-energy laser pulses initiating laser-induced ablation on solid surfaces in laser technologies and biomedicine, can simultaneously collect radiation emitted by laser-produced plasma on metal surfaces or dental tissues and deliver it in the backward direction to spectrum analyzers and detectors [6].

Fiber optic sensors are used in a wide range of applications due to their compact size, durability, immunity to electromagnetic interference, multiplexing capabilities and robust mechanics. They have been used to measure temperature, strain, pressure, acceleration, refractive index and many other physical properties with various detection methods [6]. Fiber Braggs Gratings (FBGs) have been used to measure changes in temperature, but these fiber sensors have large sensing volumes that result in unwanted sensitivity to external stress.

Optical-fiber-based sensors represent a unique or the only viable sensing solution in specific cases (e.g., in environments with electrical hazard or potentially explosive). In addition, fiber sensors are a premium choice when multiplexing capability, high sensitivity and reduced size are required. For example, the multiplexing capability of fiber sensors makes it possible to monitor the individual behavior of several sensors set in a network with a single interrogation unit [6]. This simplifies the design of a sensor network and minimizes its cost.

Holey fibers (HF) as a subgroup PCFs constitute a new class of optical fibers which has revealed many interesting phenomena paving the way for a large number of novel applications either in the telecom or in the sensing domain. The typical HF consists of pure silica or air with a periodic distribution of air holes in the cladding. In PCF light can be

guided either by effective index mechanism related to total internal reflection or through bandgap effect caused by periodically spaced air holes. HF can potentially be made highly birefringent, because the large index contrast facilitates high form geometrical birefringence. Various methods of introducing birefringence into HFs have been presented till date. PCF with elliptical air holes or/and with asymmetric core or asymmetric distribution of holes in the fiber have been applied till date to exhibit strong birefringence. Compared with elliptical hole PCF, the later two designs are more suitable for the implementation of birefringent PCF. This is due to the fact that the shape of elliptical holes is very difficult to be controlled in the fabrication process.

Since the first publication by Knight et al in 1996 on PCF [7], the optical fiber community has been continuously engaged on R&D activity around these new fibers. Indeed, the fiber structure with lattice of air holes running along its length shows remarkable properties that support a large variety of novel optical fiber devices that can be used both in communications and sensing systems. A commonly accepted classification of PCF divides them into two main classes: index-guiding PCF and photonic bandgap PCF.

The index-guiding PCF basic structure is a solid core surrounded by a micro structured cladding. Due to the presence of air holes, the effective refractive index of the cladding is below that of the core and the light is guided along the core by the principle of total internal reflection. The application of this type of fibers for sensing has been extensively researched, as outlined by Maying et al and Eggleton et al.

The second type of PCF has a hollow core and the light guidance mechanism is the result of the presence of a photonic bandgap in the cladding region for a specific range of wavelengths. This can be understood if it is imagine a multi-layer mirror that, for certain angles and optical wavelengths, coherently adds up reflections from each layer, transforming the cladding into an almost perfect 2D mirror, keeping light confined in the lower index core of the fiber. This virtually loss free mirror is called a photonic band gap, and it is created by a periodic wavelength scale lattice of microscopic holes in the cladding glass – a photonic crystal that inherently has certain angles and wavelengths or the stop bands for which light is strongly reflected. The big attraction is that by varying the size and location of the cladding holes and/or the core diameter, the fiber transmission spectrum, mode shape, nonlinearity, dispersion and birefringence can be tuned to reach values that are not achievable with

conventional fibers. This fiber structure was first demonstrated in 1996 by knight et al, and later works of maying et al established the guidance mechanisms and the main properties of these fibers. Due to the presence of a hollow core, the potential of these fibers for liquid and gas sensing or even for photonic switching if the hollow core is filled with a liquid crystal with transmittance properties dependent of an applied external voltage [7] was clear from the beginning.

After introducing the PCFs based sensors from their history and considering their useful features for sensing applications, some of the PCFs sensor application reported so far are now been discussed

- **Evanescent wave sensing:** Modeling of the modes guided through an index-guiding PCF confirms that a significant part of the evanescent field can penetrate into the air holes of a carefully designed fiber [8]. The strength of the evanescent field and the long interaction length makes index-guiding PCFs interesting for evanescent wave sensing devices. Eggleton et al measured the absorption spectrum of acetylene by inserting one end of a 75 centimeter long PCF into a pressure chamber filled with 100% acetylene gas. The fiber was subsequently removed and the absorption spectrum was measured quickly in order to minimize out-diffusion of the gas. The fiber used in this experiment had a relatively weak penetration of the optical field into the air holes, but the long interaction length provided by the PCF efficiently compensated this.
- **Enhanced Fluorescence Biosensing:** A very elegant use of PCFs for sensor applications is the improved detection efficiency within two-photon fluorescence detection compared to conventional single mode fibers by using a double-clad fiber [8]. The light used to excite the chromospheres is guided in the core defined by a defect in the triangular lattice of the inner cladding. The outer ring of air holes defines a core with a very high numerical aperture, which effectively collects the fluorescence emitted form of exited biomolecules.
- **Bend sensing:** In the stack-and-pull method used in the production of PCFs a high-index core can be defined by replacing a tube with a solid rod at the appropriate lattice position. Fabrication of multi-core fibers is hence no more complicated than fabrication of single-core fibers. Knight et al demonstrated two-dimensional bend

sensing using a PCF with three weakly interacting single-mode guiding cores. A deformation of the fiber introduces a phase shift between the beams propagating in the different cores. The bend angle is then determined by analyzing the fringes in the resulting far field interference pattern.

- **Non-Linear Properties:** The freedom in the design of the optical properties and the strong confinement of the optical field within the core of index guiding PCFs allows for strong non linear effects. One of the most intensively studied of these is the supercontinuum generation [8]. A short intense pulse generates a wide spectrum of wavelengths, which can be used in optical coherence tomography, spectroscopy and metrology. Super continua covering several hundred nanometers as well as multi-watt output have been demonstrated [8].
- **Endlessly single mode operation:** The endlessly single mode guidance seen in certain PCFs is advantageous for spectroscopy applications, where light in a very broad range of wavelengths probes the sample. Another manifestation of the endlessly single mode guidance is the large mode areas that can be obtained, while still operating in single mode. The scalability of the PCF ensures that the number of modes is determined by the d/A ratio rather than the core size, where d is core diameter and A is spacing between cladding material. PCFs with large mode areas can hence deliver single-mode high power beams, while generating only insignificant nonlinear effects.
- **Atom guides:** It is possible to guide atoms through a PCF by generating a magnetic field from driving a current through wires placed in adjacent air holes. Single atom guidance will open up for a range of highly sensitive sensors for measuring physical quantities which influence the motion of the atom. Examples of potential applications are gravitational, rotational and magnetic field sensors.
- **PBG fiber based sensors:** The majority of the sensor applications of PCFs reported in this section is based on index-guiding fibers. A significant advantage of PBG fibers for sensor applications is the possibility of guiding light in hollow cores filled with a gas or aqueous solutions of molecules. In a carefully designed PBG the majority of the mode field is guided in the sample volume, thus providing a strong interaction between light and molecules. A PBG fiber based device for absorption measurements

can evidently provide a strong interaction over several tens of centimeters while using only a few micro liters of sample volume. The index-guiding PCF also has a significant interaction between the guided light and molecules present in the air holes, but it is only the evanescent field, which penetrates into the holes. With the improved guiding properties and quality of the commercially available PBG fibers, it is expected that the number of PBG fiber based sensors will increase in the near future.

Thus the major applications areas of PCFs based sensors are described. A characteristic feature of photonic crystal fibers, which makes these particular interesting for sensor applications is the close proximity of samples positioned in the air holes and light guided through the fiber. Sensors based on evanescent-wave sensing in index-guiding PCFs has already been realized [8] and it is expected that with the improved skills of the manufacturers, sensors based on photonic band gap fibers could emerge for the sensing applications.

1.1.2 CMOS Sensors

Complementary Metal Oxide Semiconductor (CMOS) image sensors are experiencing exponential market growth due to the increasing demands of digital still and video cameras, security cameras, webcams, and mainly mobile cameras. CMOS technology has shown competitive performance but also many advantages in on-chip functionality, power consumption, pixel readout and cost, so that it has become more and more important in the image sensor Industry. Market trend for higher pixel density leads to smaller and smaller pixel size. Thus the photodiode area shrinks. On the other hand the thickness of interconnect layers scales less than the planar dimension, light has to travel through a narrower path to reach the photodiode which cause the problem of light collection. Thus optical simulation is of great importance to characterize the sensor and optimize its performance.

For small pixels that are used nowadays in CMOS image sensors, diffraction effects can substantially affect light propagation and photon collection. Thus ray-tracing description is not accurate anymore and one must use a more fundamental description to simulate these optical effects. The diffraction effects can substantially affect light propagation when the pixel size is comparable to the wavelength of light waves. So the electromagnetic simulation tools are used to do the simulation for light propagation and photon collection inside the

pixels. Most of these simulation tools make use of Finite Difference Time Domain (FDTD) method [9] for electromagnetic wave propagation analysis in the sensors.

The FDTD approach has been a popular technique that is widely used in computational electromagnetic modeling for several decades. For pixels smaller than 2 μm the FDTD substituting the classical ray-tracing model can be applied as a more accurate and rigorous methodology to model the optical propagation and diffraction effects throughout the pixel architecture of CMOS image sensors [10]. Also with the CMOS pixel size shrinking rapidly, it is more significant for a pixel to collect adequate photons onto the photosensitive area to obtain perfect device characteristics comparable to those of previous generations with larger pixel sizes. Therefore, the microlens array is essential to concentrate the incident light to improve optical efficiency. The scaling pixel dimensions lead to significant diffraction effects in the region between the microlens and the photosensitive area. Because of that the classical optical simulation methodologies like the ray-tracing model which is based entirely on the theory of geometrical optics is not sufficient to accurately describe the light-wave propagation in smaller pixel architectures. A more fundamental and rigorous method is required to characterize the optical power transmission and distribution for smaller pixels. In that case, the FDTD approach, which is based on the numerical solution of the time-dependent Maxwell's equations [11] and widely used for the electromagnetic wave propagation analysis can be introduced to investigate the CMOS pixel imaging performance. Nowadays, the pixel dimensions of CMOS image sensors are continuously being reduced down toward 1.0 μm. The current state of the art of CMOS sensors for industrial applications has a 5-megapixel and a 1.4-μm-pixel size. Smaller pixel sizes however make it increasingly difficult to provide good characteristics.

Light-guiding inside pixels can be accomplished through two mechanisms: total internal reflection (TIR) and reflection at a metal-dielectric interface. To achieve optimal light confinement, different CMOS sensor light guide designs can be implemented. Some of these designs uses air gaps within the thick oxide layer that act as a low-index cladding to channel light to the photodiode while the other consists of a high-index-core design that confines light within the pixel region and some of the sensor light guide designs uses a metal-cladding light guiding method. Essentially the one category of designs uses TIR while the other uses reflection at a metal-dielectric interface to optimize light-guiding efficiency. Using optical

efficiency and optical crosstalk as performance metrics, the FDTD modeling technique [11] may be used to understand the differences between the various optical-confinement methods.

1.2 Modeling Photonic Devices

The photonic devices that include photonic crystal, photonic crystal fibers and PCFs sensors etc, in this context are modeled by several numerical modeling techniques. The modeling includes the device design or layout, the modal properties like the reflectance and transmittance analysis and the band gap analysis in case of photonic band gap devices. All these properties are necessary to analyse a photonic device in order to use it for a specific application e.g. modeling of photonic crystal fiber is necessary to use it in PCFs sensors. So the accurate modeling of photonic devices is essential for the development of new as well as higher performance optical components and applications.

Computational electrodynamics or electromagnetic modeling is the process of modeling the interaction of electromagnetic fields with physical objects and the environment. It typically involves using computationally efficient approximations to Maxwell's equations and is used to calculate and analyse the electromagnetic wave propagation when not in free space. Many finite difference based numerical modeling methods have been developed in the past three decades. Typical among them are the finite difference time domain method of Yee’s scheme, the transmission line matrix method, the multi resolution time domain method, and the unconditionally stable finite difference time domain methods. All these methods have become powerful tools in solving electromagnetic structure problems, yet their formulations appear to be unrelated. Among these the Finite Difference Time Domain (FDTD) Analysis is a very popular numerical modeling method for solving electromagnetic problems. An increasing number of simulators based on these techniques are being developed commercially, e.g. OptiFDTD by optiwave system that has been used in this research work.

FDTD is a popular computational electromagnetic technique. It is easy to understand and easy to implement in software. Since it is a time-domain method, solutions can cover a wide frequency range with a single simulation run. FDTD belongs in the general class of grid-based differential time-domain numerical modeling methods. Maxwell's equations (in partial differential form) are modified to central-difference equations, discretized and implemented in software. The equations are solved in a cyclic manner: the electric field is solved at a given

instant in time, then the magnetic field is solved at the next instant in time, and the process is repeated over and over again. The FDTD was first introduced as a numerical method in form of space grid and time stepping algorithm for solving Maxwell's equations by Kane Yee in 1966 [l1] and pioneering work on the application of this technique in microwave domain as well as the descriptor "Finite-difference time-domain" and its corresponding "FDTD" acronym were originated by Allen Taflove [12]. Since about 1990, FDTD techniques have emerged as primary means to computationally model many scientific and engineering problems dealing with electromagnetic wave interactions with material structures. Current FDTD modeling applications range from near-DC (ultralow-frequency geophysics involving the entire Earth-ionosphere waveguide) through microwaves (radar signature technology, antennas, wireless communications devices, digital interconnects, biomedical imaging/treatment) to visible light (photonic crystals, nano-plasmonics, solitons, and bio-photonics).

FDTD is in essence an initial value problem, where an electromagnetic field is allowed to evolve as specified by the sources, in discrete time steps along a lattice including the structure to be analyzed. The evolution of the field is determined by the complex dielectric constants at each cell. At boundaries with differing dielectric constants, reflection, refraction and diffraction can be observed. The time stepping is usually carried out to several complete cycles of a sinusoidally varying source, and maximum values of the field component magnitudes during a half-cycle after the last complete cycle are stored. In this way, a steady-state solution [12] is achieved, provided the wave is allowed to propagate through the whole model space.

In the analysis, great care must be taken in choosing the boundary conditions. Since FDTD is an initial value time domain method, the propagating wave will reflect at the lattice boundaries unless special conditions are imposed on the fields at the boundary cells to make them non-reflecting i.e. absorbing. Although the absorbing boundaries [12] extend the limits of the lattice and thus reduce space of the structure to be analyzed, FDTD presents savings in memory and execution time whereas other methods require storage and computation time on the order of $(3N)^2$ and $(3N)^3$ respectively, where N is the number of cells in the model. FDTD requires only N for both. This is a direct consequence of the time domain aspect of the method. The structure analyzed with FDTD can include features down to one cell in size.

This is an important advantage in the analysis of near-field effects. Since the lattice is usually made of cells in the order of a tenth of wavelength, features of a few tens of nanometers can be included in models in the optical region. These features can be sources, or absorbers and scatterers.

In order to use FDTD a computational domain must be established. The computational domain is simply the physical region over which the simulation will be performed. The E and H fields are determined at every point in space within that computational domain. The material of each cell within the computational domain must be specified. Typically, the material is either free-space (air), metal or dielectric. Any material can be used as long as the permeability, permittivity and conductivity are specified. Once the computational domain and the grid materials are established, a source is specified. The source can be an impinging plane wave, a current on a wire or an applied electric field, depending on the application. Since the E and H fields are determined directly, the output of the simulation is usually the E or H field at a point or a series of points within the computational domain. The simulation evolves the E and H fields forward in time. Processing may be done on the E and H fields returned by the simulation. Data processing may also occur while the simulation is ongoing. While the FDTD technique computes electromagnetic fields within a compact spatial region, scattered and/or radiated far fields can be obtained via near-to-far-field transformations. FDTD is a versatile modeling technique used to solve Maxwell's equations. It is intuitive, so users can easily understand how to use it and know what to expect from a given model. FDTD is a time-domain technique, and when a broadband pulse is used as the source, then the response of the system over a wide range of frequencies can be obtained with a single simulation. This is useful in applications where resonant frequencies are not exactly known, or anytime that a broadband result is desired. Since FDTD calculates the E and H fields everywhere in the computational domain as they evolve in time, it lends itself to providing animated displays of the electromagnetic field movement through the model. This type of display is useful in understanding what is going on in the model, and to help ensure that the model is working correctly. The FDTD technique allows the user to specify the material at all points within the computational domain. A wide variety of linear and nonlinear dielectric and magnetic materials can be naturally and easily modeled. FDTD allows the effects of apertures to be determined directly. Shielding effects can be found, and the fields both inside

and outside a structure can be found directly or indirectly. FDTD uses the E and H fields directly. Since most electromagnetic modeling applications are interested in the E and H fields, it is convenient that no conversions must be made after the simulation has run to get these values.

Since FDTD requires that the entire computational domain be gridded, and the grid spatial discretization must be sufficiently fine to resolve both the smallest electromagnetic wavelength and the smallest geometrical feature in the model, very large computational domains can be developed, which results in very long solution times. Models with long, thin features like wires are difficult to model in FDTD because of the excessively large computational domain required. There is no way to determine unique values for permittivity and permeability at a material interface. FDTD finds the E/H fields directly everywhere in the computational domain. If the field values at some distance are desired, it is likely that this distance will force the computational domain to be excessively large. Far-field extensions are available for FDTD, but require some amount of post processing. Since FDTD simulations calculate the E and H fields at all points within the computational domain, the computational domain must be finite to permit its residence in the computer memory. In many cases this is achieved by inserting artificial boundaries into the simulation space. Care must be taken to minimize errors introduced by such boundaries. There are a number of available highly effective absorbing boundary conditions (ABCs) to simulate an infinite unbounded computational domain. Most modern FDTD implementations instead use a special absorbing "material", called a perfectly matched layer (PML) to implement absorbing boundaries [12]. Because FDTD is solved by propagating the fields forward in the time domain, the electromagnetic time response of the medium must be modeled explicitly. For an arbitrary response, this involves a computationally expensive time convolution, although in most cases the time response of the medium can be adequately and simply modeled using the recursive convolution (RC) technique, the auxiliary differential equation (ADE) technique or the Z-transform technique. An alternative way of solving Maxwell's equations that can treat arbitrary dispersion easily is the Pseudo Spectral Spatial-Domain method (PSSD), which instead propagates the fields forward in space.

Interest in FDTD Maxwell’s equations solvers has increased nearly exponentially over the past 20 years. Increasingly, engineers and scientists in nontraditional electromagnetics related

areas such as photonics and nanotechnology have become aware of the power of FDTD techniques. Notwithstanding the overall expansion of interest in all Computational electromagnetic techniques, there are some primary reasons for the tremendous expansion of interest in FDTD computational solution approaches for Maxwell's equations. Some of these are as follows:

- FDTD uses no linear algebra. Being a fully explicit computation, FDTD avoids the difficulties with linear algebra that limit the size of frequency domain integral-equation and finite element electromagnetics models.
- FDTD is accurate and robust. The sources of error in FDTD calculations are well understood, and can be bounded to permit accurate models for a very large variety of electromagnetic wave interaction problems.
- FDTD treats impulsive behavior naturally. Being a time-domain technique, FDTD directly calculates the impulse response of an electromagnetic system.
- FDTD is a systematic approach. With FDTD, specifying a new structure to be modeled is reduced to a problem of mesh generation rather than the potentially complex reformulation of an integral equation.
- Parallel-processing computer architectures have come to dominate supercomputing. FDTD scales with high efficiency on parallel-processing CPU-based computers, and extremely well on recently developed CPU-based accelerator technology.

These factors combine to indicate that FDTD will likely remain one of the dominant computational electrodynamics techniques for numerical modeling of photonic and related devices.

FDTD method has been used extensively in the analysis of electrically large structures in the microwave domain, but has only recently been applied to optical problems. Because of memory limitations of computers used, the method is generally restricted to configurations which extend to the order of tens of wavelengths in three dimensions, or hundreds of wavelengths in two dimensions. Optical sensor structures however are of suitable size to be modeled with FDTD and the advantages of the technique become pronounced especially in the design of photonic sensors which employ evanescence or near-field effects. Among these is the possibility to incorporate the distribution of the analyte on the sensing surface as well as the optical characteristics of the sensor in the optical model. Although the computer

resources required for arbitrary structures in three dimensions can limit the scope of analyses, it is relatively simple to use symmetry properties of the structures to relax these requirements. In addition, for planar structures, two-dimensional models are adequate for studying many aspects of sensor design. Recently, FDTD has been applied in the optical range of frequencies, as suitable problems to be analyzed with the method have emerged. Planar optical sensors are particularly good candidates for modeling with FDTD. Their structure is simple enough for the model to be used effectively, and due to the planarity only a two dimensional analysis is required for many cases. With a modern day supercomputer, structures of hundreds of wavelengths long can be analyzed in two dimensions.

1.3 Motivation

A novel class of material known as photonic crystal has opened up new ways to guide flow of light. In such structures propagation may be forbidden in any direction for certain range of frequencies called photonic band gaps (PBGs). Based on PBGs, the microstructured photonic crystal cladding running on entire length of fiber, cannot allow light propagation in cladding and hence light is trapped in central hollow core. The hollow core photonic crystal fiber with triangular array of large air holes in the cladding was first demonstrated in 1999.

Another more common type of PCFs is solid core PCF due to their relative ease of fabrication. For the solid core PCFs the guidance is attributed to modified total internal reflection, analogous to the total internal reflection in conventional optical fibers. The effective index of cladding is lower than that of core, leading to that of conventional step-index fiber. However the refractive index of microstructured cladding exhibits strong wavelength dependence allowing the PCF to possess unique properties unachievable in conventional fibers. The most striking among these properties is the single mode operation over infinite range of wavelength.

The pioneering work on these PCFs showed that they have inherently unprecedented properties and overcome many limitations of conventional optical fibers. With the versatile PCF, people can engineer the fiber properties from guiding light in vacuum to unthinkable dispersion properties, from enhanced nonlinearities by more confinement of light to minimizing the same non linear effects by using very large mode area fibers. The discovery of these attractive properties makes PCFs ideal for high power transmission without

nonlinearities, all optical signal processing, high power lasers and amplifiers, dispersion compensation, polarizing and polarization maintaining devices and novel photonic sensors.
Among the broad range of unique properties of PCF, the thesis is mainly concerned with the polarizing and modal properties that mainly include transmittance, reflectance and wave propagation analysis of photonic crystal as well as photonic crystal fibers and also the band gap analysis of the both. Since all the light properties are being analyzed for photonic crystal and photonic crystal fiber, it makes an entry into the vast field of photonic micro sensors.

1.4 Thesis Organization

Chapter 2 starts with a literature review of photonic crystal fibers, starting from basics to the advancement towards the photonic crystal fibers. After that major guiding mechanisms of the photonic crystal fiber are described. The unique properties of the PCFs that make it prime choice for the photonic applications are also included in the chapter. At last various loss mechanisms are also described in this chapter.

Chapter 3 is mainly concerned with the numerical modeling techniques of photonic crystal designs. The chapter starts with the basics of FDTD method and then the FDTD equations are described for two and three dimensional space. Various absorbing boundary conditions are also described following the FDTD equations. After that FDTD algorithm has been explained for the Telegrapher's partial difference equations. Chapter also includes the plane wave expansion method for the band gap analysis of photonic crystal structures. The PWE equations are solved to describe the dispersion relationship between the frequencies of the modes and wave vector k that usually plotted in form of band diagram.

Chapter 4 concentrates on the modeling and simulation of the photonic crystal as well as the photonic crystal fiber. After simulating the designs FDTD analysis is done firstly to describe the transmittance and reflectance properties of the designed photonic structures. The band diagrams of the designs are plotted and band gaps are located and analysed by PWE band solver and in the end the band gaps of designs are summarized that gives the frequency range of the input for which wave get strongly reflected in the designed photonic structures.
Finally, a conclusion of the thesis is given in **chapter 5.**

CHAPTER

2

PHOTONIC CRYSTAL FIBERS

2.1 Introduction

Until recently, an optical fiber was a solid thread surrounded by another material with a lower refractive index. Today the photonic crystal fibers (PCFs) are established as an alternative fiber technology. PCFs, which have been first demonstrated in 1995-96, are optical fibers with a periodic arrangement of low-index material in a background with higher refractive index. The background material in PCFs is usually undoped silica and the low-index region is typically provided by air-holes running along their entire length. Two main categories of PCFs exist: high-index guiding fibers and photonic bandgap ones. PCFs belonging to the first category are more similar to conventional optical fibers, because light is confined in a solid core by exploiting the modified total internal reflection mechanism. In fact, there is a positive refractive index difference between the core region and the photonic crystal cladding, where the air-hole presence causes a lower average refractive index. The guiding mechanism is defined as "modified" because the cladding refractive index is not a constant value as in standard optical fibers but it changes significantly with the wavelength. This characteristic as well as the high refractive index contrast between silica and air provides a range of new interesting features. Moreover, high design flexibility is one of the distinctive properties of PCFs. In particular, by changing the geometric characteristics of the air-holes in the fiber cross-section, like their dimension or position, it is possible to obtain PCFs with diametrically opposite properties. For example, PCFs with a small silica core and large air-holes, that is, with a high air-filling fraction in the transverse section have better nonlinear properties compared with conventional optical fibers and so they can be successfully used in many applications, like supercontinuum generation.

On the contrary fibers can be designed with small air-holes and large hole-to-hole distances in order to obtain a large modal area, useful for high power delivery. Differently from standard fibers PCFs with proper geometric characteristics can be endlessly single mode,

means only the fundamental mode is guided regardless of the wavelength. In addition a significant asymmetry can be introduced in a simple way in the PCF core, thus creating fibers with very high level of birefringence. Moreover the PCF dispersion properties can be tailored with high flexibility so that it is possible to move the zero-dispersion wavelength to the visible range as well as to obtain dispersion curves ultra flattened or with a strong negative slope.

When the PCF core region has a lower refractive index than the surrounding photonic crystal cladding, light is guided by a mechanism different from total internal reflection - by exploiting the presence of the photonic bandgap (PBG). In fact, the air-hole microstructure which constitutes the PCF cladding is a two dimensional photonic crystal that is a material with periodic dielectric properties characterized by a photonic bandgap, where light in certain wavelength ranges cannot propagate. The PBG effect can be also found in nature since it is responsible, for example, of the beautiful and bright colors seen in butterfly wings. PCFs with a low index core are created by introducing a defect in the photonic crystal structure, for example, an extra air-hole or an enlarged one and light is confined because the PBG makes propagation in the micro structured cladding region impossible. This guiding mechanism cannot be obtained in conventional optical fibers and it opens a whole new set of interesting possibilities. In particular light can be guided in air in PCFs with a hollow core thus providing numerous promising applications such as low-loss guidance and high-power delivery without the risk of fiber damage. Moreover air-guiding PCFs are almost insensitive to bending even for small bending diameter values and they present extreme dispersion properties, highly dominated by the waveguide component. Finally, when filled with proper gases or liquids, hollow core PCFs can be successfully employed in sensor applications or for nonlinear optics.

Since their first demonstration, PCFs have been the object of an intense research activity by the most important groups all around the world. In fact, it is particularly intriguing to study the new light-guiding mechanisms offered by PCFs and the innovative properties related to the presence of the PBG. Moreover, the possibility of modifying the air-hole geometry in the fiber cross-section is limited only by the technological feasibility of the designed PCFs. It is also very interesting to investigate how the PCF properties can be influenced by the changes

of the geometric characteristics and how far it is possible to go from the well-known and established properties of standard optical fibers.

In this chapter, starting from the description of the characteristics of photonic crystals, materials with a refractive index periodic distribution, the passage from conventional optical fibers to photonic crystal ones, introduced for the first time in 1995, is explained. Then the two light-guiding mechanisms are presented. In solid-core photonic crystal fibers, where light is confined in a higher refractive index region, modified total internal reflection is exploited, which is quite similar to the guiding mechanism of standard optical fibers. Instead, when the light is confined in a region with a refractive index lower than that of the surrounding area as in hollow-core fibers, the presence of the photonic bandgap (PBG) is necessary.

2.2 Basics of Photonic Crystal Fibers

One of the most important advantages offered by photonic crystal fibers (PCFs) is the high design flexibility. In fact, by changing the geometric characteristics of the fiber cross-section such as the air-hole dimension or disposition, it is possible to obtain fibers with diametrically opposed optical properties. PCFs with unusual guiding, dispersion and nonlinear properties can be designed and successfully used in various applications as reported in this section.

The main drawback which affects this new kind of fibers is related to the attenuation, which is higher than that of conventional optical fibers. The different loss mechanisms are thus analyzed for both solid and hollow core photonic crystal fibers. In general, a loss reduction for PCFs can be obtained by improving the fabrication process, reported in the last part of the chapter. The stack-and draw process is described with other fabrication techniques [13]. Once reached the technological maturity, the advantages offered by PCFs with respect to conventional fibers could be completely exploited for different applications [13] and the new fibers will enter concretely in the market.

2.3 From Conventional Optical Fibers to PCFs

Optical fibers which transmit information in the form of short optical pulses over long distances at exceptionally high speeds are one of the major technological successes of the 20th century. This technology has developed at an incredible rate, from the first low-loss single-mode waveguides in 1970 to being key components of the sophisticated global

telecommunication network. Optical fibers have also non-telecom applications like the in beam delivery for medicine, machining and diagnostics, sensing and a lot of other fields. Modern optical fibers represent a careful trade-off between optical losses, optical nonlinearity, group velocity, dispersion and polarization effects. After 30 years of intensive research, incremental steps have refined the capabilities of the system and the fabrication technology nearly as far as they can go. The interest of researchers and engineers in several laboratories since the 1980s has been attracted by the ability to structure materials on the scale of the optical wavelength, a fraction of micrometers or less, in order to develop new optical medium known as photonic crystals. Photonic crystals rely on a regular morphological microstructure, incorporated into the material, which radically alters its optical properties. They represent the extension of the results obtained for semiconductors into optics. In fact the band structure of semiconductors is the outcome of the interactions between electrons and the periodic variations in potential created by the crystal lattice. By solving the Schrodinger's wave equation for a periodic potential electron energy states separated by forbidden bands are obtained. PBGs can be obtained in photonic crystals where periodic variations in dielectric constant, that is in refractive index, substitute variations in electric potential as well as the classical wave equation for the magnetic field replaces the Schrodinger's equation [13]. PBG originally predicted in 1987 by Sajeev John from University of Toronto and Eli Yablonovitch from Bell Communications Research has become the really hot topic in optics in the early 1990s. The idea was to build the right structures, in order to selectively block the transmission of photons with energy levels that is wavelengths corresponding to the PBGs while allowing other wavelengths to pass freely. Moreover slight variations in the refractive index periodicity would introduce new energy levels within the PBG as it happens with the creation of energy levels within the bandgap of conventional semiconductors. Unfortunately, building the right structures has proved extremely difficult. The first PBG material was created in 1991 by Yablonovitch and his colleagues by drilling holes with a diameter of 1mm in a block of material with a refractive index of 3.6. Since the bandgap wavelength is of the order of the spacing between the air-holes in the photonic crystal, this structure had a bandgap in the microwave region. In 1991, Philip Russell [13] who was interested in Yablonovitch's research got his big "crazy" idea for "something different". Russell's idea was that light could be trapped inside a fiber hollow

core by creating a two-dimensional photonic crystal in the cladding that is a periodic wavelength scale lattice of microscopic air-holes in the glass. The basic principle is the same which is the origin of the color in butterfly wings and peacock feathers, that is all wavelength scale periodic structures exhibit ranges of angle and color, stop bands where incident light is strongly reflected. When properly designed the photonic crystal cladding running along the entire fiber length can prevent the escape of light from the hollow core. These new fibers are called PCFs since they rely on the unusual properties of photonic crystals. The first fiber with a photonic crystal structure was reported by Russell and his colleagues in 1996. Even if it was a very interesting research development, the first PCF did not have a hollow core as shown in Fig. 2(a) and consequently it did not rely on a photonic bandgap for optical confinement. In fact, in 1996 Russell's group could produce fiber with the necessary air-hole triangular lattice but the air-holes were too small to achieve a large air-filling fraction which is fundamental to realize a PBG. Measurements have shown that this solid-core fiber formed a single-mode waveguide that is only the fundamental mode was transmitted over a wide wavelength range. Moreover the first PCF had very low intrinsic losses due to the absence of doping elements in the core and a silica core with an area about ten times larger than that of a conventional single mode fiber (SMF), thus permitting a corresponding increase in optical power levels.

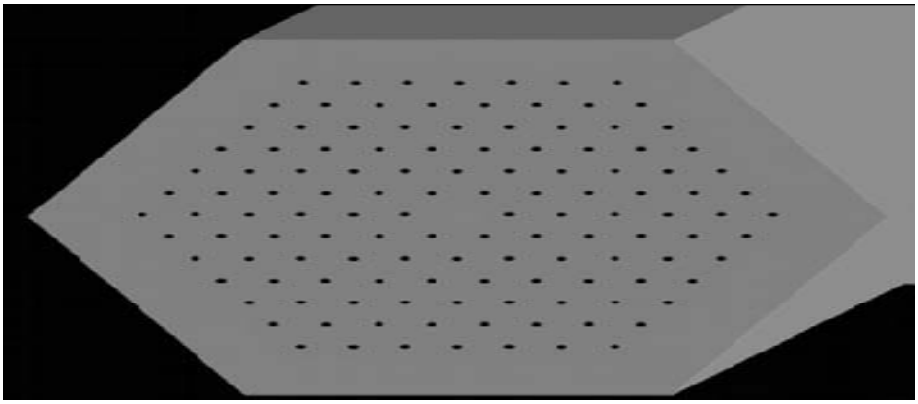

Figure 2(a): Schematic of the cross-section of the first solid-core photonic crystal fiber with air hole diameter of 300 nm and hole-to-hole spacing of 2.3 μm [13].

After moving his research group to the University of Bath where PCF fabrication techniques were steadily refined, Russell and his co-workers were able to report the first single mode

hollow-core fiber in which confinement was due by a full two dimensional PBG as reported in Fig. 2(b).

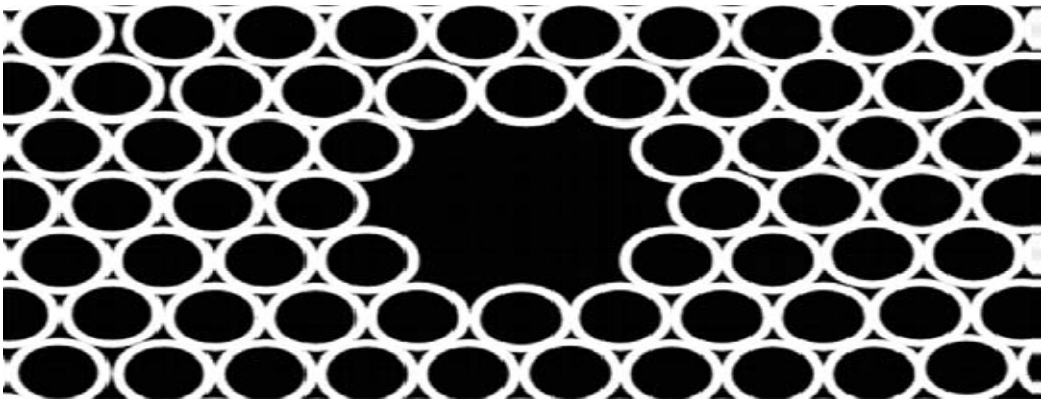

Figure 2(b): Schematic of the cross-section of the first hollow-core PCF, with hole-to-hole spacing of 4.9 μm and core diameter of 14.8 μm [13].

They realized that the photonic bandgap guiding mechanism is very robust since light remains well confined in the hollow core even if tight bends are formed in the fiber. Initial production techniques were directed simply at the task of making relatively short lengths of fiber in order to do the basic science but many research teams are now working hard to optimize their PCF production techniques in order to increase the lengths and to reduce the losses.

2.4 Guiding mechanism

In order to form a guided mode in an optical fiber, it is necessary to introduce light into the core with a value of β, which is the component of the propagation constant along the fiber axis, which cannot propagate in the cladding. The highest β value that can exist in an infinite homogeneous medium with refractive index n is $\beta = nk_0$, being k_0 the free-space propagation constant. All the smaller values of β are allowed. A two-dimensional photonic crystal like any other material is characterized by a maximum value of β which can propagate. At a particular wavelength, this corresponds to the fundamental mode of an infinite slab of the material and this β value defines the effective refractive index of the material.

2.4.1 Modified Total Internal Reflection

It is possible to use a two dimensional photonic crystal as a fiber cladding by choosing a core material with a higher refractive index than the cladding effective index. An example of this

kind of structures is the PCF with a silica solid core surrounded by a photonic crystal cladding with a triangular lattice of air-holes, shown in Fig. 2(c). These fibers also known as index-guiding PCFs guide light through a form of total internal reflection (TIR) called modified TIR. However they have many different properties with respect to conventional optical fibers.

Endlessly single-mode property

As already stated, the first solid-core PCF shown in Fig. 2(a), which consisted of a triangular lattice of air-holes did not ever seem to become multi-mode in the experiments even for short wavelengths. In fact, the guided mode always had a single central lobe filling the core [14].

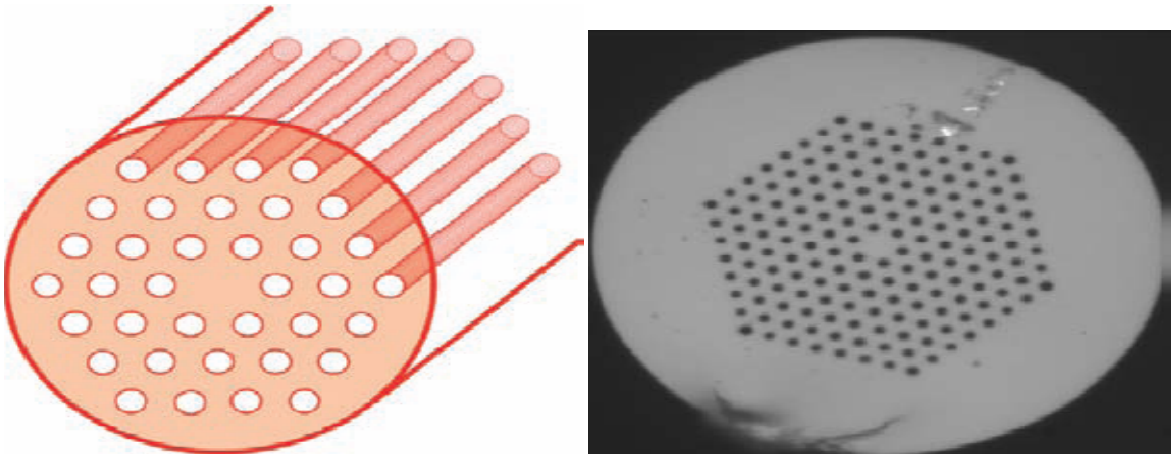

(i) (ii)

Figure 2(c): (i) Schematic of a solid-core PCF with a triangular lattice of air-holes, which guides light for modified total internal reflection. (ii) Microscope picture of a fabricated solid-core triangular PCF [14]

Russell has explained that this particular endlessly single-mode behavior can be understood by viewing the air-hole lattice as a modal filter or sieve [14]. A proper geometry design of the fiber cross-section thus guarantees that only the fundamental mode is guided. By exploiting this property, it is possible to design very large-mode area fibers which can be successfully employed for high power delivery, amplifiers and lasers. Moreover by doping the core in order to slightly reduce its refractive index light guiding can be turned off completely at wavelengths shorter than a certain threshold value.

2.4.2 Photonic Bandgap Guidance

Optical fiber designs completely different form the traditional ones result from the fact that the photonic crystal cladding have gaps in the ranges of the supported modal index β/k_0 where there are no propagating modes. These are the PBGs of the crystal which are similar to the two dimensional band gaps which characterize planar light wave circuits, but in this case they have propagation with a non-zero value of β. It is important to underline that gaps can appear for values of modal index both greater and smaller than unity, enabling the formation of hollow-core fibers with bandgap material as a cladding, as reported in Fig. 2(d).

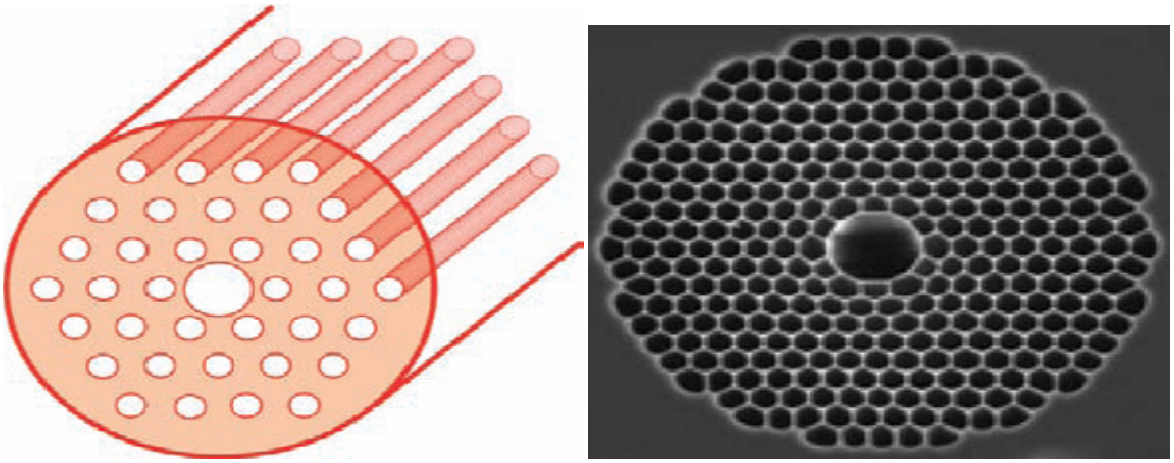

(i) (ii)

Figure 2(d): (i) Schematic of a hollow-core PCF with a triangular lattice of air-holes, which guides light through the photonic bandgap effect. (ii) Microscope picture of a fabricated hollow-core triangular PCF [14].

These fibers which cannot be made using conventional optics are related to Bragg fibers, since they do not rely on TIR to guide light. In fact, in order to guide light by TIR it is necessary a lower-index cladding material surrounding the core but there are no suitable low-loss materials with a refractive index lower than air at optical frequencies.

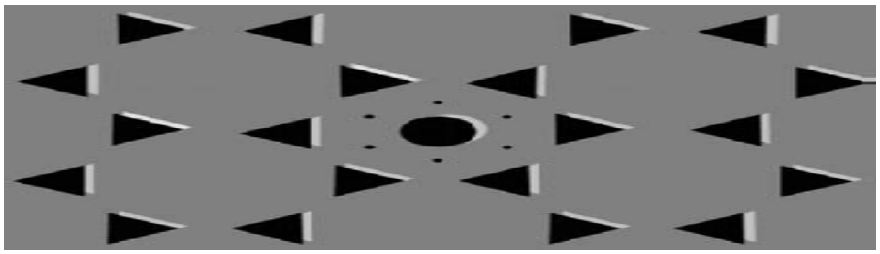

Figure 2(e): Schematic of the cross-section of the first photonic bandgap PCF with a honeycomb air-hole lattice [15].

The first PCF which exploited the PBG effect to guide light was reported in 1998 [15] and it is shown in Fig. 2(e). Notice that its core is formed by an additional air hole in a honeycomb lattice. This PCF could only guide light in silica, the higher-index material.

Hollow core guidance had to wait until 1999 when the PCF fabrication technology had advanced to the point where larger air-filling fractions required to achieve PBG for air-guiding became possible. Notice that an air guided mode must have $\beta/k_0 < 1$, since this condition guarantees that light is free to propagate and form a mode within the hollow core, while being unable to escape into the cladding. The first hollow core PCF reported in Fig. 2(b) had a simple triangular lattice of air holes and the core was formed by removing seven capillaries in the center of the fiber cross-section. By producing a relatively large core, the chances of finding a guided mode were improved. When white light is launched into the fiber core colored modes are transmitted, thus indicating that light guiding exists only in restricted wavelength ranges which coincide with the photonic band gaps [15].

2.5 Properties and Applications

Due to the huge variety of air-holes arrangements, PCFs offer a wide possibility to control the refractive index contrast between the core and the photonic crystal cladding and as a consequence, novel and unique optical properties. Since PCFs provide new or improved features beyond what conventional optical fibers offer, they are finding an increasing number of applications in ever-widening areas of science and technology.

2.5.1 Solid Core Fibers

Index-guiding PCFs with a solid glass region within a lattice of air holes offer a lot of new opportunities, also including nearly all applications related to fundamental fiber optics. These opportunities are related to some special properties of the photonic crystal cladding which are due to the large refractive index contrast and the two dimensional nature of the microstructure thus affecting the birefringence, the dispersion, the smallest attainable core size, the number of guided modes and the numerical aperture.

Highly birefringent fibers

Birefringent fibers where the two orthogonally polarized modes carried in a single-mode fiber propagate at different rates are used to maintain polarization states in optical devices and subsystems. The guided modes become birefringent if the core microstructure is

deliberately made twofold symmetric, for example, by introducing capillaries with different wall thicknesses above and below the core. By slightly changing the air-hole geometry it is possible to produce levels of birefringence that exceed the performance of conventional birefringent fiber by an order of magnitude. It is important to underline that unlike traditional polarization maintaining fibers such as bow tie, elliptical-core or Panda, which contain at least two different glasses, each one with a different thermal expansion coefficient, the birefringence obtainable with PCFs is highly insensitive to temperature, which is an important feature in many applications. An example of the cross-section of a highly birefringent PCF is reported in Fig. 2(f).

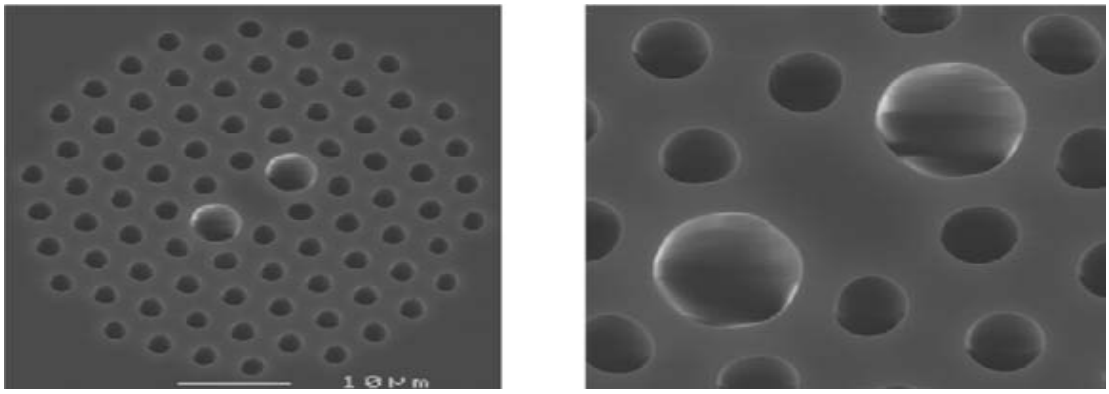

(i) (ii)

Figure 2(f): Microscope picture of (i) the cross-section and (ii) the core region of a highly birefringent triangular PCF [16].

Dispersion tailoring

The tendency for different light wavelengths to travel at different speeds is a crucial factor in the telecommunication system design. A sequence of short light pulses carries the digitized information. Each of these is formed from a spread of wavelengths and as a result of chromatic dispersion it broadens as it travels, thus obscuring the signal. The magnitude of the dispersion changes with the wavelength, passing through zero at 1.3 μm in conventional optical fibers. In PCFs the dispersion can be controlled and tailored with unprecedented freedom. In fact, due to the high refractive index difference between silica and air, and to the flexibility of changing air hole sizes and patterns, a much broader range of dispersion behaviors can be obtained with PCFs than with standard fibers.

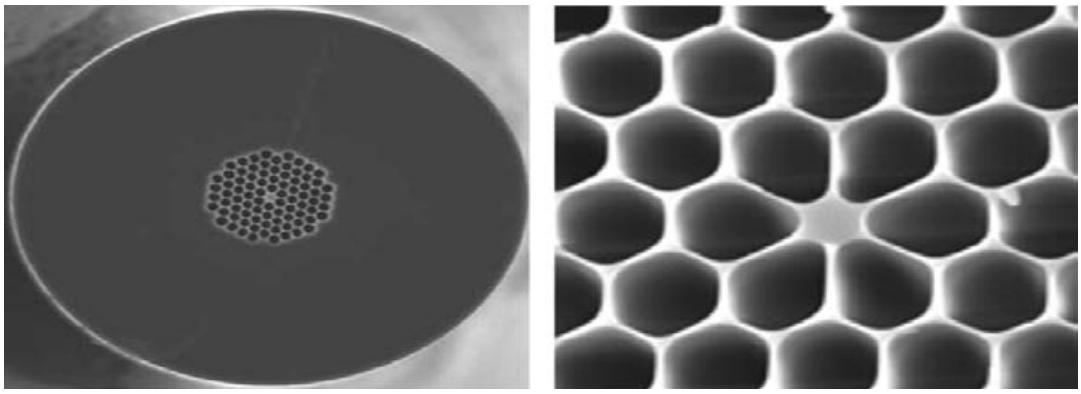

(i) (ii)

Figure 2(g): Microscope picture of (i) the cross-section and (ii) the core region of a highly nonlinear PCF, characterized by a small-silica core and large air-holes, with zero-dispersion wavelength shifted to the visible [16].

For example as the air holes get larger the PCF core becomes more and more isolated until it resembles an isolated strand of silica glass suspended by six thin webs of glass, as it is shown in Fig. 2(g). If the whole structure is made very small the zero-dispersion wavelength can be shifted to the visible since the group velocity dispersion is radically affected by pure waveguide dispersion.

Ultrahigh nonlinearities

An attractive property of solid core PCFs is that effective index contrasts much higher than in conventional optical fibers can be obtained by making large air-holes or by reducing the core dimension so that the light is forced into the silica core. In this way a strong confinement of the guided-mode can be reached, thus leading to enhanced nonlinear effects due to the high field intensity in the core. Moreover a lot of nonlinear experiments require specific dispersion properties of the fibers. As a consequence PCFs can be successfully exploited to realize nonlinear fiber devices with a proper dispersion and this is presently one of their most important applications. An important example is the so called supercontinuum generation [16], which is the formation of broad continuous spectra by the propagation of high power pulses through nonlinear media. The term supercontinuum does not indicate a specific phenomenon but rather a plethora of nonlinear effects which in combination lead to extreme spectral broadening. The determining factors for supercontinuum generation are the dispersion of the nonlinear medium relative to the pumping wavelength, the pulse length and the peak power. Since the nonlinear effects involved in the spectral broadening are highly

dependent on the medium dispersion, a proper design of the dispersion properties can significantly reduce the power requirements. The widest spectra in these can be obtained when the pump pulses are launched close to the zero dispersion wavelengths of the nonlinear media [16].

Large-mode area fibers

By changing the geometric characteristics of the fiber cross-section, it is possible to design PCFs with completely different properties like that with large effective area. The typical cross-section of this kind of fibers called large mode area (LMA) PCFs that consists of a triangular lattice of air holes where the core is defined by a missing air-hole. An example of a triangular PCF is reported in Fig. 2(c). The PCF core diameter can be defined as $d_{core} = 2\Lambda - d$, which corresponds to the distance between opposite air-hole edges in the core region. When $d/\Lambda < 0.4$, the triangular PCF is endlessly single mode. In this condition it is the core size or the pitch that determines the zero-dispersion wavelength λ_0, the mode field diameter (MFD) and the numerical aperture (NA) of the fiber. LMA PCFs are usually exploited for high-power applications, since fiber damage and nonlinear limitations are drastically reduced. In particular, LMA fibers are currently used for applications at short wavelengths, that is in ultraviolet (UV) and visible bands, like the generation and delivery of high-power optical beams for laser welding and machining, optical lasers, and amplifiers, providing significant advantages with respect to traditional optical fibers [16].

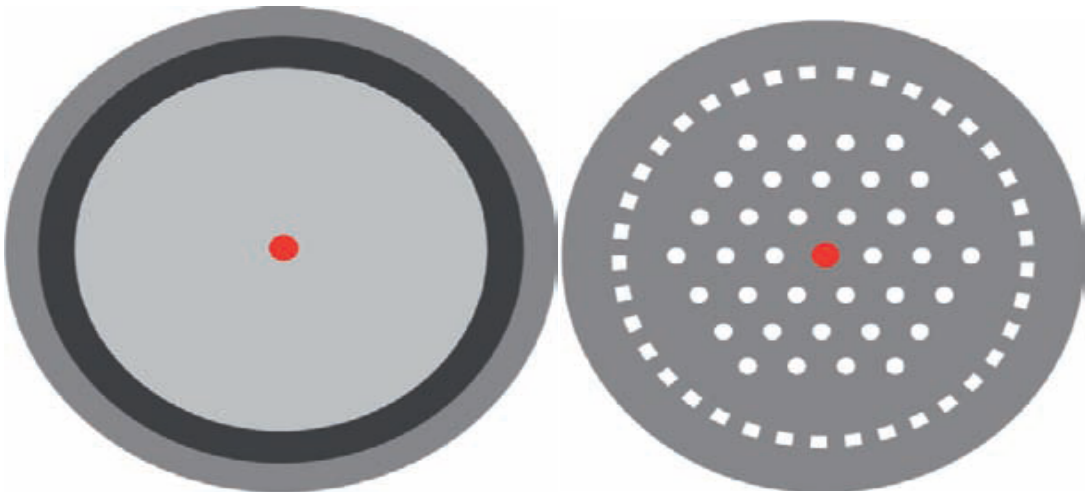

(i) (ii)

Figure 2(h): Schematic of the cross-sections of (i) standard step-index double clad fiber (ii) an air-clad PCF, where the single-mode active core is embedded in a silica-air LMA structure [16].

Conventional active fibers for lasers and amplifiers are basically standard transmission fibers whose core region has been doped with rare earth elements. These fibers also known as core-pumped are usually pumped with single mode pump lasers. Due to its power limitations, this kind of fiber is unsuitable for high-power applications. High-power fibers are usually designed with a double-cladding structure, where a second low-index region acts as a cladding for a large pump core. In the center of the pump core is located a much smaller doped signal core, as reported in Fig. 2(h{i}).

With respect to the more traditional core-pumped design, double-cladding fibers present a large pump area and high numerical aperture thus enabling pumping with relatively low-cost multimode diodes and diode bars/stacks. However it is important to underline that when considering high powers it is necessary to optimize fiber characteristics such as NA, core dimension and length, in order to obtain efficient coupling of the pump light, reduction of nonlinear effects, high conversion of pump light and good thermal properties.

Since PCF structures can provide single-mode waveguides with MFD values above 40 µm, LMA PCFs can be successfully used as active fibers for high-power applications. The PCF double-clad equivalent is shown in Fig. 2(h{ii}). It consists of a LMA structure with a doped-core inside an air clad pump guide. Very high NA values determined by the silica bridge width shown in the three fiber cross-sections reported in Fig. 2(i), are provided by the air-clad since the refractive index contrast is greatly enhanced. As a consequence, the NA is only limited by the practical handling of the fibers, being the cleaving increasingly challenging at NA values above 0.6.

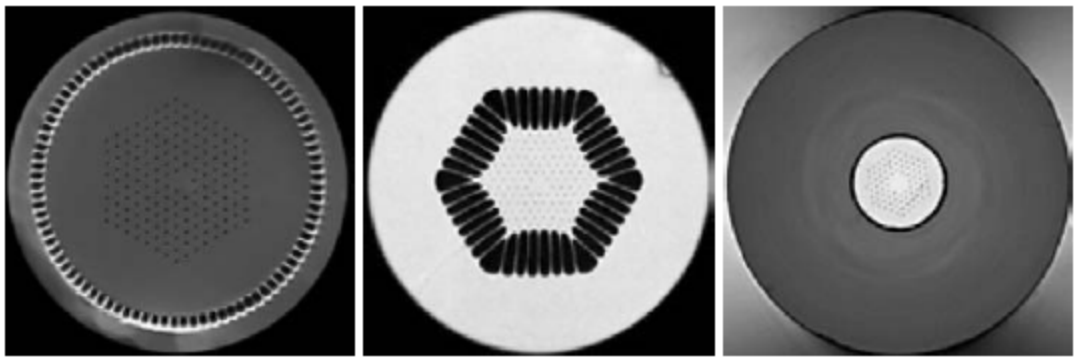

Figure 2(i): Microscope pictures of the cross-section of three different air-clad PCFs [16]

Moreover the thermal conductivity is greatly improved compared to conventional polymer clad fibers because the PCF is made only of glass and air, and there is no material degradation. The power density limit is set only by the silica damage threshold. Finally, the combination of very large MFD and high NA offered by PCFs makes it possible to fabricate lasers and amplifiers with very short fiber lengths, drastically reducing the nonlinear effects [17].

2.5.2 Hollow-core fibers

Hollow-core PCFs have great potential since they exhibit low nonlinearity and high damage threshold [17], thanks to the air-guiding in the hollow core and the resulting small overlap between silica and the propagating mode. As a consequence they are good candidates for future telecommunication transmission systems. Another application perhaps closer to fruition which can successfully exploit these advantages offered by air-guiding PCFs, is the delivery of high-power continuous wave (CW), nanosecond and sub-picoseconds laser beams which are useful for marking and laser surgery. In fact optical fibers would be the most suitable delivery means for many applications but at present they are unusable due to the fiber damage and the negative nonlinear effects caused by the high optical powers and energies as well as to the fiber group-velocity dispersion, which disperses the short pulses[17]. These limitations can be substantially relieved by considering the hollow-core fibers[17].

Moreover air-guiding PCFs are suitable for nonlinear optical processes in gases which require high intensities at low power long interaction lengths and good-quality transverse beam profiles. For example, it has been demonstrated that the threshold for stimulated Raman scattering in hollow-core fibers filled with hydrogen is orders of magnitude below that obtained in previous experiments [17]. In a similar way, PCFs with a hollow core can be used for trace gas detection or monitoring, or as gain cells for gas lasers.

2.6 Loss mechanisms

The most important factor for any optical fiber technology is loss. Losses in conventional optical fibers have been reduced over the last 30 years and a further improvement is unlikely to be reached. The minimum loss in fused silica which is around 1550nm, is slightly less than 0.2 dB/km. This limit is important since it sets the amplifier spacing in long-haul

communications systems, and thus is a major cost of a long-haul transmission system. Loss mechanisms in PCFs are here described in details, in order to understand how far the technology can go to reduce their values.

2.6.1 Intrinsic loss

Solid-core fibers

The optical loss α_{dB}, measured in dB/km, of PCFs with a sufficiently reduced confinement loss, which will be described in Section 1.4.2, can be expressed as

$$\alpha_{dB} = A/\lambda 4 + B + \alpha_{OH} + \alpha_{IR} \qquad (2a)$$

being A, B, α_{OH}, and α_{IR} the Rayleigh scattering coefficient, the imperfection loss, and OH and infrared absorption losses respectively. At the present time the losses in PCFs are dominated by OH-absorption loss and imperfection loss [18].

In a typical PCF the OH-absorption loss is more than 10dB/km at 1380 nm and this causes an additional optical loss of 0.1dB/km in the wavelength range around 1550 nm. Since this contribution is very similar to the intrinsic optical loss of 0.14dB/km for pure silica glass at this wavelength, the OH-absorption loss reduction becomes a challenging problem. Most of the OH impurities seem to penetrate the PCF core region during the fabrication process. As a consequence, a dehydration process is useful in reducing the OH-absorption loss [18].

Imperfection loss, caused mainly by air-hole surface roughness is another serious problem. In fact, during the fabrication process the air-hole surfaces can be affected by small scratches and contamination. If this surface roughness is comparable with the considered wavelength, it can significantly increase the scattering loss. Thus it is necessary to improve the polishing and etching process in order to reduce the optical loss caused by this roughness. Moreover fluctuation in the fiber diameter during the fiber drawing process can cause an additional imperfection loss if the air-hole size and pitch change along the fiber [18].

It is important to underline that the Rayleigh scattering coefficient of PCFs is the same as that of a conventional SMF. However this is higher than that of a pure silica-core fiber, although the PCF is made of pure silica glass. It is necessary to reduce the roughness further, in order to obtain a lower imperfection loss and a lower Rayleigh scattering coefficient.

It is fundamental to fabricate long PCFs with low loss, if they are to be used as transmission media.

In Fig. 2(j), the decrease of the loss for fabricated index-guiding PCFs is shown until 2006. Early in their development, solid-core PCFs had optical losses of the order of 0.24dB/m [19] and the available length was limited to several meters.

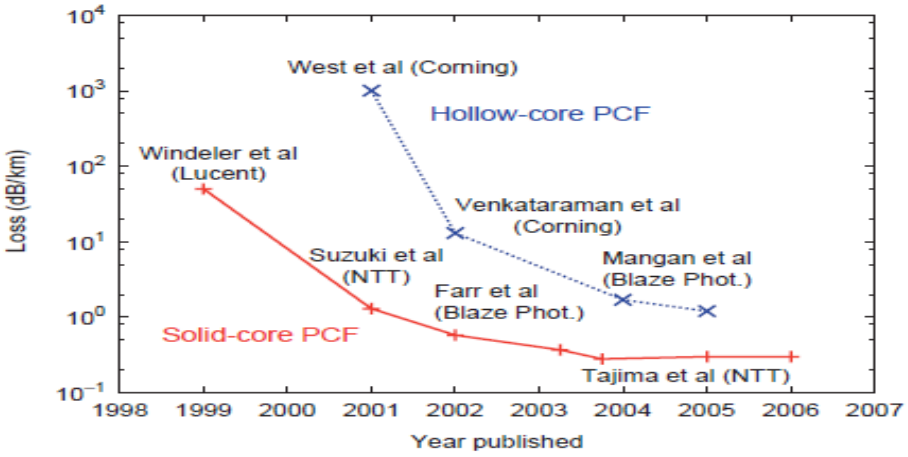

Figure 2(j): Optical loss behavior during the last years, until 2006, for solid core (+ symbols) and hollow-core (× symbols) PCFs [18].

The optical losses of PCFs were rapidly reduced to 1 dB/km by improving the fabrication process [19]. The lowest loss yet achieved is 0.28dB/km [19]. Recently a low loss that is 0.3dB/km, and long length, that is 100 km, PCF was reported [19]. The optical losses of these kinds of PCFs are still high compared with those of a conventional SMF. However, a solid-core PCF is not expected to have significantly lower losses than standard fibers.

Hollow-core fibers

Losses in hollow-core fibers are limited by the same mechanisms as in conventional fibers and in index-guiding PCFs, that is absorption, Rayleigh scattering, confinement loss, bend loss, and variations in the fiber structure along the length. However, there is the possibility to reduce them below the levels found in conventional optical fibers since the majority of the light travels in the hollow core, in which scattering and absorption could be very low.

As shown in Fig. 2(j), the attenuation values reported in literature for hollow-core PCFs are higher than those for both solid-core PCFs and standard fibers. Looking at the attenuation profiles for a range of hollow-core fibers made by Crystal Fibre, it is possible to notice two important facts. The guiding bandwidth is usually around 15% of the central wavelength and the loss scales inversely with the wavelength. As indicated by theoretical considerations, the attenuation related to mode coupling and scattering at the internal air silica interfaces scale

with the wavelength. This consideration has been confirmed by experimental observations [19] and applies to the seven-cell design, whose hollow core has been obtained by removing seven capillaries in the center of the fiber cross-section. It is important to underline that in order to reach lower losses 19-cell designs can be used, as it is demonstrated by the loss values reported in Fig. 2(k).

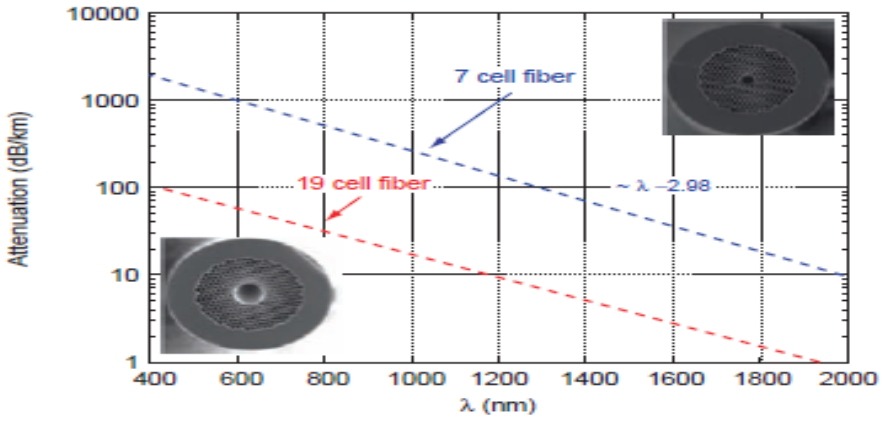

Figure 2(k): Attenuation behavior versus the wavelength for 7-cell and 19- cell hollow-core PCFs, whose cross-sections are shown as inset [19].

The minimum loss of 1.7 dB/km has been obtained with the hollow-core PCF [19] shown in Fig. 2(l), since the larger core reduces the overlap of the guided modes with silica.

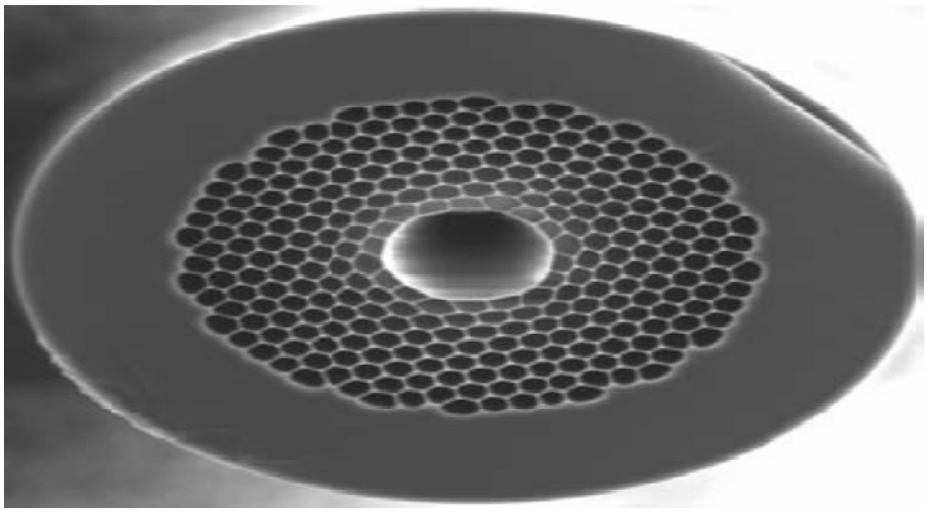

Figure 2(l): Microscope picture of a 19-cell hollow-core fiber [19].

However notice that a larger hollow core gives increased perimeters, leading to a greater density of surface modes, decreased bandwidth and also increased higher-order dispersion [19]. Reducing the hollow-core PCF loss to levels below those of conventional silica fibers

remains a challenge. For what concerns Rayleigh scattering as well as absorption, they should be reduced to below the level in bulk fibers, even if the increased scattering at the many surfaces represents potentially a problem.

Also, the biggest unknown is the level of variation in the fiber structure along its length. In fact, the band gap presents a high sensitivity to structural fluctuations that occur over long fiber lengths that is wavelengths that are guided in one section may leak away in another.

Finally, there is an excess loss in hollow-core PCFs which occurs at wavelengths where there is coupling from the air-guided fundamental mode to the confined surface modes, which have much greater overlap with the glass and, as a consequence, experience far higher loss. The presence of surface modes strongly affects the guiding properties of the air-guiding PCFs by reducing the width of their transmission window. Ideally, being the core modes completely confined in air, the small perturbations in the silica structure cause only a slight coupling with the cladding ones, which have the largest spatial overlap in the perturbed region [19].

A reduction of the silica quantity around the hollow core causes an energy increase of the surface modes which consequently move into the PBG while on the contrary the guided-mode energy is unaffected by this change. However for some hollow core dimensions there is a certain interaction between these two different kinds of modes, due to the significant field overlap in the silica regions. Thus the axial perturbations all along the fiber can provide the light coupling between the core and the surface modes. The loss mechanism related to surface modes is complete by considering that they are highly overlapped and coupled with the continuum of the extended modes in the cladding.

2.6.2 Confinement Loss

In both solid core and hollow-core PCFs it is necessary to consider another contribution to the losses, that is the leakage or confinement losses. These are due to the finite number of air-holes which can be made in the fiber cross section. As a consequence all the PCF guided modes are leaky. For example, in solid-core PCFs light is confined within a core region by the air-holes. Light will move away from the core if the confinement provided by the air-holes is inadequate. This means that it is important to design such aspects of the PCF structure as air hole diameter and hole-to-hole spacing or pitch in order to realize low-loss PCFs. In particular, the ratio between the air hole diameter and the pitch must be designed to be large enough to confine light into the core. On the other hand, a large value of the ratio

makes the PCF multi-mode. However by properly designing the structure the confinement loss of single-mode PCFs can be reduced to a negligible level.

Recently, several analyses have been performed in order to find the guidelines to design both index-guiding PCFs and PBG-based fibers with negligible leakage losses [20]. In particular leakage losses can be significantly reduced by increasing the ring number [20]. In PBG fibers the leakage loss dependence on the number of air-hole rings is much weaker than in index-guiding PCFs, whereas the confinement losses exhibit a strong dependence on the position of the localized state inside the PBG.

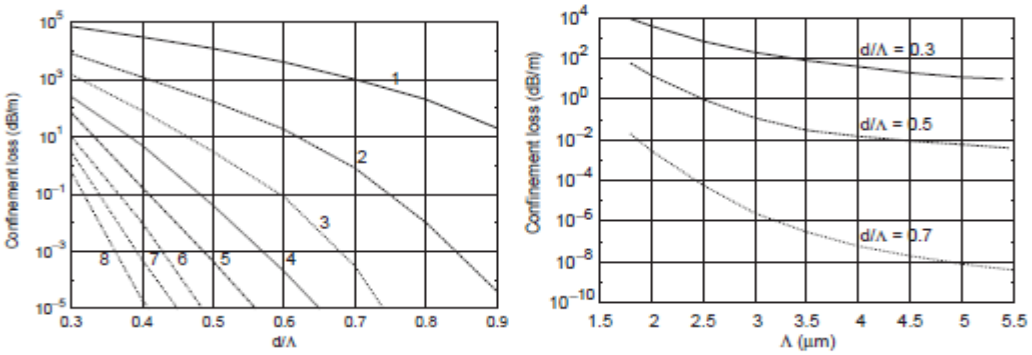

(i) (ii)

Figure 2(m): Leakage loss at 1550 nm (i) as a function of the air-hole diameter d normalized to the pitch Λ = 2.3 μm for different ring numbers and (ii) as a function of the pitch Λ for different air-filling fraction d/Λ [20].

As shown in Fig. 2(m{i}), its leakage loss quickly decreases when the air-hole ring number or the air-hole diameter increases. The reduction rate of the confinement loss increases in the same way with these geometric parameters. As expected, the loss decreases with larger Λ values for a fixed d/Λ. In this case, Λ and d are scaled in the same way, so a larger pitch corresponds to a larger silica core size and, as a consequence, to a higher field confinement. When the defect state moves closer to the PBG edges, the loss increases more quickly when the air-hole ring number is higher.

Despite the high air-filling fraction, that is d/Λ = 0.9, the dependence on the ring number is very weak, if compared with the case of solid-core PCFs. Finally, it is important to underline that there is a strong wavelength dependence of the loss. For example, the loss of the seven air-hole ring PCF increases of a decade with respect to the minimum value in a wavelength range of less than 100 nm [20].

2.6.3 Bending Loss

As already stated, an alternative route to fabricate LMA fibers is offered by PCFs, which can be designed to be endlessly single-mode, unlike conventional fibers that exhibit a cutoff wavelength below which higher-order modes are supported. As for standard optical fibers, the practical achievable mode area in PCFs is limited by the macro bending loss [21].

Conventional fibers suffer additional loss if bent more tightly than a certain critical radius. The same behavior is observed also in PCFs, which show even a short-wavelength bend loss edge [21], caused by bend-induced coupling from the fundamental to the higher-order modes which leak out of the core. In fact, at short wavelengths the guided mode is mainly confined into the silica [21] and when $\lambda << \Lambda$ the field can escape through the interstitial space between the neighboring air-holes. As a consequence, the fiber becomes more sensitive to bending. Since LMA PCFs are generally designed with $\Lambda > 7-8$ μm, the standard telecommunication window falls in the short-wavelength edge. In spite of that, it has been demonstrated that LMA PCFs exhibit bending losses comparable with those of similarly sized conventional fibers at 1550nm [21].

PCFs with larger relative air-hole diameters that is with higher d/Λ, are less sensitive to bending loss. However, the demand for single-mode operation and the need for large-mode size limit the increase of d/Λ, and other solutions must be adopted. It has been demonstrated that the bending losses of triangular PCFs can be improved by changing the air-hole configuration from the traditional single-rod core design [22]. An accurate evaluation of the advantages regarding the bending loss can be obtained by comparing suitably matched three-rod and single-rod PCFs designs [22]. Many different approaches have been proposed in literature to evaluate the bending loss in conventional optical fibers, which usually assume a circular symmetric refractive index profile. Unfortunately, these approaches are not straightforward in PCFs, due to the complex nature of their refractive index profile. As a consequence, an accurate modeling of bending loss becomes even more challenging.

The transition loss occurs where the curvature of the fiber changes suddenly, that is at the beginning or the end of the bend. This loss can be modeled as a sort of coupling loss, because the mode fields in the straight and curved sections are not aligned. The pure bend loss is the continuous loss that occurs along any curved section of fiber due to the inability of the tails of the field to keep in phase with the faster-travelling central portion of the field. In this

model, the full refractive index profile of the PCF is retained and hence the six fold field shape as well. In fact, the bent fiber is modeled as a straight fiber with an equivalent index profile given by a transformation that superimposes a gradient onto the refractive index of the straight fiber in the direction of the bend. Other theoretical approaches have been developed, which provide a correct parametric dependence of the bending loss with the PCF geometric parameters [22].

Hollow-core PCFs have different bending properties with respect to silica core ones. For applications like high-power delivery for medical use or material processing, which are suitable for air-guiding fibers, a low bending sensitivity is required, since it allows a very flexible use and an easy integration in supporting mechanical systems. After an early demonstration in a theoretical work of the low influence of bending on the hollow-core PCF guiding properties, the bending loss of air-guiding fibers have been experimentally measured [22]. The most important effect obtained with bending is a shift of the short-wavelength bandgap edge towards longer wavelengths, thus causing a PBG narrowing for the hollow-core PCFs. On the contrary, a similar shift has not been measured at the long wavelength bandgap edge. In order to understand the fact that air-guiding PCFs are bending insensitive over most of the PBG, it is useful to consider the difference between the refractive index of the core and of the PBG edge, which corresponds to the cladding. Being this difference very high which is about 2×10^{-2}, a very tight confinement of the guided-mode in the hollow-core can be obtained, which results in the robust guiding even through tightly bent PCFs [22].

CHAPTER

3

NUMERICAL MODELING TECHNIQUES

Numerical simulations play an important role for the design and modeling of photonic crystal structures. So far various modeling methods [23] in which not only a full-vector model but also an approximate scalar model is used have been developed such as effective index approach, plane-wave expansion (PWE) method, localized-function method, multipole method (MM), beam propagation method (BPM), finite-difference method (FDM), finite difference time domain method (FDTD), boundary element method (BEM) and finite-element method (FEM). An approximate-scalar model is a valuable tool for aiding fabrication efforts because it is easy to use and provides good qualitative information. However, in order to model photonic crystal structures especially PCFs accurately, it is crucial to use a full-vector model [23].

In particular, a complete vector model is necessary for predicting sensitive quantities such as dispersion and birefringence. The choice of modeling method can impact the computational time, required computational resources, and limitations of the methods, so it is important to explore the usefulness and limitations of each method.

3.1 Finite Difference Time Domain Technique

The FDTD method [24] belongs to the general class of grid based differential time domain numerical modeling methods and is one of the full vector models. The time dependent Maxwell's equations in partial differential form are discretized using central difference approximations to the space and time partial derivatives. The resulting finite-difference equations are solved in either software or hardware in a leapfrog manner: the electric field vector components in a volume of space are solved at a given instant in time; then the magnetic field vector components in the same spatial volume are solved at the next instant in time; and the process is repeated over and over again until the desired transient or steady-state electromagnetic field behavior is fully evolved. Virtually any physical system that is

governed by a time-dependent partial differential equation (PDE) can be readily simulated through the use of FDTD.

The FDTD method has been established as a powerful engineering tool for integrated and diffractive optics device simulations. This is due to its unique combination of features, such as the ability to model light propagation, scattering and diffraction, and reflection and polarization effects. It can also model material anisotropy and dispersion without any pre-assumption of field behavior such as the slowly varying amplitude approximation. The method allows for the effective and powerful simulation and analysis of sub-micron devices with very fine structural details. A sub-micron scale implies a high degree of light confinement and correspondingly, the large refractive index difference of the materials, mostly semiconductors to be used in a typical device design.

3.1.1 FDTD Basics

The basic of FDTD method starts with solving Maxwell equations in heterogeneous materials [25]. The procedure begins with two basic equations as described below.

$$\nabla \times E = -\mu \frac{\partial \vec{H}}{\partial t} \qquad (3a)$$

$$\nabla \times H = \sigma \vec{E} + \varepsilon \frac{\partial \vec{E}}{\partial t} \qquad (3b)$$

Where $\varepsilon = \varepsilon_0 \varepsilon_r$, is the dielectric permittivity and μ is the magnetic permeability of the vacuum. The refractive index is, $n = \sqrt{\varepsilon_r}$. Equation (3a) represents the Ampere's law [25] and equation (3b) represents the Faraday's law [25]. The first step is to convert the vector differential equations represented by (3a) and (3b) to the scalar differential equations. As we know

$$\nabla = \frac{\partial}{\partial x}\hat{x} + \frac{\partial}{\partial x}\hat{y} + \frac{\partial}{\partial x}\hat{z} \qquad (3c)$$

Putting the value in (3a), it becomes

$$\begin{bmatrix} \hat{x} & \hat{y} & \hat{z} \\ \partial/\partial x & \partial/\partial y & \partial/\partial z \\ E_x & E_y & E_z \end{bmatrix} = -\mu \left(\frac{\partial H_x}{\partial t}\hat{x} + \frac{\partial H_y}{\partial t}\hat{y} + \frac{\partial H_z}{\partial t}\hat{z} \right) \qquad (3d)$$

Solving right hand side of above equation we get

$$\hat{x}\left(\frac{\partial E_z}{\partial y}-\frac{\partial E_y}{\partial z}\right)-\hat{y}\left(\frac{\partial E_z}{\partial x}-\frac{\partial E_x}{\partial z}\right)+\hat{z}\left(\frac{\partial E_y}{\partial x}-\frac{\partial E_x}{\partial y}\right)=-\mu\left(\frac{\partial H_x}{\partial t}\hat{x}+\frac{\partial H_y}{\partial t}\hat{y}+\frac{\partial H_z}{\partial t}\hat{z}\right) \quad (3e)$$

Now equation (3e) can be expressed in form of three scalar differential equations by equating the coefficients of vectors (x, y, z) as

$$\frac{\partial E_z}{\partial y}-\frac{\partial E_y}{\partial z}=-\mu\frac{\partial H_x}{\partial t} \quad (3f)$$

$$\frac{\partial E_z}{\partial x}-\frac{\partial E_x}{\partial z}=\mu\frac{\partial H_y}{\partial t} \quad (3g)$$

$$\frac{\partial E_y}{\partial x}-\frac{\partial E_x}{\partial y}=-\mu\frac{\partial H_z}{\partial t} \quad (3h)$$

These equations had derivatives in both space and time. Similarly the faraday's law represented by equation (3b) can be represented in form of scalar differential equations as

$$\frac{\partial H_z}{\partial y}-\frac{\partial H_y}{\partial z}=\sigma E_x+\varepsilon\frac{\partial E_x}{\partial t} \quad (3i)$$

$$-\left(\frac{\partial H_z}{\partial x}-\frac{\partial H_x}{\partial z}\right)=\sigma E_y+\varepsilon\frac{\partial E_y}{\partial t} \quad (3j)$$

$$\frac{\partial H_y}{\partial x}-\frac{\partial H_x}{\partial y}=\sigma E_z+\varepsilon\frac{\partial E_z}{\partial t} \quad (3k)$$

Discretizing the FDTD grid

The next step is to convert the scalar differential equations to the difference equations and this is done by discretizing the 3-D FDTD grid. The FDTD grid is shown in the figure below

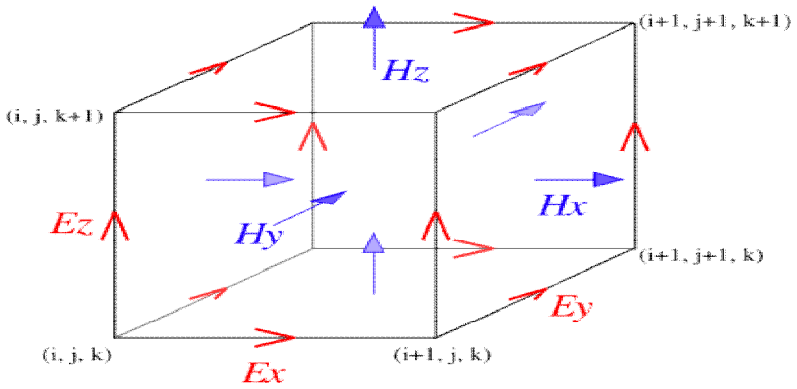

Figure 3(a): FDTD grid showing E and H components [25].

The electric field and magnetic field components are shown in the grid. Each scalar differential equation can be converted into the difference equation in terms the field components as well as space and time steps. Taking equation (3h) the left hand side of the equation becomes

$$\left(\frac{E_y(i+1,j,k)-E_y(i,j,k)}{\Delta x}\right)-\left(\frac{E_x(i,j+1,k)-E_x(i,j,k)}{\Delta y}\right)$$

Now from this difference term representing RHS of equation (3h).the location of H_z is (i,j,k). To represent LHS of same equation let us consider the time derivative. For this the division of electric field and magnetic field in time is presented as

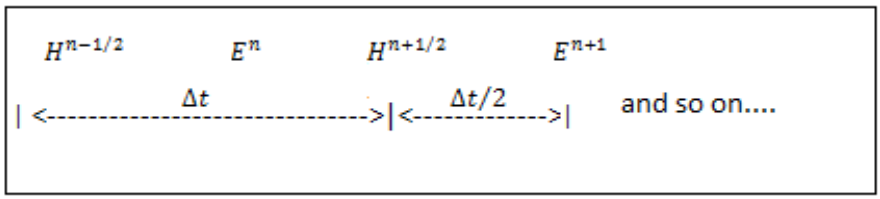

Figure 3(b): Time division of electric and magnetic field components [25]

So it is shown that magnetic field components are at ½ time steps and electric field components are at full time steps. Now if we consider electric field of above equation at nth time step then the complete difference equation becomes

$$\left(\frac{E_y^n(i+1,j,k)-E_y^n(i,j,k)}{\Delta x}\right)-\left(\frac{E_x^n(i,j+1,k)-E_x^n(i,j,k)}{\Delta y}\right)$$
$$=\mu(i.j,k)\left(\frac{H_z^{n+1/2}(i,j,k)-H_z^{n-1/2}(i,j,k)}{\Delta t}\right) \quad (3l)$$

Similarly the other two electric field scalar differential equations can be represented in terms of difference equation discretized in space and time.

Next task is to convert magnetic field scalar differential equations to the same form as the electric field equations are represented. Considering the same time division the LHS of equation (3j) becomes

$$-\left[\left(\frac{H_z(i,j,k)-H_z(i-1,j,k)}{\Delta x}\right)-\left(\frac{H_x(i,j,k)-H_x(i,j,k-1)}{\Delta z}\right)\right]$$

The position of E_y will now be (i, j, k) and to find the RHS of the equation, considering the magnetic field at $H^{n+1/2}$ the complete equation becomes

$$-\left[\left(\frac{H_z^{n+1/2}(i,j,k)-H_z^{n+1/2}(i-1,j,k)}{\Delta x}\right)-\left(\frac{H_x^{n+1/2}(i,j,k)-H_x^{n+1/2}(i,j,k-1)}{\Delta z}\right)\right]$$

$$=\sigma(i,j,k)\left(\frac{E_n+E_{n+1}}{2}\right)+\left(\frac{E_y^{n+1}(i,j,k)-E_y^{n}(i,j,k)}{\Delta t}\right) \quad (3m)$$

So the values of electric and magnetic fields are updated from their previous values to define a crystal lattice that contains a defined number of FDTD grids. The magnetic field and electric field difference equations are also known as FDTD equations in context to the FDTD method. Since these equations are defined for a single grid, we can use them to define 1D, 2D and 3D crystal consisting of the same grids.

3.1.2 2D FDTD Equations

The FDTD approach is based on a direct numerical solution of the time-dependent Maxwell's curl equations [26].The photonic device is laid out in the X-Z plane. The propagation is along Z. The Y-direction is assumed to be infinite. This assumption removes all the $\partial/\partial y$derivatives from Maxwell's equations and splits them into two (TE and TM) independent sets of equations. The 2D computational domain is shown in Figure 3(c). The space steps in the X and Z directions are Δx and Δz, respectively. Each mesh point is associated with a specific type of material and contains information about its properties such as refractive index and dispersion parameters [27].

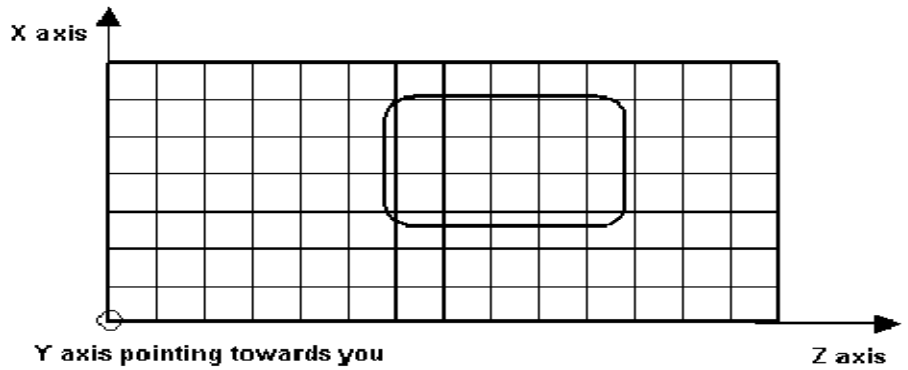

Figure 3(c): The 2-D computational domain [27].

TE waves

In the 2D TE case where H_x, E_y, H_z are nonzero components, propagation is along Z and transverse field variations along X, in lossless media, Maxwell's equations take the following form

$$\mu \frac{\partial H_x}{\partial t} = \frac{\partial E_y}{\partial z} \qquad (a)$$

$$\mu \frac{\partial H_z}{\partial t} = -\frac{\partial E_y}{\partial x} \qquad (b) \qquad (3n)$$

$$\varepsilon \frac{\partial E_y}{\partial t} + \sigma E_y = \frac{\partial H_x}{\partial z} - \frac{\partial H_z}{\partial x} \qquad (c)$$

where $\varepsilon = \varepsilon_0 \varepsilon_r$is the dielectric permittivity and μ is the magnetic permeability of the vacuum. The refractive index is $n = \sqrt{\varepsilon_r}$.

Each field is represented by a 2D array as E_y (i, k), H_x (i, k) and H_z (i, k) corresponding to the 2D mesh grid given in Figure 3(c). The indices i and k account for the number of space steps in the X and Z direction, respectively. In the case of TE, the location of the fields in the mesh is shown in Figure 3(d) below.

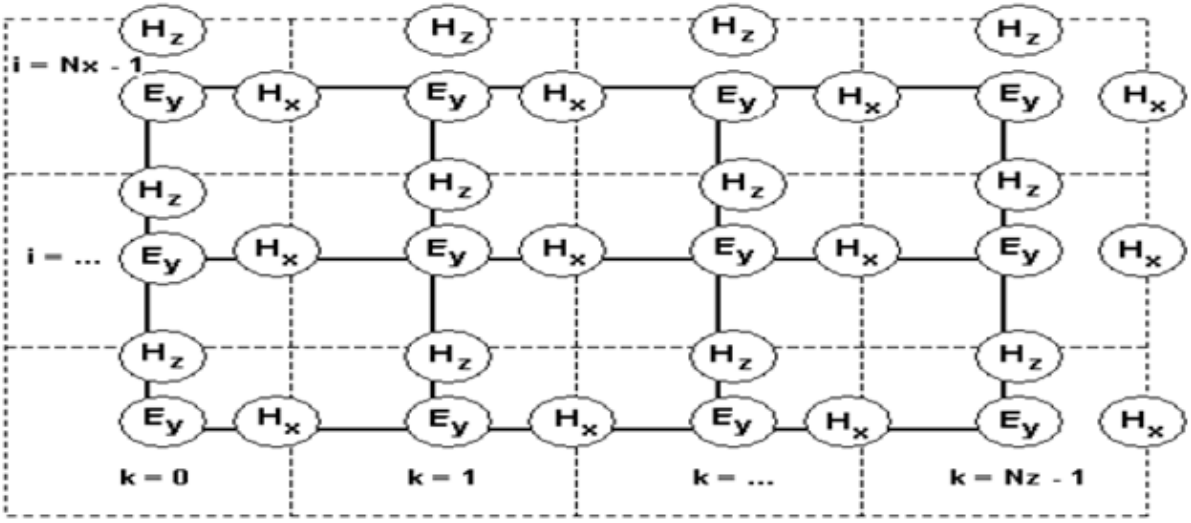

Figure 3(d): Location of the TE fields in the computational domain [27].

The TE fields stencil can be explained as follows. The E_y field locations coincide with the mesh nodes given in Figure 3(c). In Figure 3(d), the solid lines represent the mesh given in Figure 3(c). The E_y field is considered to be the center of the FDTD space cell. The dashed lines form the FDTD cells. The magnetic fields H_x and H_z are associated with cell edges. The locations of the electric fields are associated with integer values of the indices i and k. The H_x field is associated with integer i and (k + 0.5) indices. The H_z field is associated with (i + 0.5) and integer k indices.

The indices i and k label the space steps and along the x and z directions, respectively. This is the so-called Yee's numerical scheme [27] applied to the 2D TE case. It uses central

difference approximations for the numerical derivatives in space and time, both having second order accuracy. The sampling in space is on a sub-wavelength scale [28]. Typically, 10 to 20 steps per wavelength are needed. The sampling in time is selected to ensure numerical stability of the algorithm. The time step is determined by the Courant limit:

$$\Delta t \leq 1/\left(c\sqrt{1/(\Delta x)^2 + 1/(\Delta z)^2}\right) \qquad (3n\{i\})$$

TM waves

In the 2D TM case where E_x, H_y and E_z are nonzero components, propagation along Z and transverse field variations along X, in lossless media, Maxwell's equations take the following form:

$$\mu \frac{\partial H_y}{\partial t} = \frac{\partial E_z}{\partial x} - \frac{\partial E_x}{\partial z} \qquad (a)$$

$$\varepsilon \frac{\partial E_x}{\partial t} + \sigma E_x = -\frac{\partial H_y}{\partial z} \qquad (b) \qquad (3o)$$

$$\mu \frac{\partial E_z}{\partial t} + \sigma E_z = \frac{\partial H_y}{\partial x} \qquad (c)$$

The location of the TM fields in the computational domain follows the same philosophy and is shown in Figure 3(e) below.

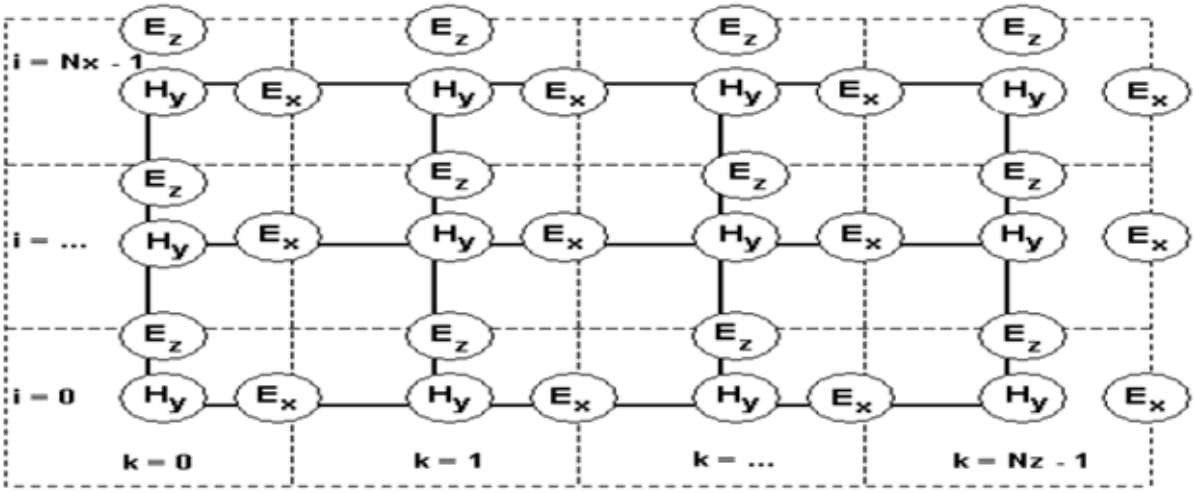

Figure 3(e): Location of the TM fields in the computational domain [27].

Now, the electric field components E_x and E_z are associated with the cell edges, while the magnetic field H_y is located at the cell center. The TM algorithm can be presented in a way similar to Equation (3n). In this way the magnetic field and electric field components are updated accordingly and the grid is continued up to the defined time steps.

3.1.3 3D FDTD Equations

In 3D crystal, the lattice structure is a cubic box, the space steps are D_x, D_y and D_z in x, y and z directions respectively.

Each field components is presented by a 3D array $E_x(i, j, k)$, $E_y(i, j, k)$, $E_z(i, j, k)$, $H_x(i, j, k)$, $H_y(i, j, k)$, $H_z(i, j, k)$. The field components position in Yee's Cell are shown in Figure 3(f). These placements and the notation show that the E and H components are interleaved at intervals of 1/2Dh and 1 /2Dt in space and for the purpose of implementing a leapfrog algorithm.

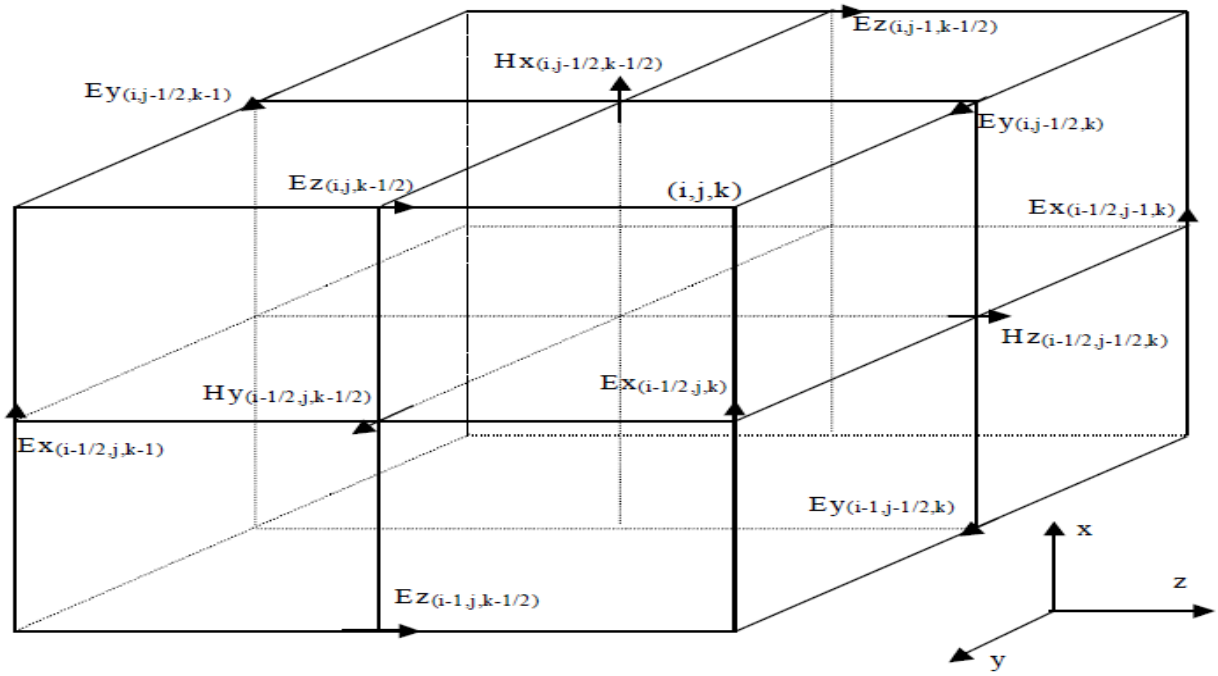

Figure 3(f): Displacement of the electric and magnetic field vector components about a cubic unit cell of the Yee space lattice [27].

Now we can apply the above finite-difference ideas, notations, and field displacements to achieve a numerical approximation of Maxwell's equation. The FDTD equations for electric and magnetic field components can be written as

Equation (3p)

$$H_x^{n+1/2}(i, j-1/2, k-1/2) = H_x^{n-1/2}(i, j-1/2, k-1/2) + \frac{\Delta t}{\mu \Delta z}\left(E_y^n(i, j-1/2, k) - E_y^n(i, j-1/2, k-1)\right) - \frac{\Delta t}{\mu \Delta y}\left(E_z^n(i, j, k-1/2) - E_z^n(i, j-1, k-1/2)\right)$$

Equation (3q)

$$H_y^{n+1/2}(i-1/2,j,k-1/2) = H_y^{n-1/2}(i-1/2,j,k-1/2) + \frac{\Delta t}{\mu\Delta x}\left(E_z^n(i,j,k-1/2) - E_z^n(i,j-1,k-1/2)\right) - \frac{\Delta t}{\mu\Delta z}\left(E_x^n(i-1/2,j,k) - E_x^n(i-1/2,j,k-1)\right)$$

Equation (3r)

$$H_z^{n+1/2}(i-1/2,j-1/2,k) = H_z^{n-1/2}(i-1/2,j-1/2,k) + \frac{\Delta t}{\mu\Delta y}\left(E_x^n(i-1/2,j,k) - E_x^n(i-1/2,j-1,k)\right) - \frac{\Delta t}{\mu\Delta x}\left(E_y^n(i,j-1/2,k) - E_y^n(i-1,j-1/2,k)\right)$$

Equation (3s)

$$E_x^{n+1}(i-1/2,j,k) = \frac{2\varepsilon-\sigma\Delta t}{2\varepsilon+\sigma\Delta t}E_x^n(i-1/2,j,k) + \frac{2\Delta t}{(2\varepsilon+\sigma\Delta t)\Delta y}\left(H_z^{n+1/2}(i-1/2,j+1/2,k) - H_z^{n+1/2}(i-1/2,j-1/2,k)\right) - \frac{2\Delta t}{(2\varepsilon+\sigma\Delta t)\Delta z}\left(H_y^{n+1/2}(i-1/2,j,k+1/2) - H_y^{n+1/2}(i-1/2,j,k-1/2)\right)$$

Equation (3t)

$$E_y^{n+1}(i,j-1/2,k) = \frac{2\varepsilon-\sigma\Delta t}{2\varepsilon+\sigma\Delta t}E_y^n(i,j-1/2,k) + \frac{2\Delta t}{(2\varepsilon+\sigma\Delta t)\Delta z}\left(H_x^{n+1/2}(i,j-1/2,k+1/2) - H_x^{n+1/2}(i,j-1/2,k-1/2)\right) - \frac{2\Delta t}{(2\varepsilon+\sigma\Delta t)\Delta x}\left(H_z^{n+1/2}(i+1/2,j-1/2,k) - H_z^{n+1/2}(i-1/2,j-1/2,k)\right)$$

Equation (3u)

$$E_z^{n+1}(i,j,k-1/2) = \frac{2\varepsilon-\sigma\Delta t}{2\varepsilon+\sigma\Delta t}E_z^n(i,j,k-1/2) + \frac{2\Delta t}{(2\varepsilon+\sigma\Delta t)\Delta x}\left(H_y^{n+1/2}(i+1/2,j,k-1/2) - H_y^{n+1/2}(i-1/2,j,k-1/2)\right) - \frac{2\Delta t}{(2\varepsilon+\sigma\Delta t)\Delta y}\left(H_x^{n+1/2}(i,j+1/2,k-1/2) - H_x^{n+1/2}(i,j-1/2,k-1/2)\right)$$

Equation (3p) to (3u) represented the electric field and magnetic field components in all three directions for the 3D structure that uses these equations to update itself in time as well as space when it is modeled by FDTD method. Hence these equations are the base to model a three dimensional structure in FDTD.

3.1.4 Space Step and Time Step

The fundamental constraint of FDTD method is the step size both for the time and space. Space and time steps relate to the accuracy, numerical dispersion, and the stability of the FDTD method. In general, to keep the results as accurate as possible, with a low numerical dispersive, the mesh size often quoted is "10 cells per wavelength", meaning that the side of each cell should be 1/10 or less at the highest frequency (shortest wavelength).

The FDTD is a volumetric computational method, so that if some portion of the computational space is filled with penetrable material, the wavelength in the material must be used to determine the maximum cell size.

The following equation is for the suggested mesh size:

$$minimun(\Delta x,\Delta y,\Delta z) = \frac{\lambda_{min}}{10n_{max}} \qquad (3v)$$

Where n_{max} is the maximum refractive index value in the computational domain. Once the cell size is determined, the maximum size for the time step Δt immediately follows the Courant-Friedrichs-Levy (CFL) condition [29].

For 3D FDTD simulation, the CFL condition is:

$$\Delta t \leq \frac{1}{v\sqrt{\frac{1}{(\Delta x)^2}+\frac{1}{(\Delta y)^2}+\frac{1}{(\Delta z)^2}}} \qquad (3w)$$

Where v is the speed of the light in medium.

For 2D simulations, the above CFL condition can be simplified as:

$$\Delta t \leq \frac{1}{v\sqrt{\frac{1}{(\Delta x)^2}+\frac{1}{(\Delta z)^2}}} \qquad (3x)$$

Thus the defined assumptions for space step size and time step size must be considered while defining a two or three dimensional crystal that is to be modeled using FDTD method.

3.2 FDTD Boundary Conditions

The basic FDTD algorithm must be modified at the boundaries of the computational window where suitable numerical absorbing boundary conditions (ABC) are applied. This is one of the most challenging parts of FDTD simulations. There are several choices for the type of boundary conditions [30]. The Perfectly Matched Layer (PML) boundary conditions have the best performance. Most FDTD simulator uses the Anisotropic PML or so-called Un-split PML (UPML) version. The UPML boundary conditions are physical rather than numerical because their implementation is based on a Maxwellian formulation rather than on a mathematical model. Their absorbing properties are physically equivalent to the properties of an absorbing uni-axial anisotropic medium with the following permittivity and permeability tensors:

$$\hat{\varepsilon} = \varepsilon\,\hat{S}, \hat{\mu} = \mu_0\hat{S}, \hat{S} = \begin{pmatrix} s^{-1} & 0 & 0 \\ 0 & s & 0 \\ 0 & 0 & s \end{pmatrix}, s = \kappa - i\,\frac{\sigma}{\varepsilon_0\omega} \qquad (3y)$$

A plane wave incident on a half space composed of the above uni-axial medium with an interface in the x that equals constant plane is purely transmitted into it. The reflectionless property is completely independent of the angle of incidence, polarization and frequency of the incident wave. The numerical implementation of the UPML in a 2D (X-Z) computational window requires the introduction of such perfectly matched absorbing layers on all the sides. The corner regions need special attention. In these regions the tensor from Equation (3y) must be modified to:

$$\hat{S} = \begin{pmatrix} s_x^{-1} & 0 & 0 \\ 0 & s_x & 0 \\ 0 & 0 & s_x \end{pmatrix} \begin{pmatrix} s_z & 0 & 0 \\ 0 & s_z & 0 \\ 0 & 0 & s_z^{-1} \end{pmatrix}, s_x = \kappa_x - i \frac{\sigma_x}{\varepsilon_0 \omega}, s_z = \kappa_z - i \frac{\sigma_z}{\varepsilon_0 \omega} \qquad (3z)$$

The minimization of the numerical reflectance of the Anisotropic PML layers requires spatial scaling of the conductivity profile from zero (at the interface of the PML) to a maximum value at the end of the computational window:

$$\sigma(x) = \sigma_{max} \left(\frac{x}{L}\right)^m, \quad \kappa(x) = 1 + (\kappa_{max} - 1)\left(\frac{x}{L}\right)^m \qquad (3aa)$$

Where L is the thickness of Anisotropic PML [30]. Typical values for the parameter *m* are between 2 and 4.

3.2.1 PMC/PEC Boundary Conditions and Plane Wave Simulation

The FDTD simulators have options to use Perfect Electrical Conductor (PEC) and Perfect Magnetic Conductor (PMC) boundary conditions. The boundaries that use the new conditions can be chosen, and Anisotropic PML can be used for the remaining boundaries. With this PEC/PMC/Anisotropic PML combination, the following simulations may be obtained:

- Plane wave simulation
- Domain reduced simulation for symmetric, periodic, or photonic band gap structures

3.2.2 Image Value of PEC/ PMC

The following graphs show the field set up in the PEC/PMC wall (zero thickness) and its image value

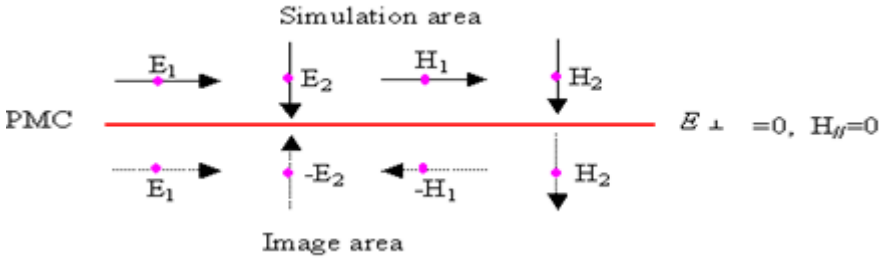

Figure 3(g): Field in PMC and image area [31].

Here $E_\perp$ is the vertical electric component in the PMC wall, and is the parallel magnetic component $H_\parallel$ in the PMC wall.

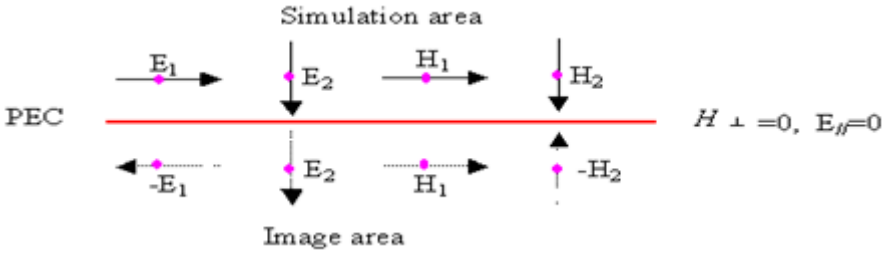

Figure 3(h): Field in PEC and image area [31].

As we can see from Figure 3(g), PMC is a symmetric wall for the symmetric structure with symmetric wave propagation. The following two cases detail the results when PMC occurs.

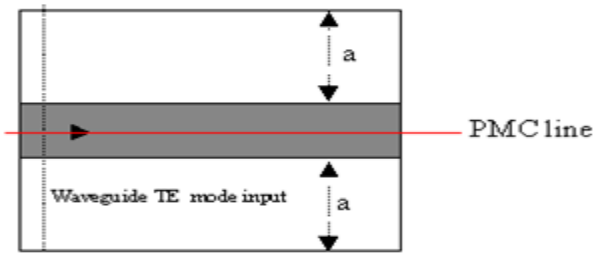

Figure 3(i): PMC wall in a symmetric waveguide excited by symmetric TE waveguide mode[31].

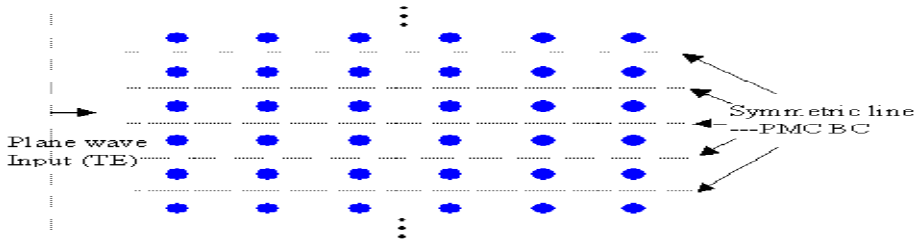

Figure 3(j): PMC wall in a periodic structure for TE plane wave propagation [31].

PMC can be seen as the special case for Bloch's boundary condition [31] (periodic boundary condition) where the k-vector is set to zero in the corresponding direction. PEC line is the complement of PMC, so in Figure 3(i) and Figure 3(j), the PMC line will become the PEC line if the wave polarization is changed to TM.

3.2.3 Plane Wave Realized in Symmetric/Periodic Structure

Figure 3(k) shows how the plane wave simulation can be realized for a symmetric structure. For a 2D TE simulation, the edge of transverse plane should be set to the PMC boundary condition to realize the plane wave.

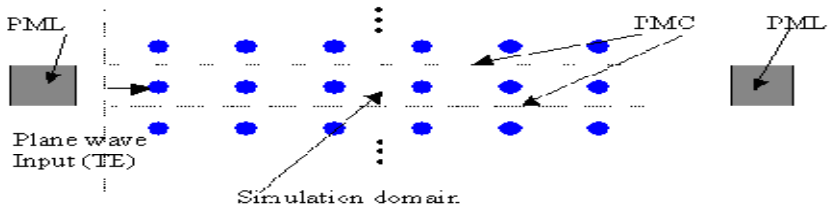

Figure 3(k): Plane wave in TE simulation [31].

For a 2D TM simulation, the edge of transverse plane should set to the PEC boundary condition to realize the plane wave as shown in figure 3(l).

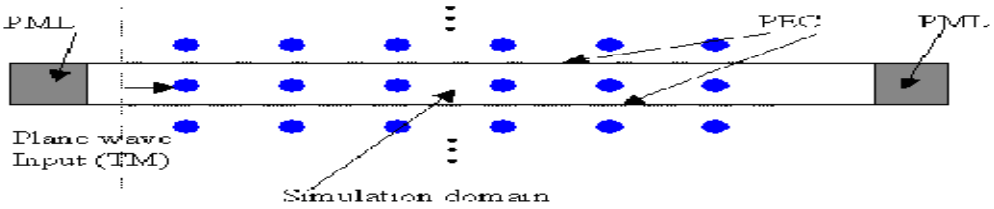

Figure 3(l): Plane wave in TM simulation [31].

For a 3D simulation, the plane wave realization depends on the wave polarization and the boundary condition setup at different edges of the transverse plane. If the wave goes in z-direction, and the input wave is in y-direction polarization, then the y plane (x-z) edge should be set to the PEC and x-plane (y-z plane) edge set to the PMC boundary as shown in figure 3(m).

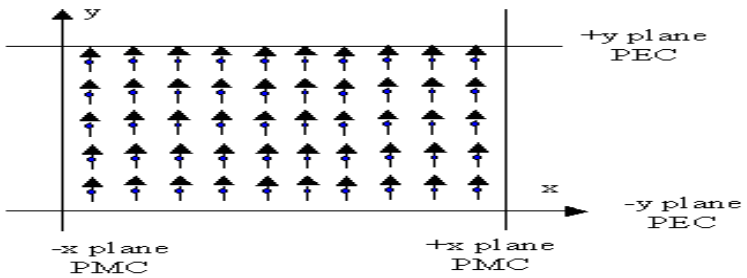

Figure 3(m): Y-polarization plane wave in z-direction of propagation with boundary conditions [31].

For 3D simulation, if the wave goes in z-direction, and the input wave is in x-direction polarization, then the y plane (x-z) edge should be set to the PMC and x-plane (y-z plane) edge set to the PEC boundary as shown in figure 3(n)

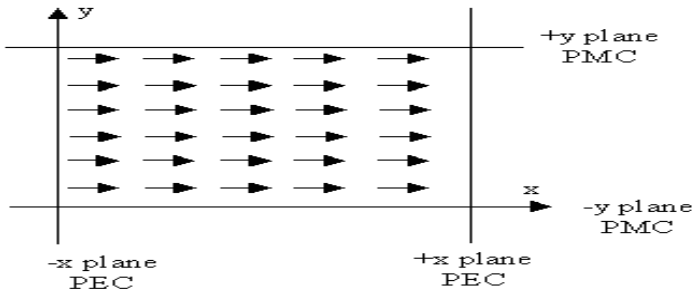

Figure 3(n): X-polarization plane wave in z-direction of propagation with boundary conditions [31].

The plane wave shape can be set by setting the rectangular wave parameters in the input wave properties. Currently, plane wave does not support the tilting angle. Currently, the plane wave simulation is only effective for symmetrical structures [32].

3.2.4 Periodic Boundary Conditions

Some of the FDTD simulators provide the option to use simplified Periodic Boundary Condition (PBC). PBC can work with other boundary conditions such as Anisotropic PML, PMC and PEC. With PBC, a simple plane wave simulation or periodic layout simulations can be generated.

The simplified PBC [33] is based on the Bloch's Theorem:

- For the periodic layout, the wave function is written as the combination of a cell periodic component and a wave-like component:

$$\psi(\gamma + \Delta\gamma) = \varphi(\gamma) \cdot \exp(jk\Delta\gamma)$$

- The equation above needs to have a pre-defined value for the k-vector; which is not so feasible for an FDTD simulation, especially for Pulse input.

Therefore, we simplified the application by setting the k-vector in one specific direction as zero, which then leads to the input wave being the axis-propagated wave, and then the equation becomes:

$$\psi(\gamma + \Delta\gamma) = \varphi(\gamma)$$

$\varphi(\gamma)$ is the field component at the edge of the simulation domain. $\psi(\gamma + \Delta\gamma)$ is the corresponding field value at the boundary of the opposite edge of the $\varphi(\gamma)$. The following graph [33] shows the relationship.

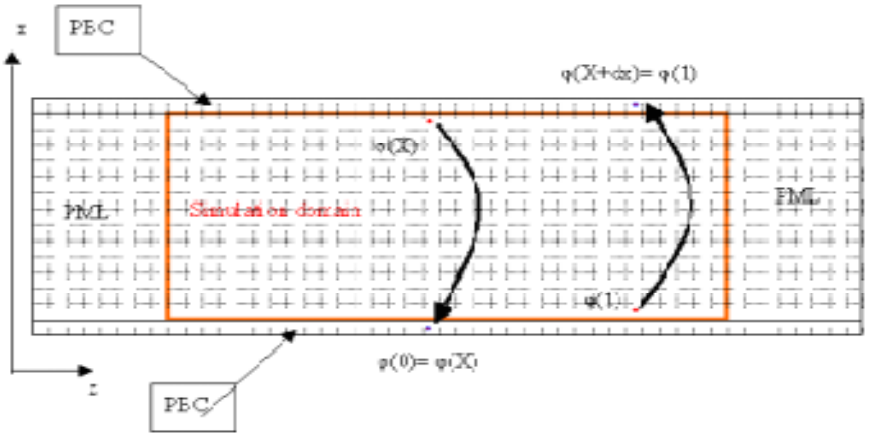

3.3 The FDTD Algorithm

Since the finite difference time domain (FDTD) technique has been explained starting from the basics of technique to the boundary conditions. Now the FDTD algorithm can be defined that is being used in the modeling and simulations of the defined structures.

The FDTD algorithm [34] is an especially popular tool because it is Simple, robust and easy to understand. Here the FDTD algorithm has been explained by considering the Telegrapher's equations [35] which are in form of Partial differential equation in space and time.

3.3.1 The Telegrapher's Equations

The telegrapher's equations are basically nothing more than a pair of coupled partial differential equations (PDEs) in space and time. Together, they represent the fundamental governing equations of all transmission line theory [35], and are given as

$$-\frac{\partial v(z,t)}{\partial z} = R'i(z,t) + L'\frac{\partial i(z,t)}{\partial t}, \qquad (3ab)$$

$$-\frac{\partial i(z,t)}{\partial z} = G'v(z,t) + C'\frac{\partial v(z,t)}{\partial t}, \qquad (3ac)$$

Where v(z, t) and i(z ,t) represent the instantaneous voltage and current at position z and time t. The R', L', G', and C terms represent the resistance, inductance, conductance, and capacitance per unit length.

Because computers only have a finite capacity for memory storage, the first step in applying FDTD is to define a mesh, which is a set of discrete points in space and time that will sample

the functions. Shown in figure 3(o), this is done by fixing a grid spacing of A_z in space and A_t in time. The points that lie on the mesh are then defined as

$$z_k = k\Delta z \qquad (3ad)$$

$$t_n = n\Delta t \qquad (3ae)$$

Where k and n are the integers confined by sets (1 < k < K) and *(1* < n < N).

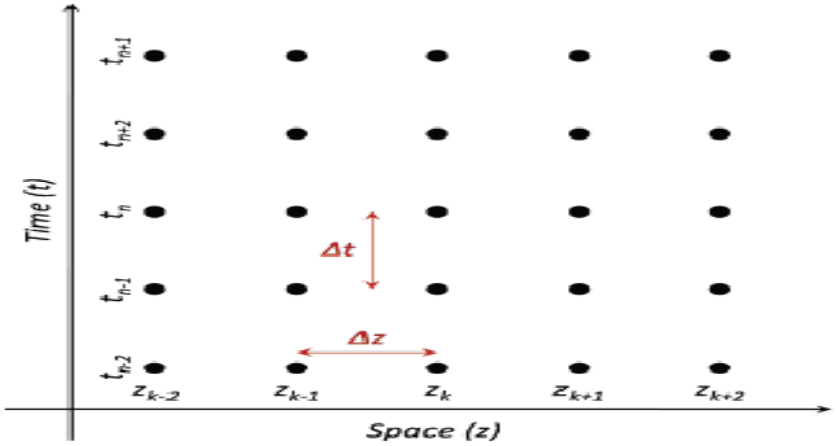

Figure 3(o): A simple FDTD mesh defined in space and time [35].

Now that the voltage and current functions have been sampled on a discrete, finite grid, we are ready to define a stencil, which is simply a numerical approximation for the derivative that uses neighboring points along the mesh. For example, the spatial derivative acting on the voltage function can be approximated through the use of forward finite-difference:

$$\frac{\partial v(z,t)}{\partial z} \approx \frac{v(z+\Delta z,t)-v(z,t)}{\Delta z} \qquad (3af)$$

At this point, it is convenient to introduce a more compact notation for the function v (z_k, t_n) by simply shortening it to v_k^n. In other words, the subscript index represents the spatial grid point, while the superscript index represents the temporal grid point. Using this notation, the numerical derivative is rewritten as

$$\frac{\partial}{\partial x} v_k^n \approx \frac{v_k^{n+1}-v_k^n}{\Delta z} \qquad (3ag)$$

Note that as long as the difference length A_z is very small, this approximation can provide us with reasonably accurate results. Nevertheless, we still would like to minimize the error from this approximation. It is therefore best to approximate all of our derivatives by using the central-difference method because it is more accurate than either forward or backwards-differences [36].We shall therefore impose the approximation

$$\frac{\partial}{\partial x} v_k^n \approx \frac{v_{k+1}^n - v_{k-1}^n}{2\Delta z} \qquad (3ah)$$

Similarly, the same approximation to the time-derivatives can be applied. For example, the time derivative on the current function i (z, t) can be rewritten as

$$\frac{\partial}{\partial t} i_k^n \approx \frac{i_k^{n+1} - i_k^{n-1}}{2\Delta t} \qquad (3ai)$$

Using these new expressions, the telegrapher's equations are to be transformed into a pair of coupled, finite-difference equations. In terms of the new stencil notation, this is written as

$$-\frac{v_{k+1}^n - v_{k-1}^n}{2\Delta z} = R' i_k^n + L' \frac{i_k^{n+1} - i_k^{n-1}}{2\Delta t} \qquad (3aj)$$

$$-\frac{i_{k+1}^n - i_{k-1}^n}{2\Delta z} = G' i_k^n + C' \frac{v_k^{n+1} - v_k^{n-1}}{2\Delta t} \qquad (3ak)$$

The voltage mesh is staggered from the current mesh in both space and time by the convention

$v_k^n = v_{k+1/2}^n$ and $i_k^n = i_{k+1/2}^n$. and is shown in figure 3(p) also.

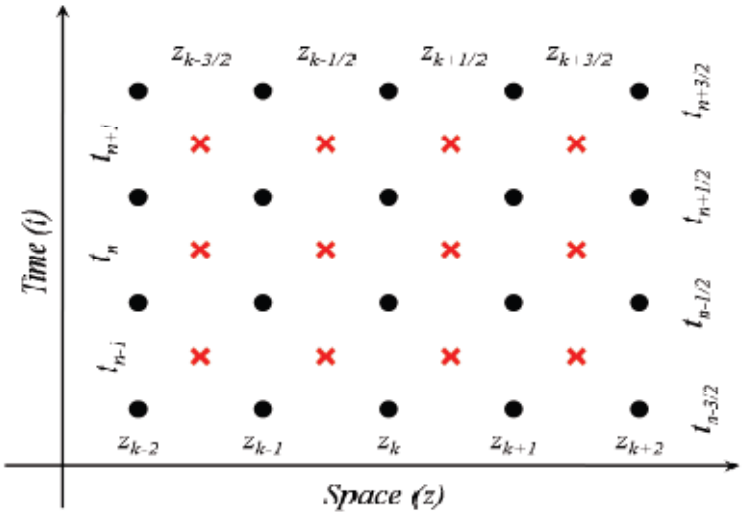

Figure 3(p): Revised FDTD mesh using the staggered grid [35].

The reason for redefining the meshes this way is so that we can approximate the spatial derivative on v as

$$\frac{\partial}{\partial t} v_k^n \approx \frac{v_{k+1/2}^n - v_{k-1/2}^n}{\Delta z} \qquad (3al)$$

Similarly the temporal derivative on the current is approximated by centering around the nth time step using

$$\frac{\partial}{\partial t} i_k^n \approx \frac{i_k^{n+1} - i_k^{n-1}}{\Delta t} \qquad (3am)$$

Applying these to (3ab) and (3ac) new set of finite difference equations becomes

$$\frac{v_{k+1/2}^n - v_{k-1/2}^n}{\Delta z} = R' i_k^n + L' \frac{i_k^{n+1/2} - i_k^{n-1/2}}{\Delta t} \qquad (3an)$$

$$-\frac{i_{k+1}^{n+1/2} - i_k^{n-1/2}}{\Delta z} = G' v_{k+1/2}^{n+1/2} + C' \frac{v_{k+1/2}^{n+1} - v_{k+1/2}^n}{\Delta t} \qquad (3ao)$$

3.3.2 Update Equations

The key concept behind the FDTD algorithm is to begin with some given "present" state for a system and then solve for the nearest "future" state. This is accomplished by taking the numerical telegrapher's equations and solving for the "future" terms.

$$i_k^{n+1/2} = c_1\left(v_{k+1/2}^n - v_{k-1/2}^n\right) + c_2\left(i_k^{n-1/2}\right) \quad (3ap)$$

and

$$v_{k+1/2}^{n+1} = c_3\left(i_{k+1}^{n+1/2} - i_k^{n+1/2}\right) + c_4\left(v_{k+1/2}^n\right) \quad (3aq)$$

Where

$$c_1 = -\frac{2\Delta t}{\Delta t \Delta z R' + 2\Delta z L'} \qquad (3ar)$$

$$c_2 = \frac{2L' - \Delta t R'}{2L' + 2\Delta t R'} \qquad (3as)$$

$$c_3 = -\frac{2\Delta t}{\Delta t \Delta z G' + 2\Delta z C'} \qquad (3at)$$

$$c_4 = \frac{2C' - \Delta t G'}{2C' + \Delta t G'} \qquad (3au)$$

The importance of equations (3ap) and (3aq) is that they provide a way to solve for the future state of the system in terms of surrounding points in space and time. A summary of the algorithm is provided as follows:

- Instantiate the samples of voltage and current over the simulation domain to their initial values.
- Loop over all values of k and solve for the future state of the current.
- Loop over all values of k and solve for future state of the voltage.
- Increment n.
- Process the new state of the system (ie, plot a graph, compute power flow, etc).

- If n is greater than the desired simulation time N, terminate the loop. Else, return to 2nd step.

This is the algorithm to initialize the FDTD grid given E and H at t=0 and then to update the grid till the defined time steps.

3.4 Plane Wave Expansion Method

The discovery of photonic crystals, periodic materials with photonic band gap, has opened up new methods for controlling light. In order to design photonic crystals to take advantage of their unique properties, a calculation method is necessary to determine how light will propagate through a particular crystal structure. Specifically, given any periodic dielectric structure, the allowable frequencies also known as eigen frequencies or eigen modes for light propagation in all crystal directions must be detected and the field distributions in the crystal for any frequency of light must be calculated. There are several capable techniques, but one of the most studied and reliable method is the plane wave expansion method. It was used in some of the earliest studies of photonic crystals and is simple enough to be easily implemented. The method allows the computation of eigen frequencies for a photonic crystal to any prescribed accuracy, commensurate with computing time.

The plane wave expansion (PWE) method [37] is for the band structure calculations of the general periodic structures, where the structures extend periodically in all dimensions. Plane wave expansion method refers to a computational technique in electromagnetics to solve the Maxwell's equations by formulating an eigen value problem [38] out of the equation. This method is popular among the photonic crystal community as a method of solving for the band structure or the dispersion relation of specific photonic crystal geometries. PWE is traceable to the analytical formulations, and is useful in calculating modal solutions of Maxwell's equations over an inhomogeneous or periodic geometry. It is specifically tuned to solving problems in time-harmonic forms, with non-dispersive media.

The Maxwell equation in a transparent, time-invariant, source free and non-magnetic medium can be written in the following form:

$$\nabla \times \frac{1}{\varepsilon(\vec{r})} \nabla \times \vec{H}(\vec{r}) = \frac{\omega^2}{c^2} \vec{H}(\vec{r}) \qquad (3av)$$

Where $\varepsilon(\vec{r})$the space dependent dielectric function, c is is speed of light in vacuum and $\vec{H}(\vec{r})$is the optical magnetic field vector of a definite frequency ω with time dependence e^{iwt}.

This equation is sometimes called master equation [38] and represents a Hermitian Eigen problem [38] which could not be said if the wave equation were derived in terms of the electric field.

The Bloch theorem [39] says that due to the infinite periodicity, the magnetic field will take a form of

$$\vec{H}(\vec{r}) = e^{i\vec{k}\vec{r}}\vec{h}_k(\vec{r}), \qquad (3aw)$$

Where $\vec{h}(\vec{r}) = \vec{h}(\vec{r} + \vec{R})$for all combinations of lattice vectors $\vec{R}$. Thus we end up with the master equation in operator form:

$$(\nabla + i\vec{k}) \times \left\{\frac{1}{\varepsilon(\vec{r})}(\nabla + i\vec{k})\right\} \times \vec{h}_k = \frac{\omega^2}{c^2}\vec{h}_k \qquad (3ax)$$

This is the fundamental equation, which needs to be solved. The equation is transformed into a finite problem by expanding the magnetic field in a finite basis of simple plane waves. Different approaches can be explored to solve the final discretized problem. The result of solving the discretized problem is the dispersion relationship between the frequencies of the modes and wave vector $\overrightarrow{R}$, usually plotted in the form of a band diagram.

PWE expansions are rigorous solutions. PWE is extremely well suited to the modal solution problem. Large size problems can be solved using iterative techniques. For both generalized and normal eigen value problems, just a few band index plots in the band-structure diagrams are required, usually lying on the brillouin zone edges [39]. This corresponds to eigen modes solutions using iterative techniques, as opposed to diagonalization of the entire matrix.

Though plane wave method is quite successful in photonic band gap calculations, it has several limitations. The computation grows exponentially when the problem size increases. For complicated problems, such as three dimensional photonic band gap calculations, the computation is intensive. A less computationally intensive eigen solver is critical to reduce computation effectively.

CHAPTER 4

SIMULATIONS AND RESULTS

In this chapter, the one dimensional and two dimensional photonic crystals has been designed and modeled. After that the photonic crystal fiber has been designed as a holey fiber. All the structures are designed as a finite difference time domain model using the LAYOUT DESIGNER of OptiFDTD tool. The PROFILE DESIGNER of OptiFDTD tool has been used to define channel as well as material, with user defined refractive index, that is used to design the structure. OptiFDTD Analyzer is used to study the transmittance and reflectance properties of the design and PWE Band Solver is used to study the band gap characteristics of the design. The anisotropic perfectly matched layers (APML) have been used as boundary conditions in all the designs

4.1 One Dimensional Photonic Crystal Design

The one dimensional photonic crystal consisting of alternating layers of materials is known as Braggs Grating Crystal. The Bragg Grating Crystal that consists of alternating layers with permittivity contrast 1/13 has been designed using the OptiFDTD Layout Designer.

The waveguide channel is defined to be the material of refractive index 3.6056 or permittivity 13 and the default wafer material is air with refractive index or permittivity 1. Hence alternating layers of materials having permittivity contrast 1/13 forms the layout of crystal. This crystal structure is also known as Braggs grating crystal. The waveguide width is 10μm and wafer dimensions are 10μm × 10μm.

The layout is drawn taking the default rectangular lattice and specify the Lattice dimensions (1, 1, 8). This will create 1D lattice with 8 unit cells along Z-direction i.e the horizontal direction. Center the lattice on the layout by setting the origin as (2, 0) (horizontal, vertical). New linear waveguide atom is added to each of the 8 unit cells. The input wave is taken to be continuous wave with wavelength 1.5μm. The input plane is placed at z-position 0.625μm. The layout is shown in figure 4(a).

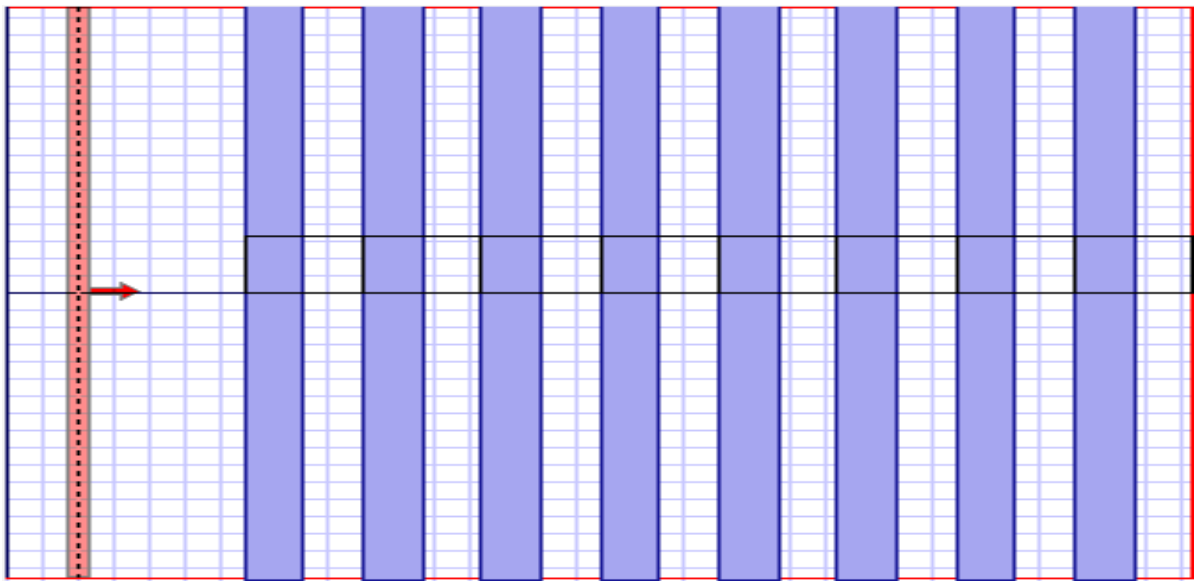

Figure 4(a): Layout of one dimensional photonic crystal.

In the layout the vertical dotted line having arrow at its centre is the input plane and the eight alternate vertical lines are unit cells of 1D lattice having refractive index 3.6056 or permittivity 13 and the base material of 1D lattice as shown by crossed area in between the shaded lines is the default material air with permittivity 1. Hence the permittivity contrast of 1/13 is formed in the design.

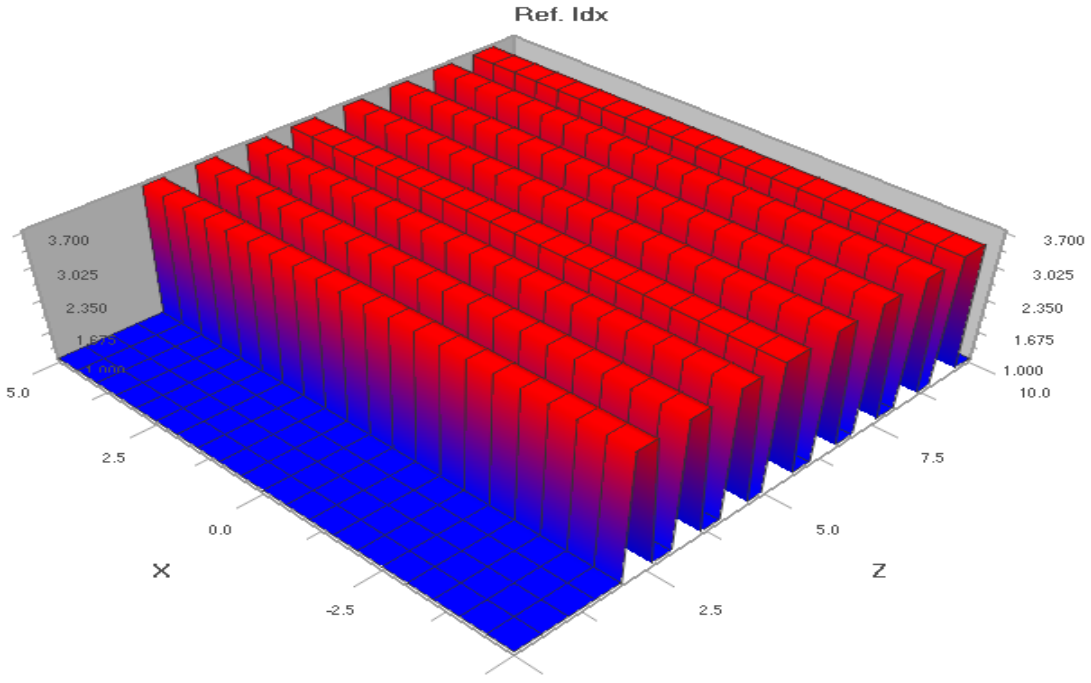

Figure 4(b): Refractive index distribution profile of one dimensional photonic crystal.

To observe the transmittance and reflectance properties of the defined structure, the FDTD simulation is done taking the TE waves. The mesh delta size is 0.1µm × 0.1µm and numbers of mesh cells are 100 × 100. The minimum memory requirements are 36.54MB and wafter size is 10µm × 10µm as already defined. The simulation is done for 3000 time steps. The refractive index distribution profile for the structure is shown in figure 4(b).

The amplitude variation of Discretized Fourier Transform (DFT) output of all the components of TE wave and the poynting vector with the variations in Z-direction (position) at the end of simulation has been shown below.

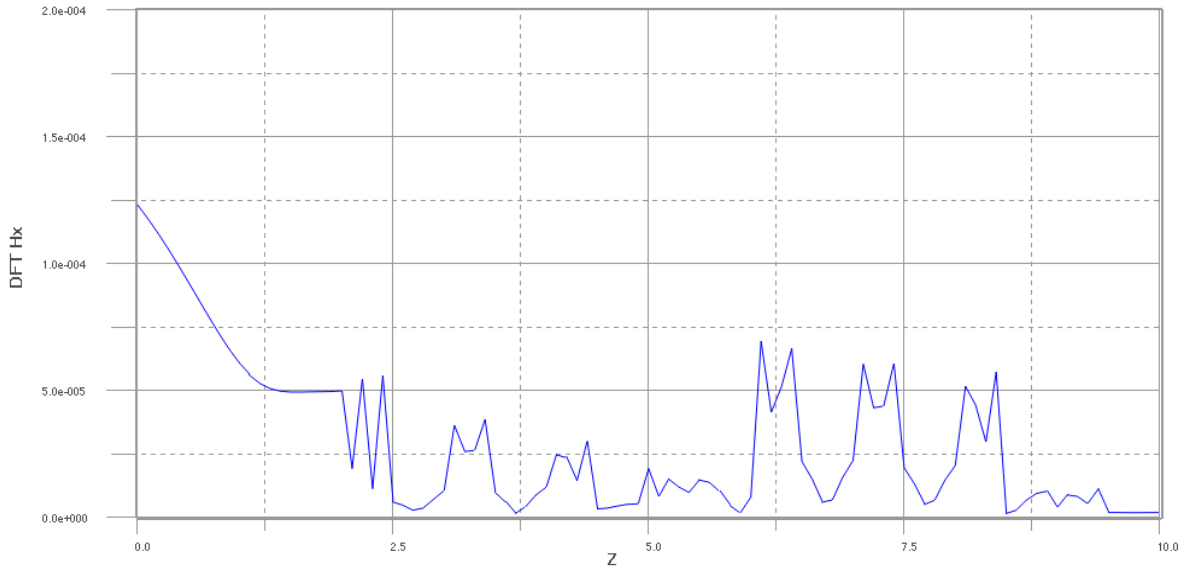

Figure 4(c): DFT output of amplitude variation of H_x along horizontal plane.

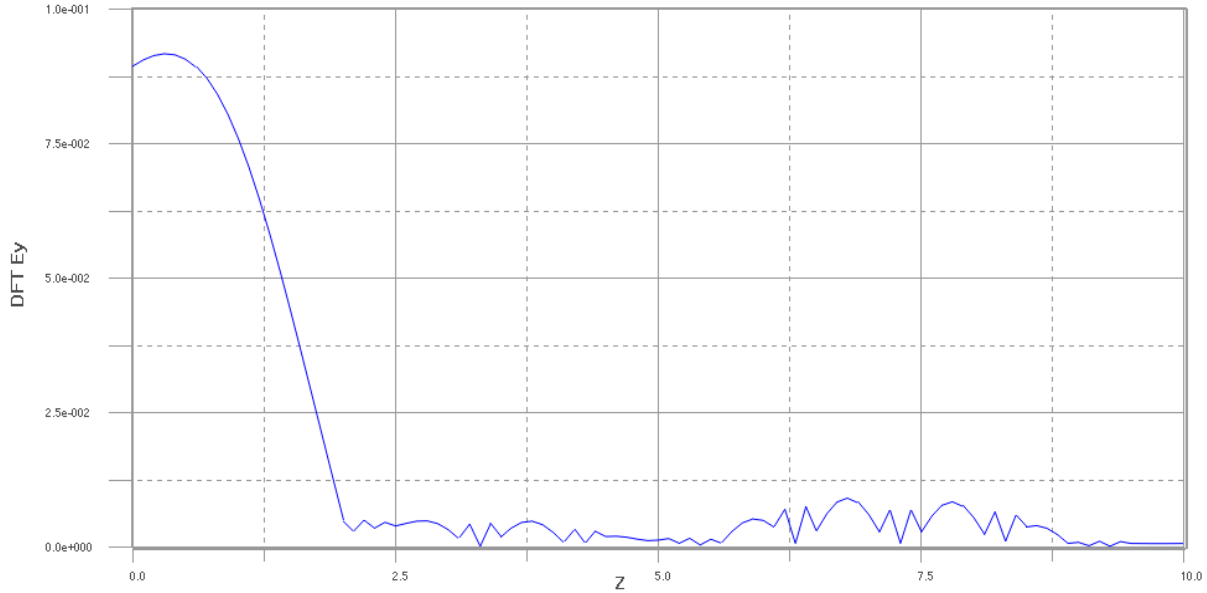

Figure 4(d): DFT output of amplitude variation of E_y along horizontal plane.

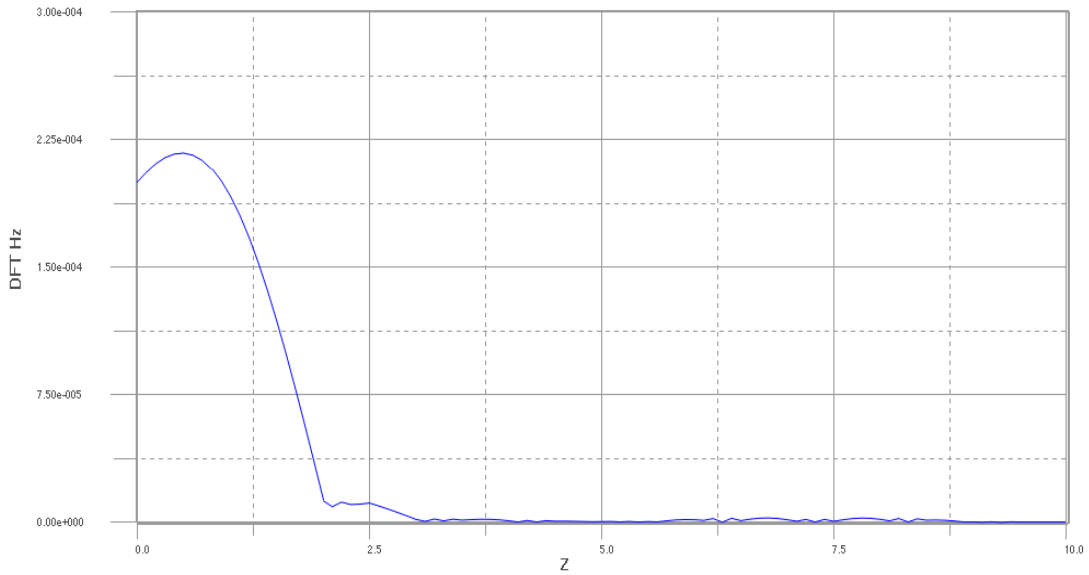

Figure 4(e): DFT output of amplitude variation of H_z along horizontal plane.

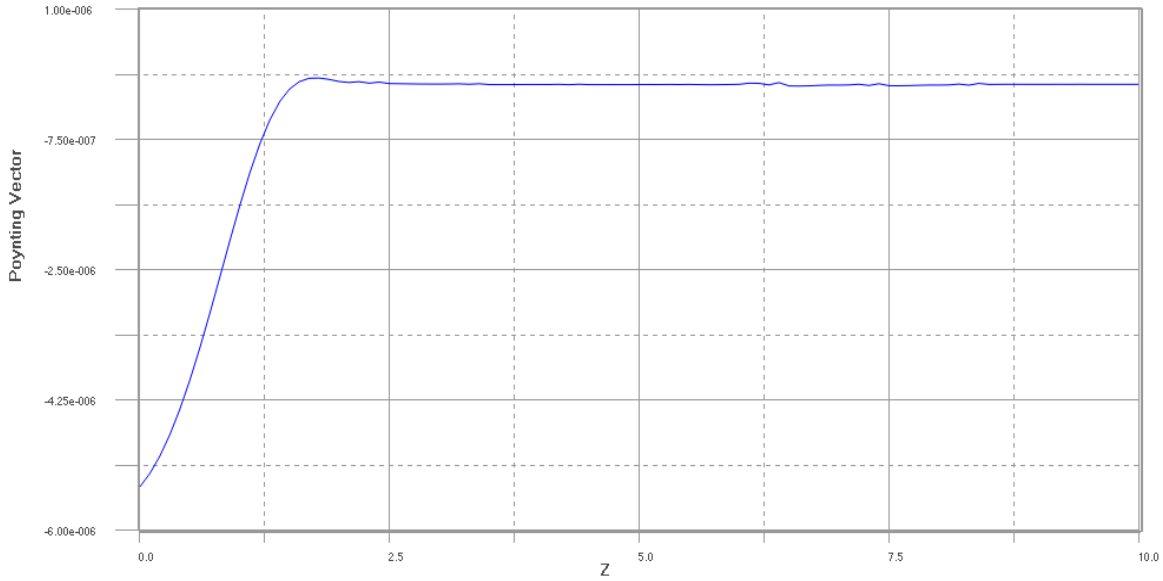

Figure 4(f): Variation of poynting vector along horizontal plane.

These outputs indicate how the wave components will be varied for the designed photonic structure, that is how the electric and magnetic field components are varied with horizontal plane. It has been observed that the DFT amplitude is maximum at beginning and goes on falling as soon as the wave falls on the first horizontal layer and after that minor variations are there as the wave passes through the alternating layers of air and defined material. It is seen that variations of H_x component are more verse as compared to others because the input wave is along x-direction. Figure 4(f) shows the variations of poynting vector that is minimum at

beginning, goes on increasing and attains a nearly steady state value as soon as wave falls on first horizontal layer.

Next the band gap characteristics of defined photonic band gap structure are observed and it is done by Plane Wave Expansion (PWE) method. The PWE band solver simulation is done for the same and band gaps are observed. The PWE band solver has taken 1D structure and TE polarization. The mesh delta size is taken to be 0.0625µm in vertical direction and numbers of mesh steps are taken as 16. For the tolerance value 0.1 the band solver output is as follows

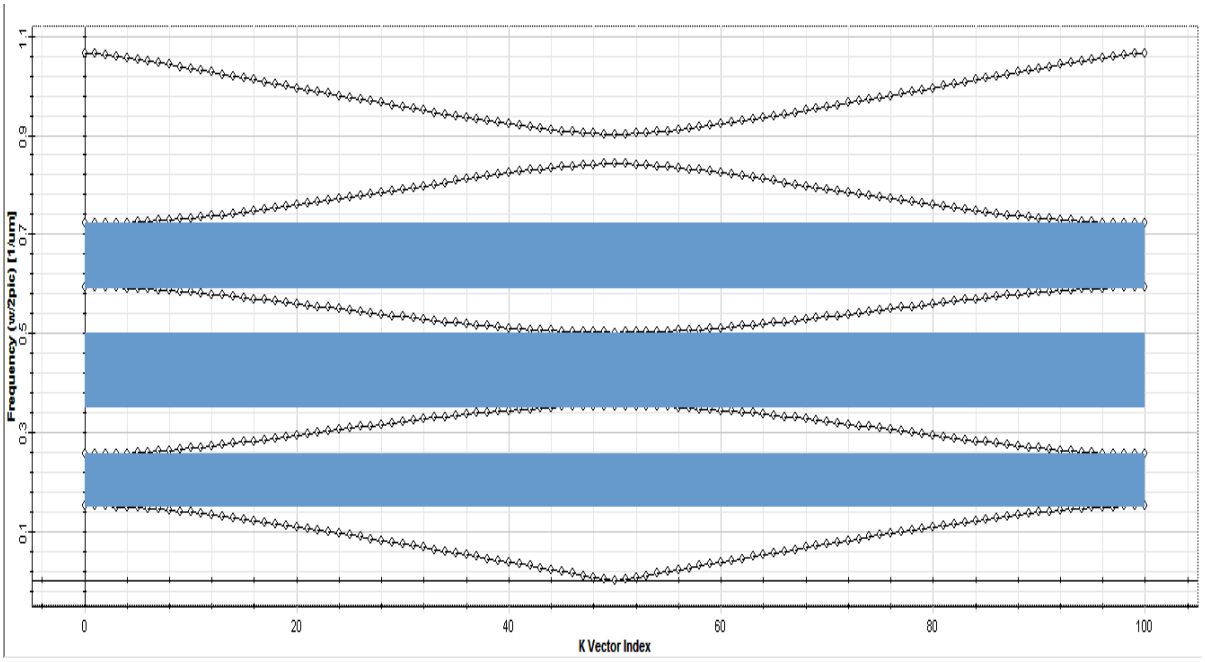

Figure 4(g): Band diagram of 1D photonic crystal.

Three band gaps are found as shown by shaded area in the graph. The number of band gaps found could depend on tolerance value. The band gap result summary is shown below

```
Simulation ... OK:
Tolerance = 0.1: Band gap(s) found = 3:
Band gap 0: (0.151232, 0.256058), gap = 0.104826:
Band gap 1: (0.353862, 0.501916), gap = 0.148053:
Band gap 2: (0.592998, 0.721837), gap = 0.128839:
```

Figure 4(h): Band Gap result summary of 1D photonic crystal.

So the band gap defines the frequency range for the design corresponding to which the wave gets strongly reflected. For all three frequency range or band gaps as shown in figure 4(h), the input wave having frequency within these ranges will get strongly reflected.

4.2 Two Dimensional Photonic Crystal Design

The first and foremost reason to consider a two dimensional photonic crystal design is to improve the band gap as the band gap for the one dimensional structure is considerably high even by optimizing the refractive index profile of the channel.

The 2D rectangular lattice photonic crystal that consists of alternating layers in both horizontal and vertical directions with permittivity contrast 1/8.9 has been designed in the OptiFDTD designer. OptiFDTD analyzer is used to observe the transmittance and reflectance properties of the design and PWE Band Solver is used for the band gap characteristics of the design.

The waveguide channel is defined to be the material of refractive index 2.98 or permittivity 8.9 and the default wafer material is air with refractive index or permittivity 1. Hence alternating layers of materials having permittivity contrast 1/8.9 in both horizontal and vertical direction forms the layout of the design. The waveguide width is 1µm and wafer dimensions are 10µm × 10µm that are same as the one dimensional design.

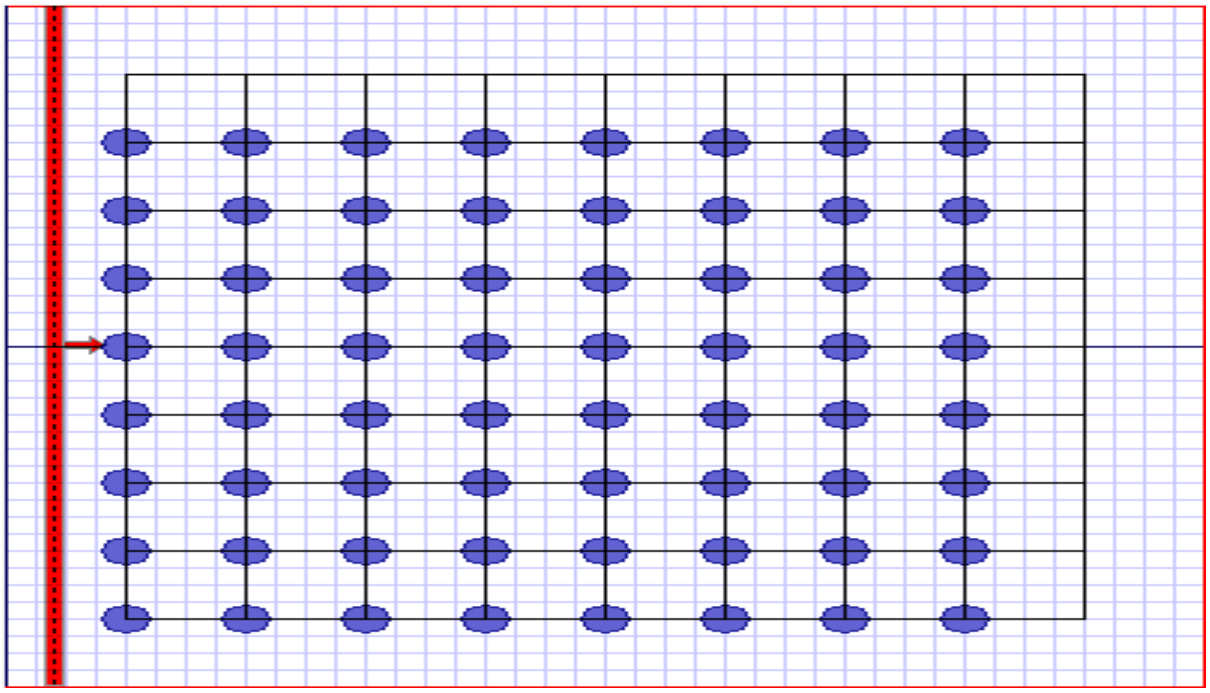

Figure 4(i): Layout of two dimensional photonic crystal.

Next step is to create 2D rectangular lattice with alternating layers in horizontal and vertical directions represented by elliptical waveguides. So the 2D layout is drawn taking the default rectangular lattice and specify the Lattice dimensions (8, 1, 8). This will create 2D lattice with 8 unit cells along X and Z direction i.e the vertical and horizontal direction respectively. Center the

lattice on the layout by setting the origin as (2, 0) (horizontal, vertical). New elliptical waveguide atom is added to each of the unit cells.

The input wave is taken to be continuous wave with wavelength 1.55µm. The input plane is placed at Z-position 0.40µm. The layout is shown in figure 4(i).

In the layout the vertical dotted line having arrow at its centre is the input plane and the dotted points are unit cells of 2D lattice having refractive index 2.98 or permittivity 8.9 and the base material of 2D lattice as shown by crossed area in between the dotted points is the default material air with permittivity 1. Hence the permittivity contrast of 1/8.9 is formed in the design.

To observe the transmittance and reflectance properties of the defined structure, the 2D simulation is done taking the TM waves. The mesh delta size is 0.05µm × 0.05µm and numbers of mesh cells are 200 × 200. The minimum memory requirements are 37.80MB and wafer size is 10µm × 10µm as already defined. The simulation is done for 1000 time steps.

Here is the refractive index distribution profile for the structure.

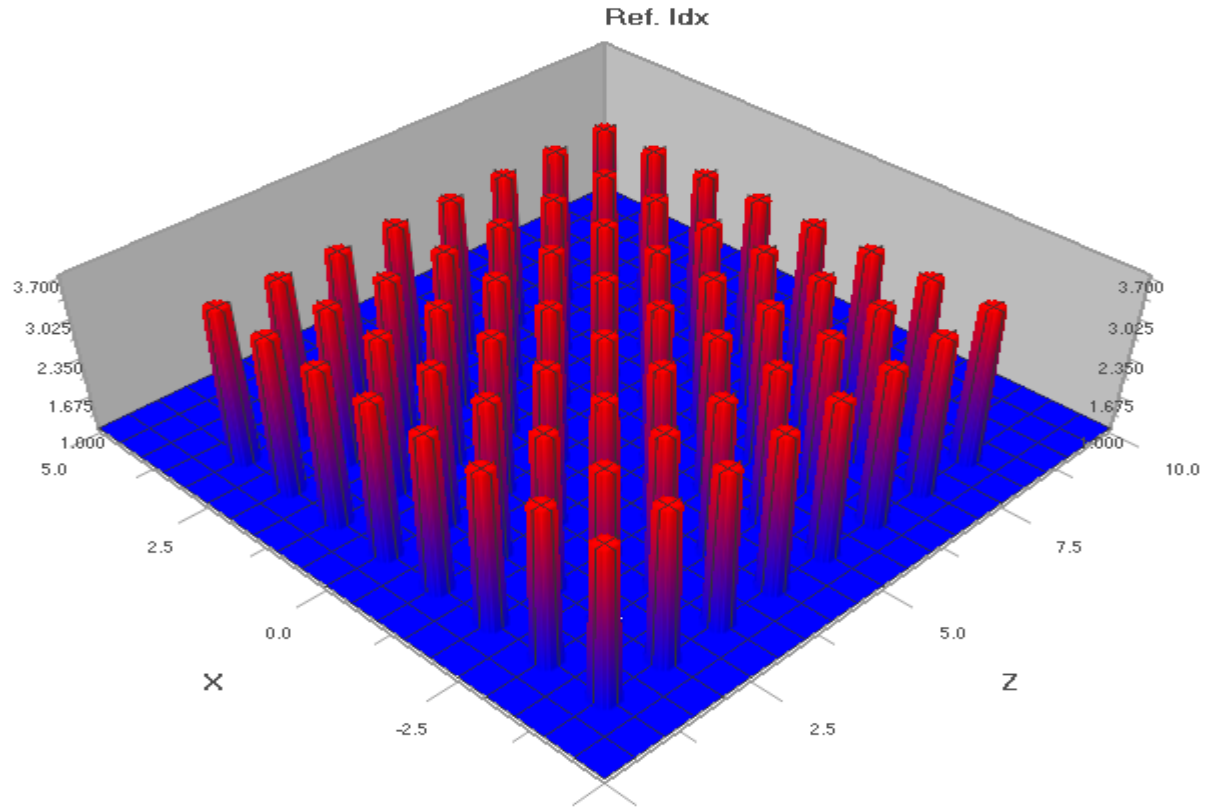

Figure 4(j): Refractive index distribution profile of one dimensional photonic crystal.

The amplitude of Discretized Fourier Transform (DFT) output of all the components of TM wave and the poynting vector with the variations in Z-direction (position) at the end of simulation has been shown below.

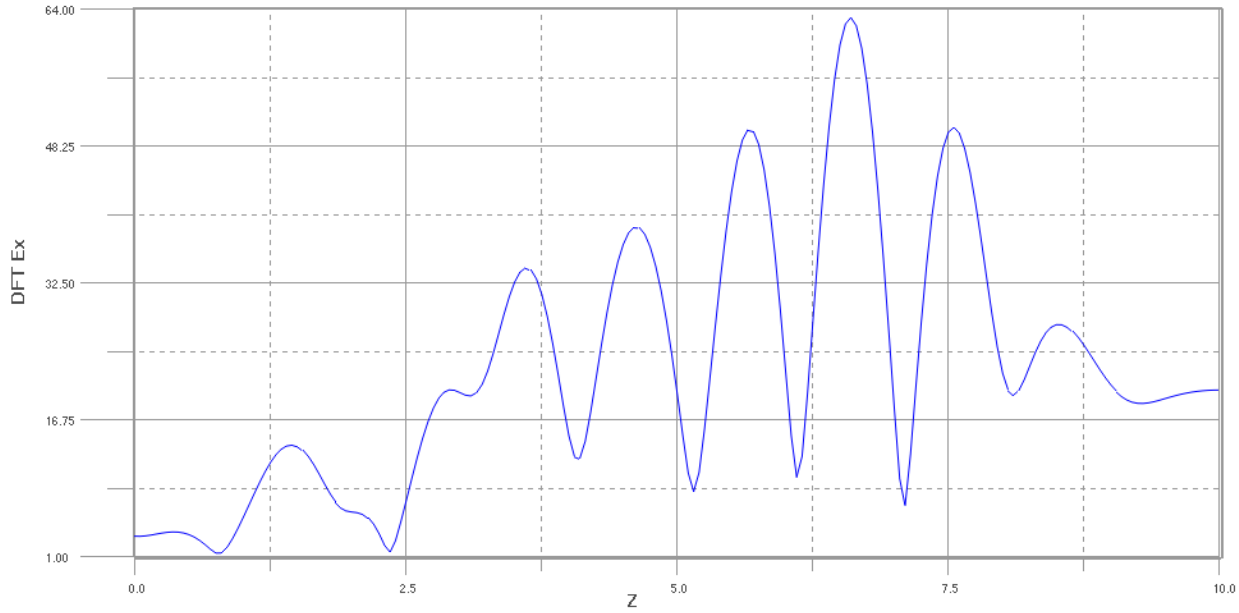

Figure 4(k): DFT output of amplitude variation of E_x along horizontal plane.

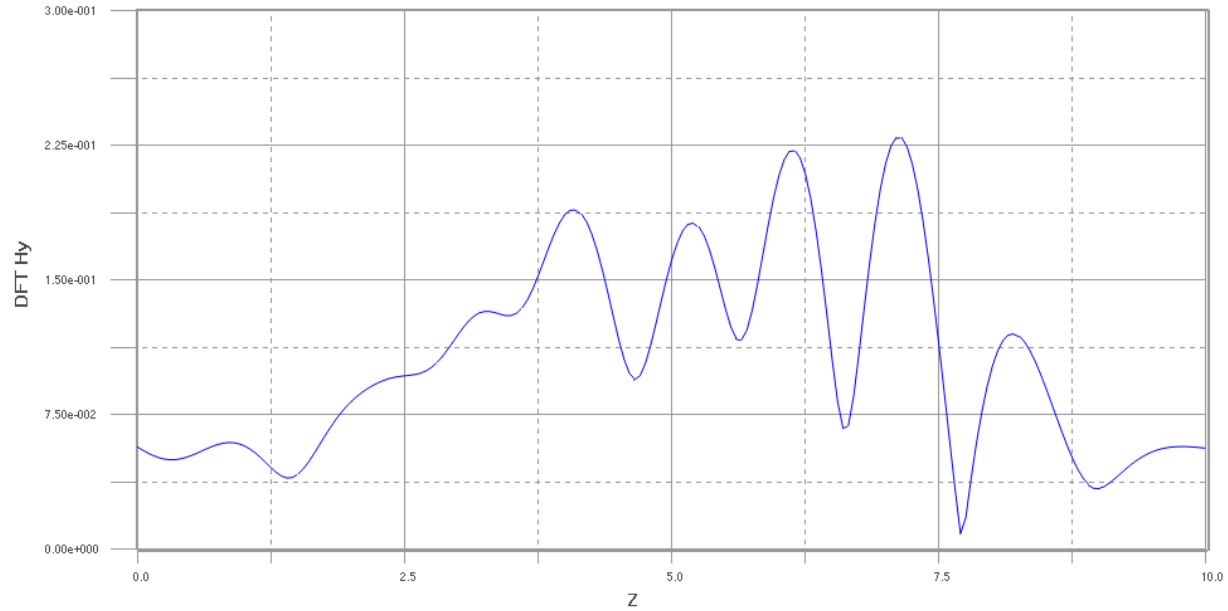

Figure 4(l): DFT output of amplitude variation of H_y along horizontal plane.

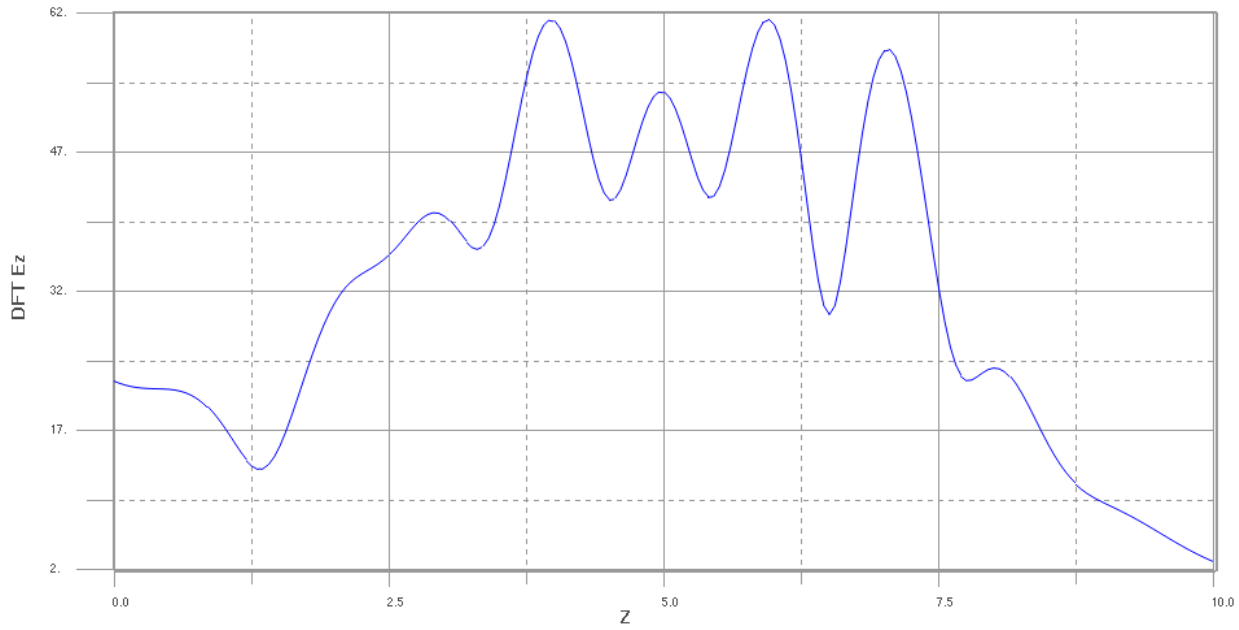

Figure 4(m): DFT output of amplitude variation of E_z along horizontal plane.

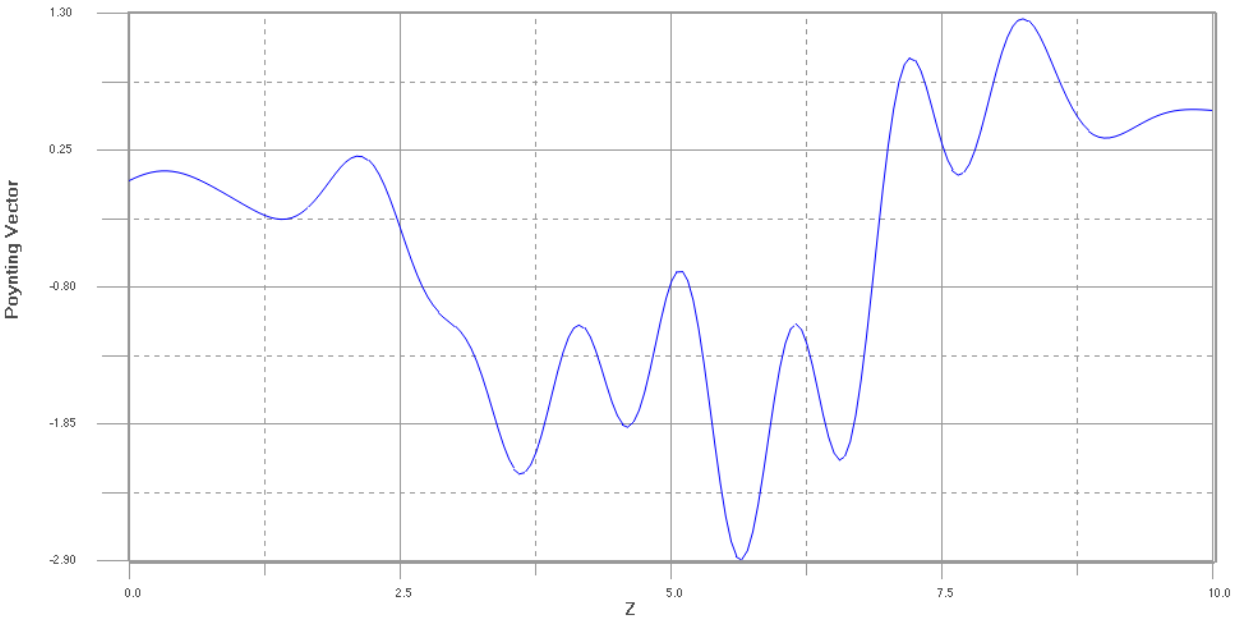

Figure 4(n): Variation of poynting vector along horizontal plane.

These outputs indicate how the TM wave components will be varied along horizontal plane for the designed photonic structure. It has been observed that the DFT amplitude variations are more verse at centre. It is seen that variations of all component are nearly same and E_z component has minimum value at the end which indicates that the electric field component of input wave in z direction will attain a minimum value. Figure 4(n) shows the variations of poynting vector that attains a negative value at centre due to intense variations of electric and magnetic field

components at centre but at the end the poynting vector achieves a positive value which is more than its amplitude at beginning.

Next the band gap characteristics of defined photonic band gap structure are observed and it is done by plane wave expansion method using PWE band solver. The PWE band solver simulation is done for the design and band gaps are observed. The PWE band solver has taken 2D structure and TE polarization. The mesh delta size is taken to be 0.0625 μm in horizontal and vertical direction and numbers of mesh steps are taken as 16 in both horizontal and vertical direction. For the tolerance value 0.1 the band solver output is shown below.

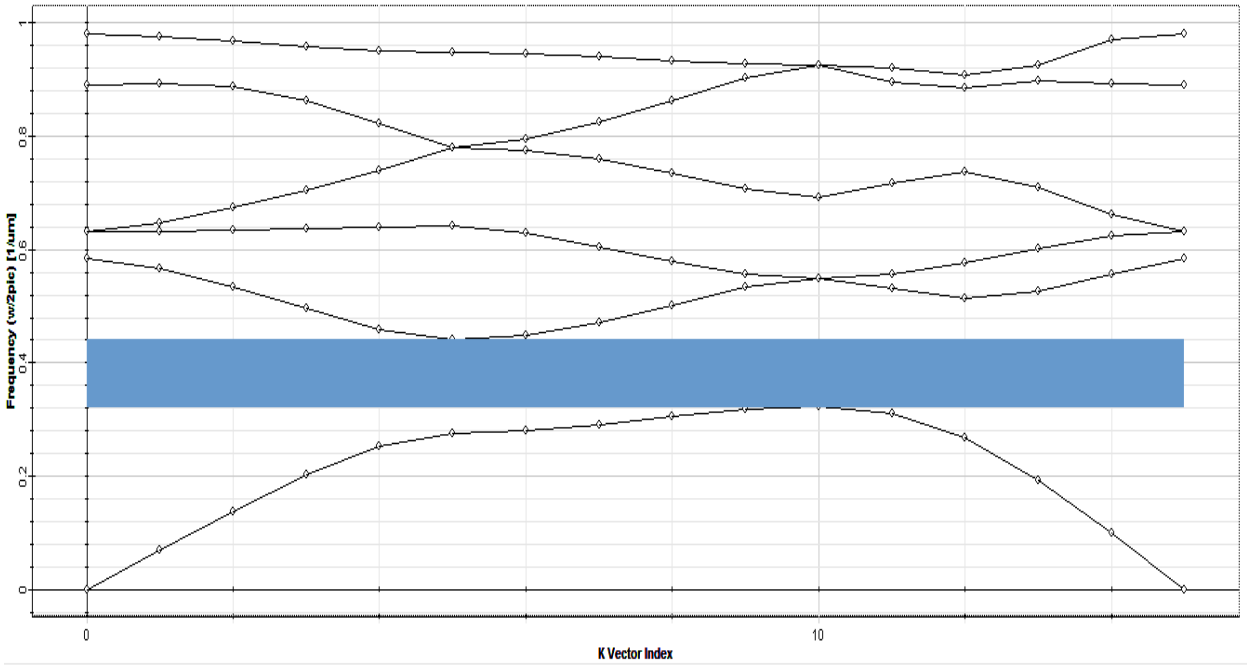

Figure 4(o): Band diagram of 2D photonic crystal.

Only one band gap is found as shown by shaded area in the graph. The tolerance value is same as taken in one dimensional design. The band gap result summary is shown below.

Figure 4(p): Band Gap result summary of 2D photonic crystal.

It is seen that the band gap characteristics are much improved by migrating to 2D design. Only a single band gap is found in the 2D design. Hence only the wave having frequency within this single range would get strongly reflected if made to fall on the designed photonic crystal.

4.3 Photonic Crystal Fiber Design

The design work for PCF starts from defining a rectangular structure as done for photonic crystals and then to modify it by defining the core region and the layers in such a way to confine the modes within the fiber.

The cladding of PCF comprises 2D hexagonal lattice consists of alternating layers in both horizontal and vertical directions with permittivity contrast 1/2.13 has been designed in the OptiFDTD designer. OptiFDTD analyzer is used to study the TE input wave behavior in terms of its components and poynting vector and PWE Band Solver is used to study the band gap characteristics of the design. The LAYOUT DESIGNER has been used to define the PCF layout. In case of PCF, the wafer as well as the waveguide channel materials and their properties are defined in variable form for convenience. The variables are

Table 4.1: Variables for Waveguide and Wafer Materials and Properties.

Name	value	Definition
a	2.3um	Lattice constant
b	a*sin(pi/3)	Height of triangle cell
lngth	11*a	Length of domain
wdth	11*b	Width of domain
c	-5*b	Original point of lattice
R	0.6um	Radius of air hole

All these variables are defined initially in Variables and Functions of layout designer before defining the wafer and channel properties.

The channel is defined to be the material of refractive index 1.46 or permittivity 2.13 and the default wafer material is air with refractive index or permittivity 1. The waveguide width is 0.6μm and wafer dimensions are lngth × wdth that are in form of predefined variables.

Next step is to create 2D hexagonal lattice with alternating layers in horizontal and vertical directions represented by elliptical waveguides. So the layout is drawn taking the default rectangular lattice and specify the Lattice dimensions (11, 1, 12). This will create the specified unit cells in defined directions. New elliptical waveguide atom is added to each of the unit cells.

The initial layout is in the form as shown in figure 4(q)

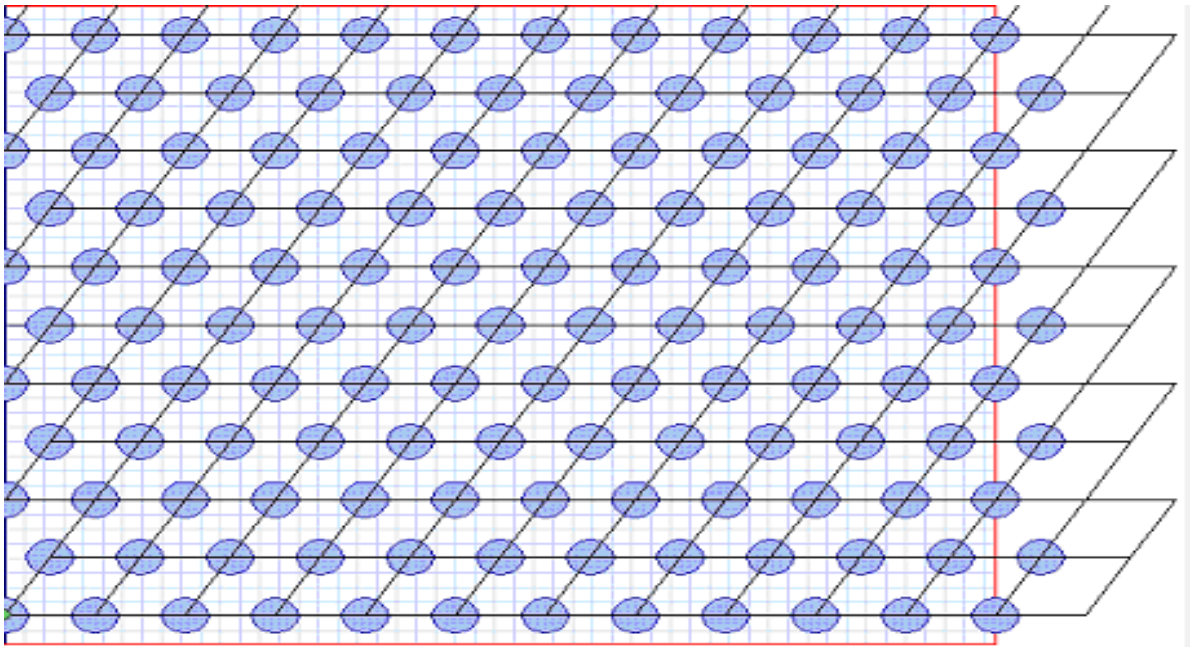

Figure 4(q): Initial layout for the PCF design.

Next step is to define the core region of the PCF as well as the layers for a holey PCF. Since number of cells along vertical direction is 11, a maximum of five layers can be defined for which the desired cells are made off or disappear. To define the core region the centre cell is also made to disappear. One missing cell defines the core region. The layout of five layers holey PCF is shown below.

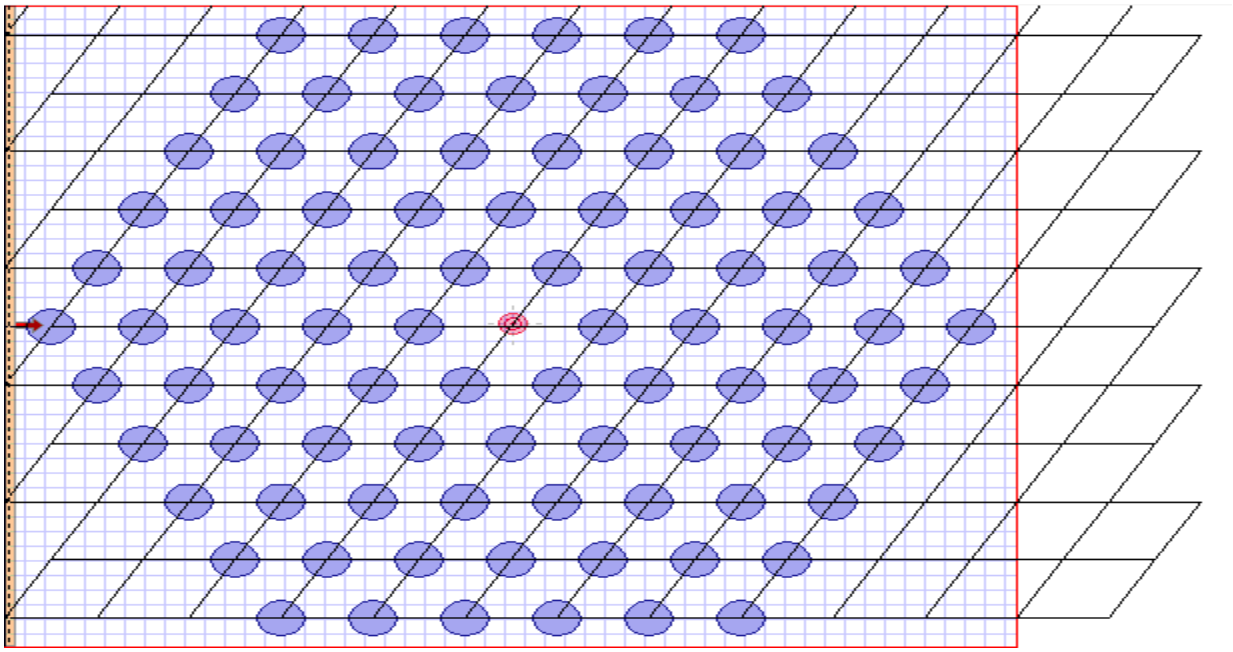

Figure 4(r): Layout of five layer PCF fiber.

The five layers have been defined only to confine the wave within the fiber. A point source having Gaussian modulated continuous wave of wavelength 1.3µm has been placed at the centre, to observe the refractive index distribution. The vertical input plane is also placed at z-position of 0.1µm having continuous wave of wavelength 1.55µm and is shown as a dashed line with arrow at its centre. The input plane has been defined is only for band analysis as PWE band solver does not works without the input plane.

To observe the wave behavior that is made to fall on defined PCF structure, the 2D simulation is done for the input point source at centre, taking the TE waves. The mesh delta size is 0.08µm × 0.08µm and numbers of mesh cells are 273 × 316. The minimum memory requirements are 39.64MB and wafer size is 25.30µm × 21.92µm as calculated from defined variables. The simulation is done for 1000 time steps. The refractive index profile is shown below.

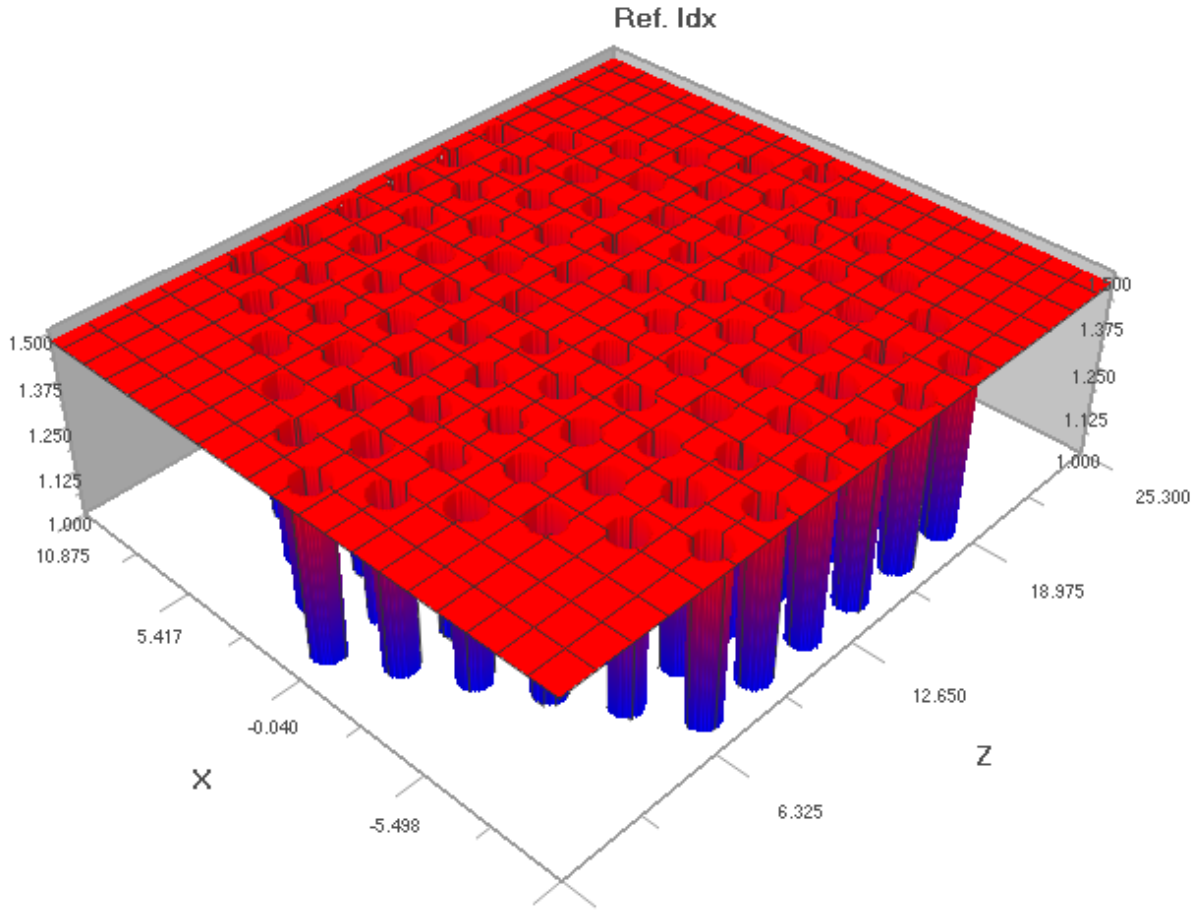

Figure 4(s): Refractive index distribution profile of PCF.

The amplitude of Discretized Fourier Transform (DFT) output of all the components of TE wave and the poynting vector with the variations in Z-direction (position) at the end of simulation has been shown below.

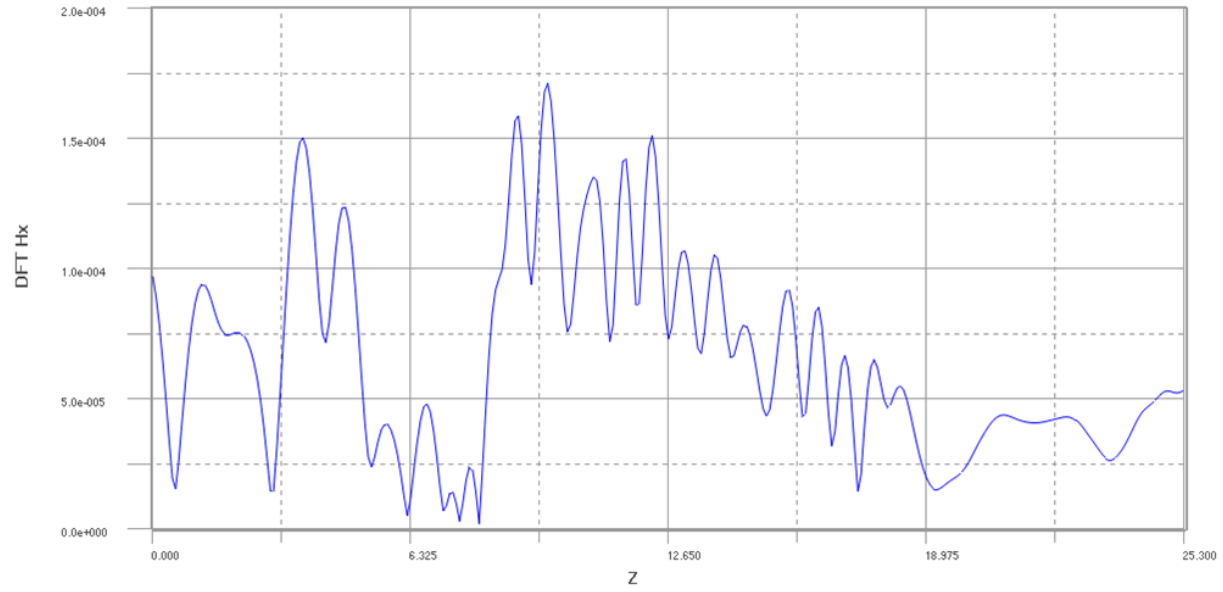

Figure 4(t): DFT output of amplitude variation of H_x along horizontal plane.

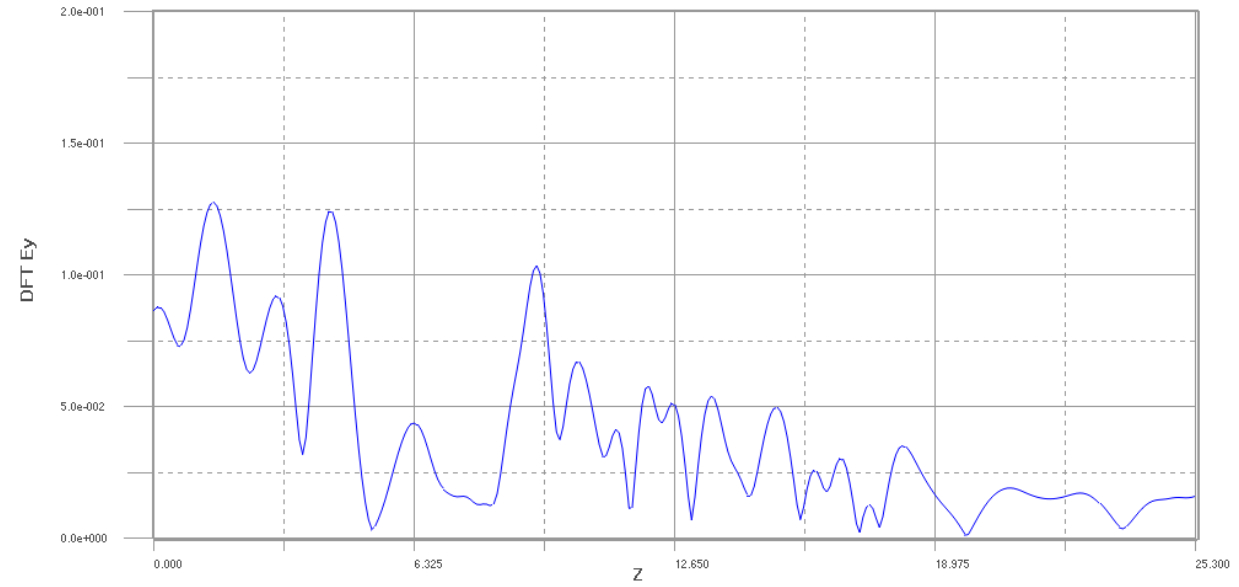

Figure 4(u): DFT output of amplitude variation of E_y along horizontal plane.

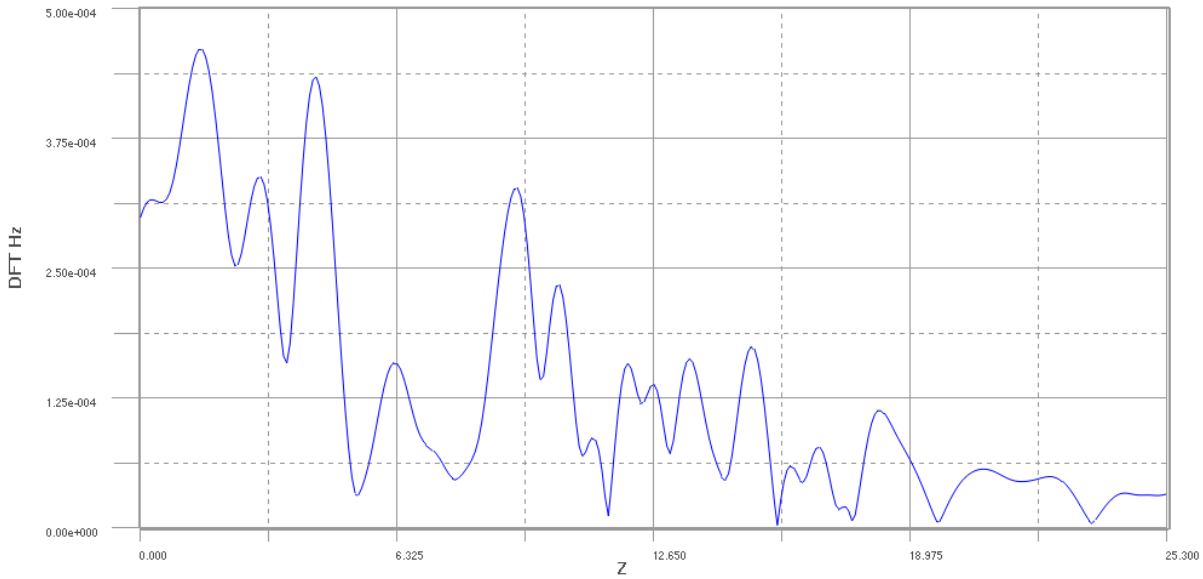

Figure 4(v): DFT output of amplitude variation of E_x along horizontal plane.

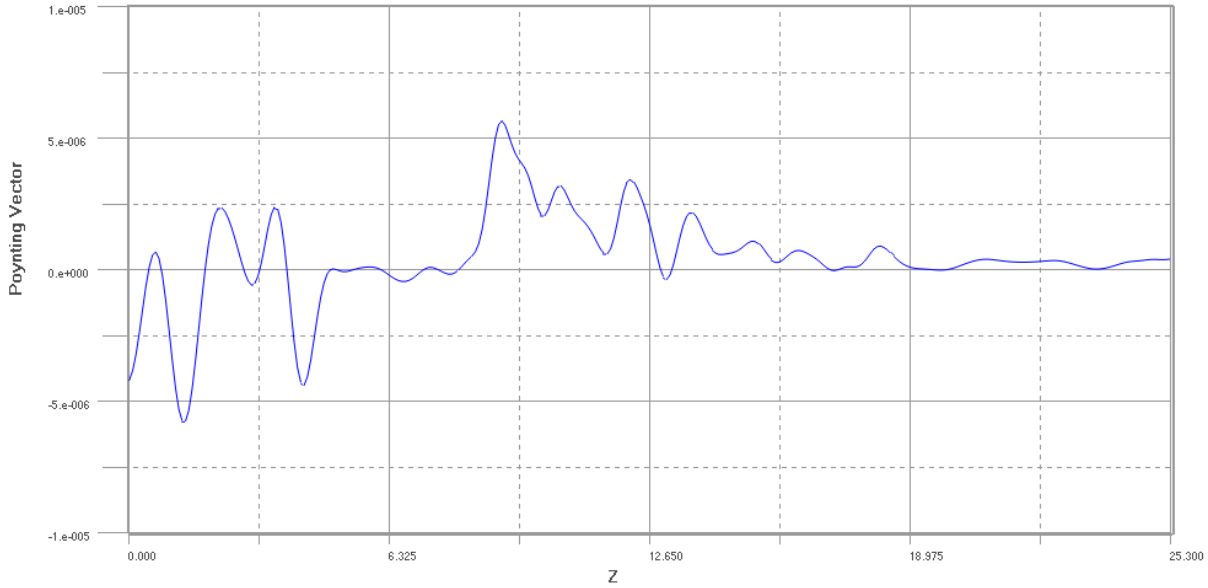

Figure 4(w): Variation of poynting vector along horizontal plane.

It has been observed that the DFT amplitude of all components undergoes high amount of variations from start till the end of simulation. Since the input source is taken at centre the wave components continues to vary right from the beginning however the magnetic field component has the maximum variation at centre as compared to other components. So the components shows that the TE wave will get propagation as well as reflection for the given wavelength as specified by the defined high and low variation of DFT amplitude.

Next is the band gap analysis of the PCF which is done by plane wave expansion method Using PWE Band Solver of optiFDTD tool. As already defined the vertical input plane must be considered for the band gap analysis.

The PWE band solver is made to run in 2D form and TE polarization. The mesh delta size is taken to be 0.14375 µm in horizontal and vertical direction and numbers of mesh steps are taken as 16 in both horizontal and vertical direction. For the tolerance value 0.01 the band solver output is shown below

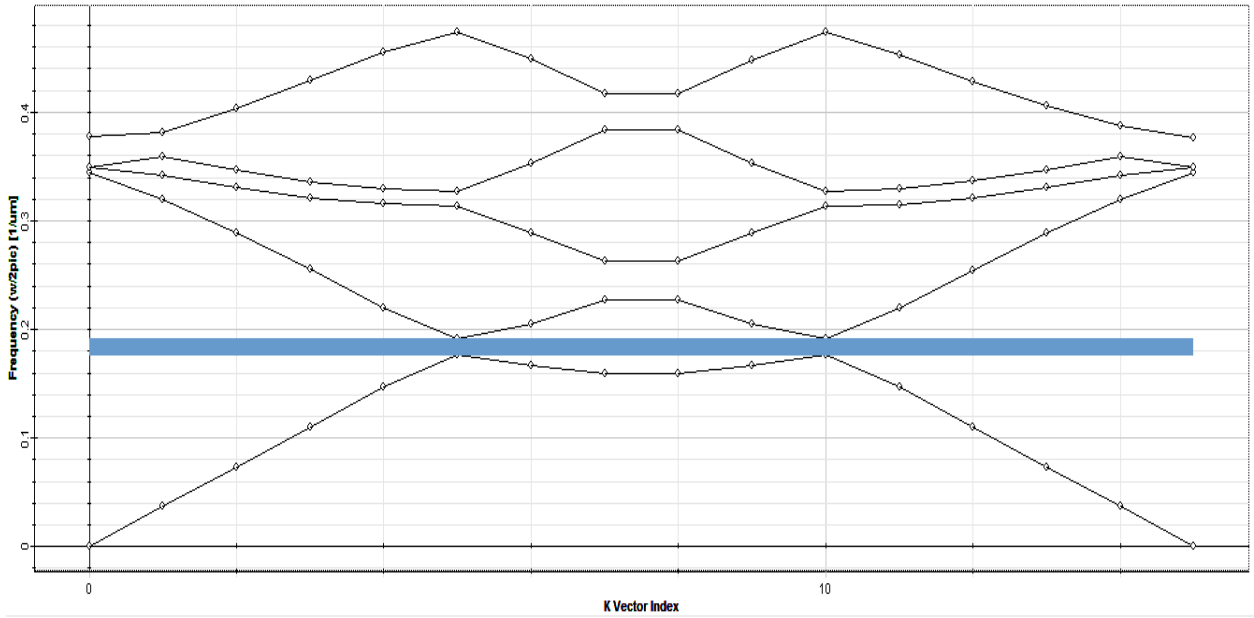

Figure 4(x): Band diagram of PCF.

It has been observed that band gap characteristics are far different from the cases of photonic crystals. Only one band gap has been found and that too is very narrow as compared to previous designs. As a result more combinations of input wave can be used for this PCF design, when used for Sensor applications, as the exceptional frequency range for input wave is very narrow, as shown by band gap result summary below.

```
Simulation ... OK:
Tolerance = 0.01: Band gap(s) found = 1:
Band gap 0: (0.176327, 0.191016), gap = 0.0146892:
```

Figure 4(y): Band Gap result summary of PCF.

In PCF case the tolerance value is taken to be 0.01 and decreasing tolerance value after this range will not affects the band gap.

4.4 The Band Gap Analysis-A Comparison

As the mode analysis and band gap analysis is done for three designs, the band gap characteristics have been improved from the one dimensional photonic crystal to the photonic crystal fiber. Since the band gap analysis is done for photonic sensor applications a narrower and single band gap is observed at the end. A comparison is shown in the table 4.2 for all three designs.

Table 4.2: Band Gap Comparison for Designed Photonic Structures.

Structure	No. of Band Gaps	Bandgap Range(frequency)	Tolerance
1D Photonic Crystal	3	0.151232-0.256028	0.1
		0.353862-0.501916	
		0.592998-0.721837	
2D Photonic Crystal	1	0.324152-0.441990	0.1
Photonic Crystal Fiber	1	0.176327-0.191016	0.01

As the table indicates, it can be easily concluded that no. of band gaps as well as band gap frequency range comes out to be minimum for the PCF which makes it a desirable choice for photonic sensor application.

CHAPTER

5

CONCLUSIONS

Photonic crystal structures and devices reveal great potential and underexplored possibilities for both basic and applied research, opening new perspectives in the field of photonic micro sensors. Photonic crystal structures are at the forefront of micro sensor technology. In this thesis photonic crystal structures and the devices has been designed and some of the novel optical properties provided by photonic crystals are analysed and their implementation within micro sensors are summarized.

The one dimensional and two dimensional photonic crystals as well as a hollow core photonic crystal fiber have been designed as the finite difference time domain models. The band gap analysis has been done by using plane wave expansion method. The band gap analysis of all three designs has been done taking into consideration their micro sensor implementations.

It has been observed that for one dimensional photonic crystal design, the poynting vector amplitude comes out to be constant in horizontal direction of crystal for range 1.5μm-10μm. Hence this whole area can be used for photonic sensor implementation however when the band gap analysis is done the band gap in this case comes out to be very high in all three bands calculated through plane wave expansion method. So the frequency range of the input wave should not be in the band gap range otherwise it will be fully reflected.

The poynting vector amplitude for two dimensional design is nearly constant for a horizontal range of 3.9μ-6.2μm that defines the area for micro sensor implementation. The number of band gaps in this case were also reduced however width of the one and only calculated band gap is quite more that defines somewhat wider range of frequency that should be taken care of while propagating a wave through the two dimensional photonic crystal design.

In the photonic crystal fiber design, the poynting vector is nearly constant in horizontal direction from 8.6μm to 12.8μm. so a range of about 4μm horizontal can be used for the photonic crystal fiber based sensor implementations. The band gap in this design comes out

to be very narrow. Hence photonic crystal fiber design minimized the band gap so that except from a narrow range of frequencies, all the waves will be able to propagate through this device that widens the design space.

It has been concluded that photonic crystal devices and structures comes out to be distinctive for photonic micro sensor implementations.

REFERENCES

[1] J. Knight, T. Birks, B. Mangan and P. St. James Russell, “New solutions in fiber optics,” Optics Photonics News, vol. 13, pp. 26–30, Mar. 2002.

[2] Y. Wang, H. Bartelt, W. Ecke, R. Willsch, J. Kobelke, M. Kautz, S. Brueckner and M. Rothhardt, “Sensing properties of fiber Bragg gratings in small-core Ge-doped photonic crystal fibers,” Optical Communication, pp. 1129–1134, 2009.

[3] L. Rindorf and O. Bang, “Sensitivity of photonic crystal fiber grating sensors: biosensing, refractive index, strain and temperature sensing,” J. Opt. Soc. Am. B 25(3), pp. 310–324, 2008.

[4] M. T. Myaing, J. Y. Ye, T. B. Norris, T. Thomas, J. R. Baker Jr., W. J. Wadsworth, G. Bouwmans, J. C. Knight and P. St. J. Russell, “Enhanced two-photon biosensing with double-clad photonic crystal fibers”, Optics Letter 28, pp. 1224-1226, 2003.

[5]. B. J. Eggleton, C. Kerbage, P. Westbrook, R. S. Windeler, and A. Hale, "Microstructured optical fiber devices," Opt. Express 9, pp. 698-713, 2001.

[6] J. Broeng, S.E. Barkou, T. Sondergaard, A. Bjarklev, “Analysis of air-guiding photonic bandgap fibers”, Optics Letter 25, pp. 96-98, 2000

[7] J.C. Knight, Opt. Letter 21, 1547 (1996), 22, 484 (1997).

[8] D. Akimov, M. Schmitt, R. Maksimenka, K. Dukel.skii, Y. Kondrat.ev, A. Khokhlov, V. Shevandin, W. Kiefer and A. M. Zheltikov, “Supercontinuum generation in a multiple-submicron-core microstructure fiber: toward limiting waveguide enhancement of nonlinear-optical processes,” Appl. Phys. B 77, pp. 299-305, 2003.

[9] James R. Nagel, “The Finite-Difference Time-Domain (FDTD) Algorithm’’ University of Utah

[10] H. Mutoh, “Optical and Electrical simulation for CMOS image sensors,” IEEE Trans. Electron Devices, vol. 50, no. 1, pp. 19–25, Jan. 2003.

[11] K. Yee, “Numerical solution of initial boundary value problems involving Maxwell’s equations in isotropic media,” IEEE Trans. Antennas Propag., vol. AP-14, no. 3, pp. 302–307, May 1966.

[12] A. Taflove, "Application of the finite difference time domain method to sinusoidal steady state electromagnetic-penetration problems," IEEE Trans. Electromagn. Compat., vol. EMC-22, no. 3, pp. 191–202, Aug. 1980.

[13] J. D. Joannopoulos, R. D. Meade, and J. N. Winn, "Photonic Crystals: Molding the Flow of Light," Princeton University Press, Princeton, NJ, 1995.

[14] P. St. J. Russell, "Photonic crystal fibers," Opt. Science, vol. 299, pp. 358–362, Jan. 2003.

[15] J. C. Knight, J. Broeng, T. A. Birks, and P. St. J. Russell, "Photonic band gap guidance in optical fibers," Opt Science, vol. 282, pp. 1476–1478, Nov. 1998.

[16] W. H. Reeves, J. C. Knight, P. St. J. Russell and P. J. Roberts, "Demonstration of ultra-flattened dispersion in photonic crystal fibers," Optics Express, vol. 10, pp. 609–613, July 2002.

[17] R. E. Kristiansen, K. P. Hansen, J. Broeng, P. M. W. Skovgaard, M. D. Nielsen, A. Petersson, T. P. Hansen, B. Mangan, C. Jakobsen and H. R. Simonsen, "Microstructured fibers and their applications," in OPTOEL 2005, Elche, Spain, July 13–15, 2005.

[18] K. Kurokawa, K. Tajima, K. Tsujikawa and K. Nakajima, "Reducing the losses in photonic crystal fibres," in Proc. European Conference on Optical Communication-ECOC 2005, Glasgow, Scotland, Sept. 25–29, 2005.

[19] K. Tajima, J. Zhou, K. Nakajima, and K. Sato, "Ultra low loss and long length photonic crystal fiber," in Proc. Optical Fiber Communications Conference-OFC 2003, Atlanta, Georgia, USA, Mar. 23–28, pp. PD1.1–PD1.3, 2003.

[20] L. Vincetti, D. Ferrarini, M. Zoboli, A. Cucinotta, F. Poli, and S. Selleri, "Leakage losses in photonic band gap fibers," in Proc. European Conference on Optical Communication-ECOC 2003, Rimini, Italy, Sept. 21–25, 2003.

[21] K. Miyake, M. Hachiwaka, T. Kinoshita, S. Yamaguchi, H. Kubota, and S. Kawanishi, "Bend resistant photonic crystal fiber compatible with conventional single mode fiber," in Proc. European Conference on Optical Communication-ECOC 2004, Stockholm, Sweden, Sept. 5–9,2004.

[22] T. P. Hansen, J. Broeng, C. Jakobsen, G. Vienne, H. R. Simonsen, M. D. Nielsen, P. M. W. Skovgaard, J. R. Folkenberg and A. Bjarklev, "Air-guiding photonic bandgap fibers:

spectral properties, macrobending loss, and practical handling," IEEE/OSA Journal of Lightwave Technology, vol. 22, pp. 11–15, Jan. 2004.

[23] B.M.dillion and J.P.Webb, "A comparison of formulation for vector finite element analysis of photonic waveguides", IEEE transactions on microwave theory and techniques, Vol.42, pp.308-316, Feb.1994.

[24] D. M. Sullivan, "Electromagnetic Simulation using the FDTD Method," Piscataway, NY: IEEE Press, 2000.

[25] A. Taflove and M. E. Brodwin, "Numerical solution of steady-state electromagnetic scattering problems using the time-dependent Maxwell's equations," IEEE Transactions on Microwave Theory and Techniques, vol. 23, pp. 623–630, Aug.1975

[26] K. R. Umashankar and A. Taflove, "A novel method to analyze electromagnetic scattering of complex objects". IEEE Transactions on Electromagnetic Compatibility, vol. 24, pp. 397–405, 1982.

[27] Taflove, Alen "Computational Electrodynamics: The FDTD method" Artech house, Boston, 1995.

[28] Zhili Lin, Chunxi Zhang, Pan Ou, Yudong Jia and Lishuang Feng. "A Generally Optimized FDTD Model for Simulating Arbitrary Dispersion sub wavelength model Based on the Maclaurin Series Expansion" Journal Of Lightwave Technology, vol. 28, no. 19, October 1, 2010.

[29] D. H. Choi and W. J. Hoefer , "The finite difference time-domain method and its application to eigenvalue problems," IEEE Transactions on Microwave Theory and Techniques, vol.34, pp. 1464–1470, 1986.

[30] J. Berenger, "A perfectly matched layer for the absorption of electromagnetic waves". Journal of Computational Physics, vol. 114, pp. 185–200, Aug. 1994.

[31] S. D. Gedney, "An anisotropic perfectly matched layer absorbing media for the truncation of FDTD lattices," IEEE Transactions on Antennas and Propagation, vol. 44, pp. 1630–1639, 1996.

[32] B. Engquist and A. Majda, "Absorbing boundary conditions for the numerical simulation of symmetric waves," Math Comp, vol. 31, pp. 629-651, July 1977.

[33] R. R. McLeod, "Finite difference time domain boundary conditions class notes," pp. 31–59, Sept. 2004.

[34] G.P. Agarwal, “Non linear fiber optics”, fourth edition, Academic press-UK, 2007.

[35] James R. Nagel, “The One-Dimensional Finite difference Time Domain(FDTD) Algorithm Applied to the telegrapher equation” university of Utah

[36] A. Soriano, “Analysis of the finite difference time domain technique to solve the Schroginer equation for quantum devices,” Journal of Applied Physics, Vol. 95, N12, June 2004.

[37] S.Guo, S.Albin, “Simple plane wave implementation for photonic crystal calculations,” Optics Express 11, no.2, p.167-175, 2003.

[38] D. H. Choi and W. J. Hoefer , "The finite-difference time-domain method and its application to eigenvalue problems" IEEE Transactions on Microwave Theory and Techniques, vol. 34, pp. 1464–1470, Nov. 1986.

[39] Okamoto K., “Fundamentals of Optical Waveguides,” Academic Press, San Diego 2000.